

General Disclaimer

One or more of the Following Statements may affect this Document

- This document has been reproduced from the best copy furnished by the organizational source. It is being released in the interest of making available as much information as possible.
- This document may contain data, which exceeds the sheet parameters. It was furnished in this condition by the organizational source and is the best copy available.
- This document may contain tone-on-tone or color graphs, charts and/or pictures, which have been reproduced in black and white.
- This document is paginated as submitted by the original source.
- Portions of this document are not fully legible due to the historical nature of some of the material. However, it is the best reproduction available from the original submission.

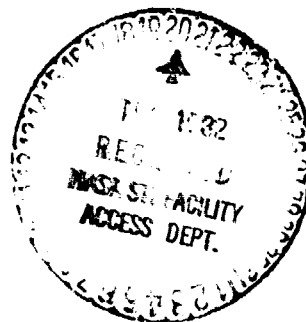
9950-725'

FINAL REPORT

A HIGH-TEMPERATURE CERAMIC HEAT EXCHANGER ELEMENT FOR A SOLAR THERMAL RECEIVER

81-18452

March 23, 1982



(NASA-CR-169625) A HIGH TEMPERATURE CERAMIC
HEAT EXCHANGER ELEMENT FOR A SOLAR THERMAL
RECEIVER Final Report (AiResearch Mfg. Co.,
Los Angeles, Calif.) 114 p HC A06/MF A01

N83-14666

Unclass
01676

CSCL 10A G3/44

Prepared for
Jet Propulsion Laboratory
California Institute of Technology
Pasadena, California 91103



AIRESEARCH MANUFACTURING COMPANY

FINAL REPORT

A HIGH-TEMPERATURE CERAMIC HEAT EXCHANGER ELEMENT FOR A SOLAR THERMAL RECEIVER

81-18452

March 23, 1982

Prepared by

**Hal J. Strumpf
David M. Kotchick
Murray G. Coombs**

Approved by


W.J. O'Reilly

**Chief Engineer, Heat Transfer
and Cryogenic Systems**

Prepared for

**Jet Propulsion Laboratory
California Institute of Technology
Pasadena, California 91103**



AIRESEARCH MANUFACTURING COMPANY

FOREWORD

This report describes the results of a study conducted by AiResearch Manufacturing Company, a division of The Garrett Corporation, on the development of a high-temperature ceramic heat exchanger element. The study was performed for the Jet Propulsion Laboratory (JPL) under Contract 955875. The JPL contract monitor was Dr. Al Kudirka and the AiResearch program manager was Mr. M. Coombs.

PRECEDING PAGE BLANK NOT FILMED



AIRESEARCH MANUFACTURING COMPANY

**ORIGINAL PAGE IS
OF POOR QUALITY**

ABSTRACT

A study has been performed by AiResearch Manufacturing Company, a division of The Garrett Corporation, on the development of a high-temperature ceramic heat exchanger element to be integrated into a solar receiver producing heated air. A number of conceptual designs were developed for heat exchanger elements of differing configuration. These were evaluated with respect to thermal performance, pressure drop, structural integrity, and fabricability. The fabrication analysis was performed by the Norton Company, a ceramic manufacturer acting as a subcontractor to AiResearch on this study. The final design selection identified a finned ceramic shell as the most favorable concept. The shell is surrounded by a larger metallic shell. The flanges of the two shells are sealed to provide a leak-tight pressure vessel. The ceramic shell is to be fabricated by an innovative combination of slip casting the receiver walls and precision casting the heat transfer finned plates. The fins are bonded to the shell during firing. The unit is sized to produce 2150°F air at 2.7 atm pressure, with a pressure drop of about 2 percent of the inlet pressure. This size is compatible with a solar collector providing a receiver input of 85 kw(th). Fabrication of a one-half scale demonstrator ceramic receiver has been completed by Norton.



ACKNOWLEDGEMENTS

The authors of this report would like to acknowledge the significant contributions made to the study by C. C. Wright and W. T. Aboufasha of AiResearch Manufacturing Company and D. P. Reed of the Norton Company.

**ORIGINAL PAGE IS
OF POOR QUALITY**



**ORIGINAL PAGE IS
OF POOR QUALITY**

CONTENTS

<u>Section</u>		<u>Page</u>
1	INTRODUCTION	1-1
2	TASK 1, CONCEPTUAL DESIGNS AND EVALUATIONS	2-1
	Establishment of Design Requirements	2-1
	Conceptual Designs	2-3
	Concept Definition	2-5
	Thermal Analysis and Sizing	2-14
	Structural Analysis	2-26
	Drawings	2-31
	Fabrication Analysis	2-31
	Concept Evaluation and Selection	2-49
3	TASK 2A, PRELIMINARY DESIGNS AND EVALUATIONS	3-1
	Refined Design for Ceramic-Lined Metal Shell	3-1
	Concept Selection	3-8
	Fabrication Options	3-9
	Preliminary Designs	3-13
	Final Design Configuration	3-13
	Stress Levels	3-18
	Component Reliability	3-20
4	TASK 2B, FABRICATION DEMONSTRATION	4-1
	Fabrication of the Finned Plates	4-3
	Fabrication of the Cylinder/Flange Unit	4-3
	Assembly of the Finned Plates to the Cylinder/Flange Unit	4-3
	Siliconization/Bonding of the Assembly	4-9
<u>Appendix</u>		
A	ALTERNATE MATERIAL SYSTEM DESIGN	A-1
B	DESIGN WITH CERAMIC MATERIALS	B-1



SECTION 1

INTRODUCTION

A study has been performed by AiResearch Manufacturing Company, a division of The Garrett Corporation, on the development of a high-temperature ceramic heat exchanger element to be integrated into a solar receiver producing heated air. The study was funded by the Jet Propulsion Laboratory (JPL).

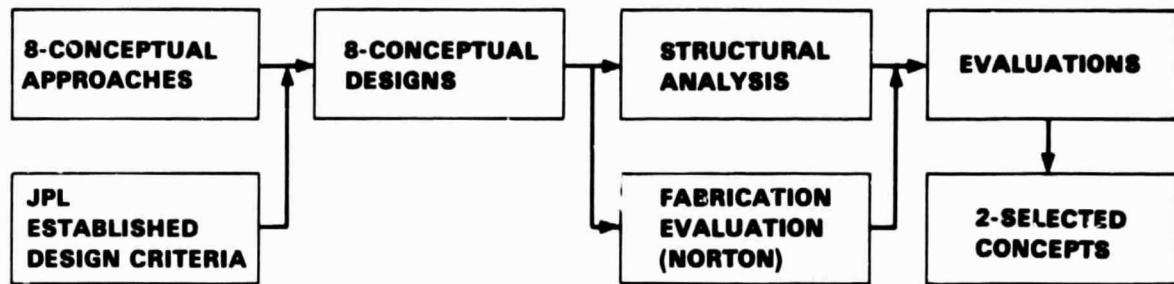
Eight conceptual designs were developed for heat exchanger elements of differing configuration. These were evaluated with respect to thermal performance, pressure drop, structural integrity, and fabricability based on the established design criteria. The fabrication analysis was performed by the Norton Company, a ceramic manufacturer acting as a subcontractor to AiResearch on this study.

The two most favorable designs were chosen for further evaluation. From this evaluation, the selected concept emerged. A detailed preliminary design and fabrication analysis was performed for this concept. In addition, a fabrication demonstration program was conducted by Norton. The outline of the study program is shown in Figure 1-1.

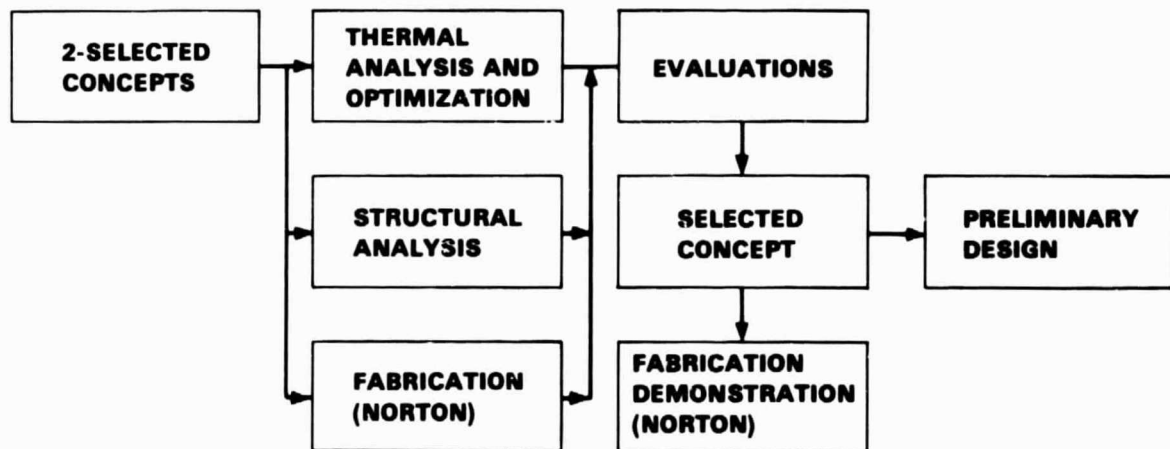
The work was performed during the calendar year 1981. The program schedule is shown in Figure 1-2.



ORIGINAL PAGE IS
OF POOR QUALITY



TASK 1



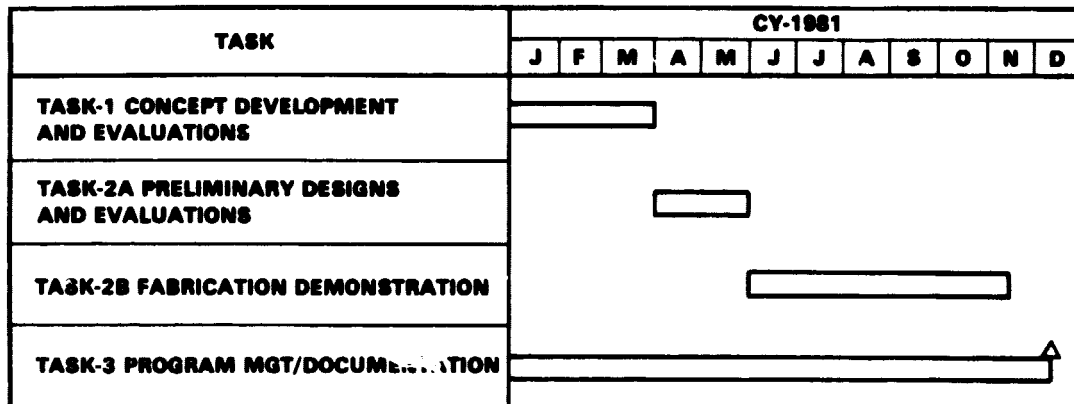
TASK 2

A-16638

Figure 1-1. Program Approach



ORIGINAL PAGE IS
OF POOR QUALITY



△ FINAL REPORT

A-16632-A

Figure 1-2. Program Schedule



SECTION 2

TASK 1, CONCEPTUAL DESIGNS AND EVALUATIONS

ESTABLISHMENT OF DESIGN REQUIREMENTS

The function of the cavity receiver is to absorb sunlight, using the energy to heat the working fluid (air). The sunlight is focused by a concentrator; the focal point of the concentrator is located at the receiver aperture. Figure 2-1 shows a conceptual concentrator and solar receiver system.

The concentrated incident solar flux is distributed on the interior walls and heat transfer surfaces of the receiver. Most of the energy is absorbed by the air; the remaining energy escapes back through the aperture or is lost from the outer surfaces of the receiver. A generalized schematic of a solar receiver is shown in Figure 2-2.

The applications for the hot air produced by the ceramic solar receiver may be in the areas of electric power, fuels and chemicals, or industrial process heat. It is clear that precise design requirements cannot be developed until, at the very least, the receiver application is selected. It is necessary, however, to develop problem conditions in order to conduct the present study. A convenient and typical set of conditions is available for a power-producing solarized automotive gas turbine (SAGT) engine being developed by the Garrett Turbine Engine Company. This engine configuration is referred to as the Mod I. The design point for the SAGT receiver is given in Table 2-1. These conditions are typical of high-temperature receivers and are used for all designs in the present study. A ceramic heat exchanger element is required since metallic material limits would be exceeded. The material selected for the present study, siliconized-silicon carbide (NC-430) manufactured by the Norton Company, has an upper temperature limitation of around 2400°F.

JPL has specified an 8-in. aperture diameter. In order to limit incident flux spillage outside the aperture, a concentrator with a slope error of no greater than 1 mrad is required. Based on representative flux distribution curves for concentrators of this accuracy (supplied by JPL), cavity wall incident flux distribution maps were developed for various size cavities (all with 8-in. diameter apertures) using AiResearch-developed flux mapping techniques. These techniques are described in the Air Brayton Solar Receiver (ABSR) Phase I Final Report, para. 2.3.2.4.* All generated incident flux distributions were symmetrical in the circumferential direction of the receiver.

The thermal input to the working fluid is not specified. Therefore, neither the working fluid flow rate nor the desired cavity efficiency is

*Eastwood, J. C., Open Cycle Air Brayton Solar Receiver Phase I Final Report, AiResearch Report 79-15677, February 1979.



ORIGINAL PAGE IS
OF POOR QUALITY

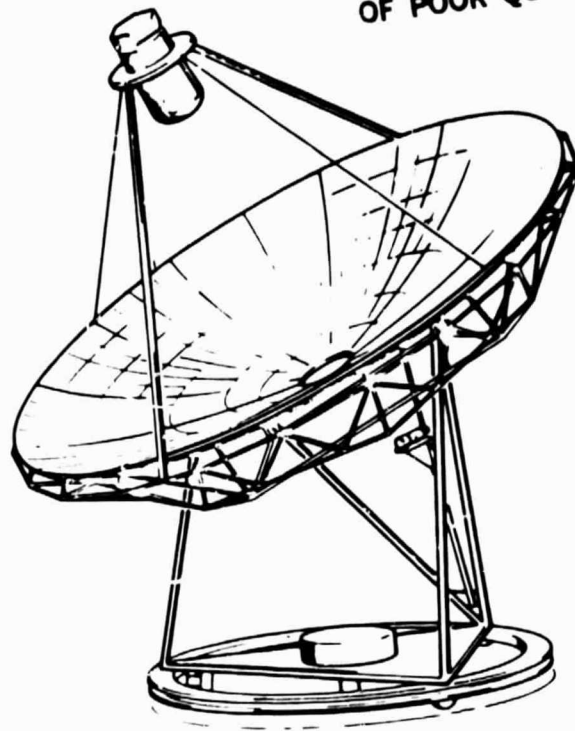
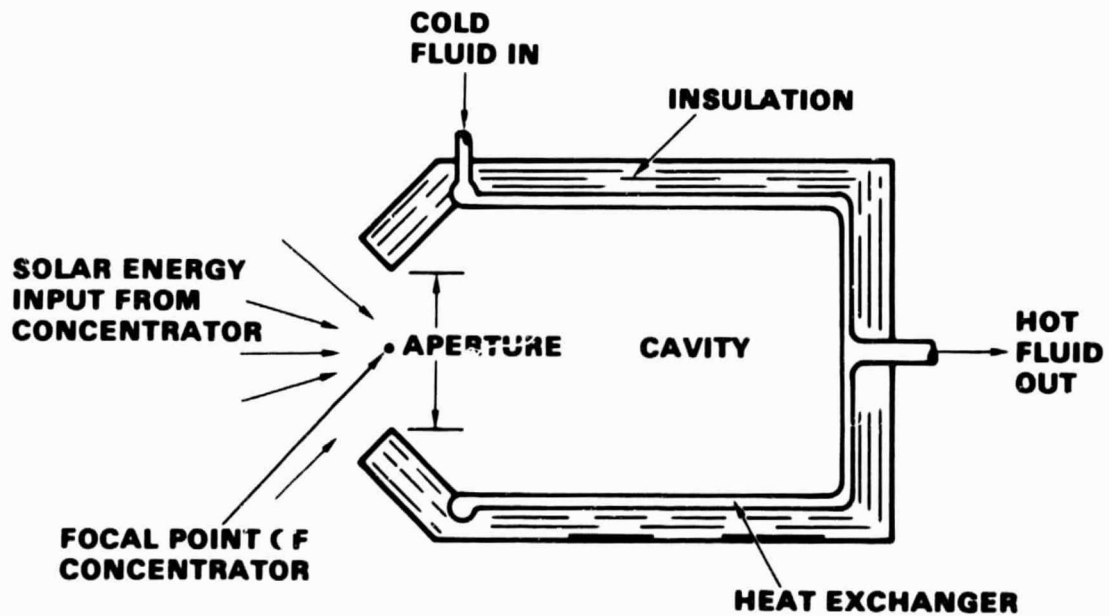


Figure 2-1. Solar Collector Module



A-18855

A-24346

Figure 2-2. Solar Receiver Schematic



AIRESEARCH MANUFACTURING COMPANY

81-18452
Page 2-2

TABLE 2-1

RECEIVER DESIGN POINT

Working Fluid	Air
Outlet Air Temperature	2150°F
Inlet Air Temperature	1580°F
Inlet Pressure	2.7 atm
Maximum Pressure Drop	4.0 percent of inlet pressure
Receiver Input Power	85 kw(th)

given. The cavity efficiency is defined as the ratio of the working fluid thermal input to the specified receiver thermal input. The cavity efficiency takes into account the receiver thermal losses. These include radiation and convection losses out of the aperture opening and losses from the receiver outer surface. The cavity efficiency is a function of receiver geometry and temperature level.

CONCEPTUAL DESIGNS

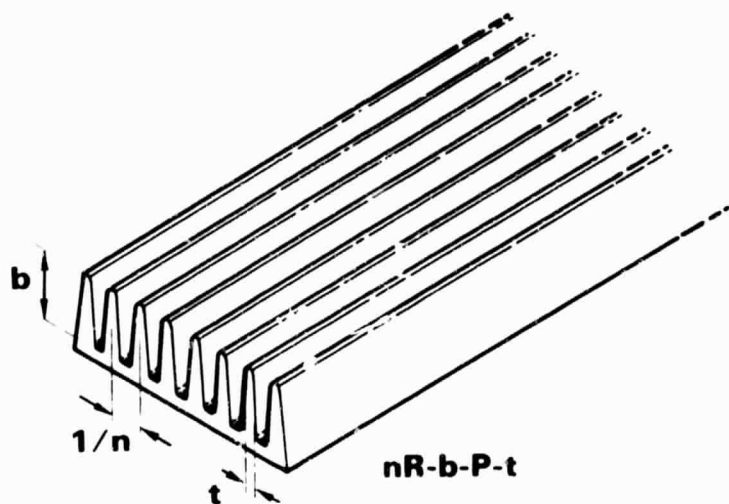
As described in the following paragraphs, various ceramic receiver conceptual designs were prepared to meet the above specifications. The scope of the study effort permitted the consideration only of the steady-state design point. For each conceptual design, the study consisted of the following: concept definition, sizing and thermal analysis, structural analysis, drawing preparation, and fabrication analysis.

It is desired to minimize receiver size and weight, as small size improves fabricability and enhances survival probability (as discussed in Appendix E). In addition, small size aids in mounting and packaging of the receiver. A secondary consideration is to maximize the receiver cavity efficiency.

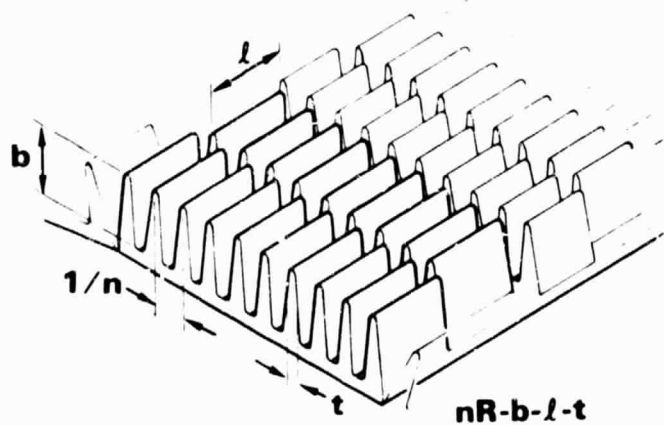
A number of the proposed concepts are of the plate-fin type. The fins can be either plain or offset. Plain fins form a series of discrete flow passages that enable hydrodynamic and thermal development of the flow. Offset fins form interrupted flow passages with accompanying flow migration among the passages. The offsets preclude the development of the flow by disrupting the fluid boundary layer. This results in an increase in the fluid heat transfer coefficient and pressure drop. Sketches of ceramic-type plain and offset fins are shown in Figure 2-3, along with the AiResearch fin geometry designation. The designation is self-explanatory and is used throughout this report.



ORIGINAL PAGE IS
OF POOR QUALITY



a. PLAIN FINS



b. OFFSET FINS

A-10029

Figure 2-3. AiResearch Ceramic Fin Designations



AIRESEARCH MANUFACTURING COMPANY

In general, the receiver structure, excepting the heat exchanger element, is similar for the various designs. The receiver consists of a cylindrical main body, a flat or hemispherical closed end, a conical aperture end, and an incident radiation reflection skirt located around the aperture. The skirt helps direct any incident flux that spills over the aperture opening into the cavity. The closed end and cylindrical body of the receiver are covered with insulating material. An outer case surrounds the insulation. This is the general arrangement shown in Figure 2-2 (the reflector skirt is not shown, however). From Figure 2-2, it can be seen that the fluid inlet section is located at the aperture end, and the outlet section is at the closed end. Due to the nature of the flux distribution, this arrangement has been found to yield a lower maximum wall temperature and a higher cavity efficiency than an otherwise identical receiver with opposite flow direction.

Concept Definition

1. Continuous Plate-Fin

This concept is shown schematically in Figure 2-4. The design consists of a single layer of formed fins between two plates, which act as the inner and outer shells of the fluid containment structure. The fins and plates can be fabricated separately and bonded together during assembly. Alternatively, the fins could be cast on one of the plates and bonded to the other plate. As shown in Figure 2-4, the manifolds are made integral with the plates. The fluid enters the inlet manifold at the bottom of the cylinder and is distributed to the fin passages. The fluid flows upward through the fins and is collected at the top by the outlet manifold.

This concept is similar in geometry to the metallic plate-fin receiver used in the AiResearch ABSR.

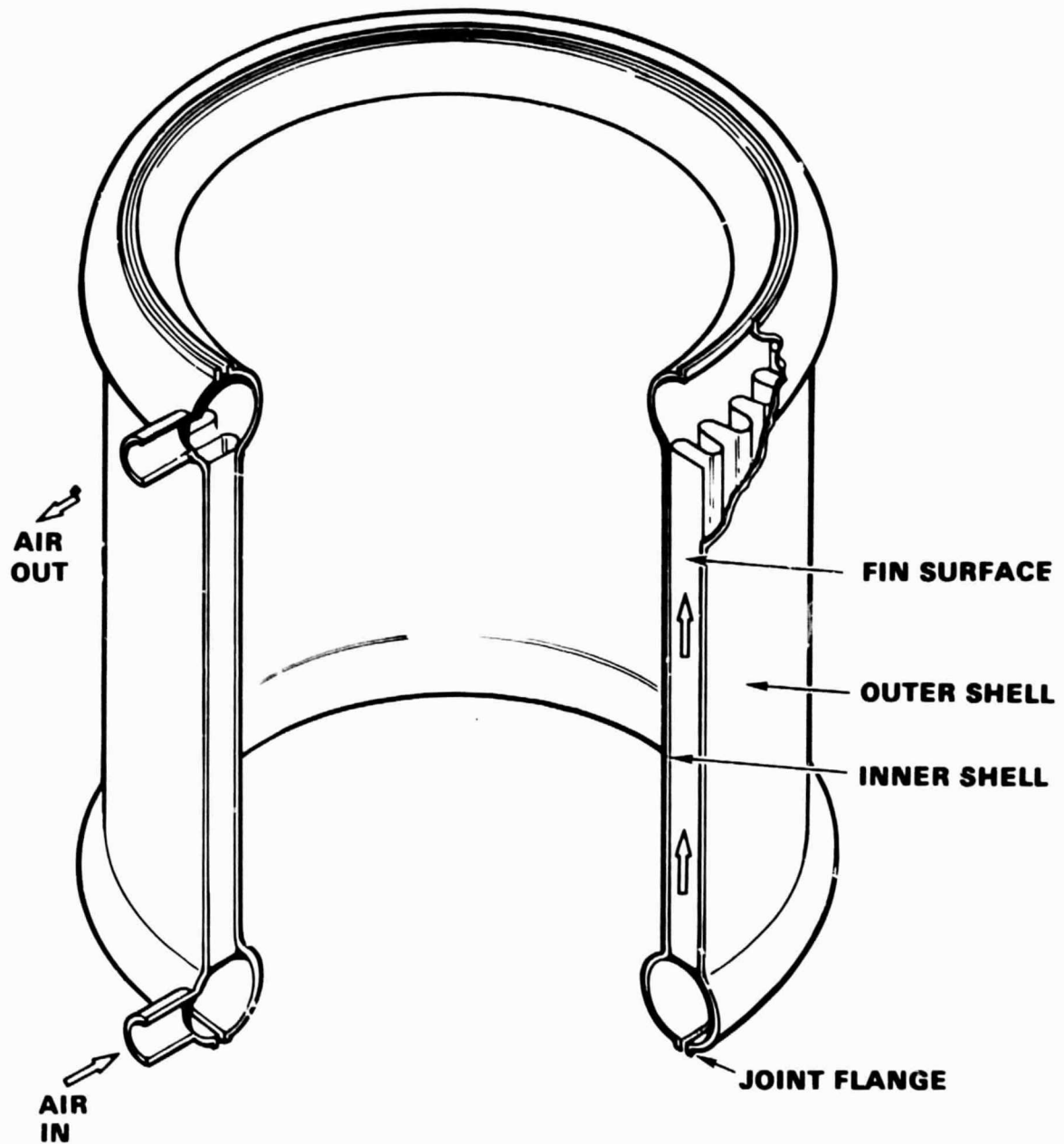
2. Plate-Fin Stacked Ring

This concept is illustrated in Figure 2-5. It consists of a series of individual ring segments that (when stacked and bonded together) form a cylindrical receiver cavity. The individual rings have radial fins that connect the inner and outer walls of the ring. The mating surfaces of the rings have an interlocking tongue-and-groove arrangement to aid in stacking the rings. Individual rings are formed first, and the cylindrical assembly is formed from the rings. Manifolds are similarly and separately formed and can be bonded to the top and bottom of the cylindrical assembly. The fluid enters the inlet manifold at the bottom of the cylinder and is distributed to the fin passages. The fluid flows upward through the fins and is collected at the top by the outlet manifold. The receiver aperture is at the fluid inlet location.

3. Concentric Cylinders with Vertical Ribs

This concept is illustrated in Figure 2-6. It consists of two concentric cylinders, bonded together. Grooves are cast in the cylinders so that flow passages are created upon bonding. The grooves define parallel flow passages separated by vertical ribs, as can be seen from the unrolled view in Figure 2-6a. The flow passages can be any desired shape; square passages were selected for the present study, as shown in the passage cross section in Figure 2-6b.





A 2131

Figure 2-4. Continuous Plate-Fin Concept



ORIGINAL PAGE IS
OF POOR QUALITY

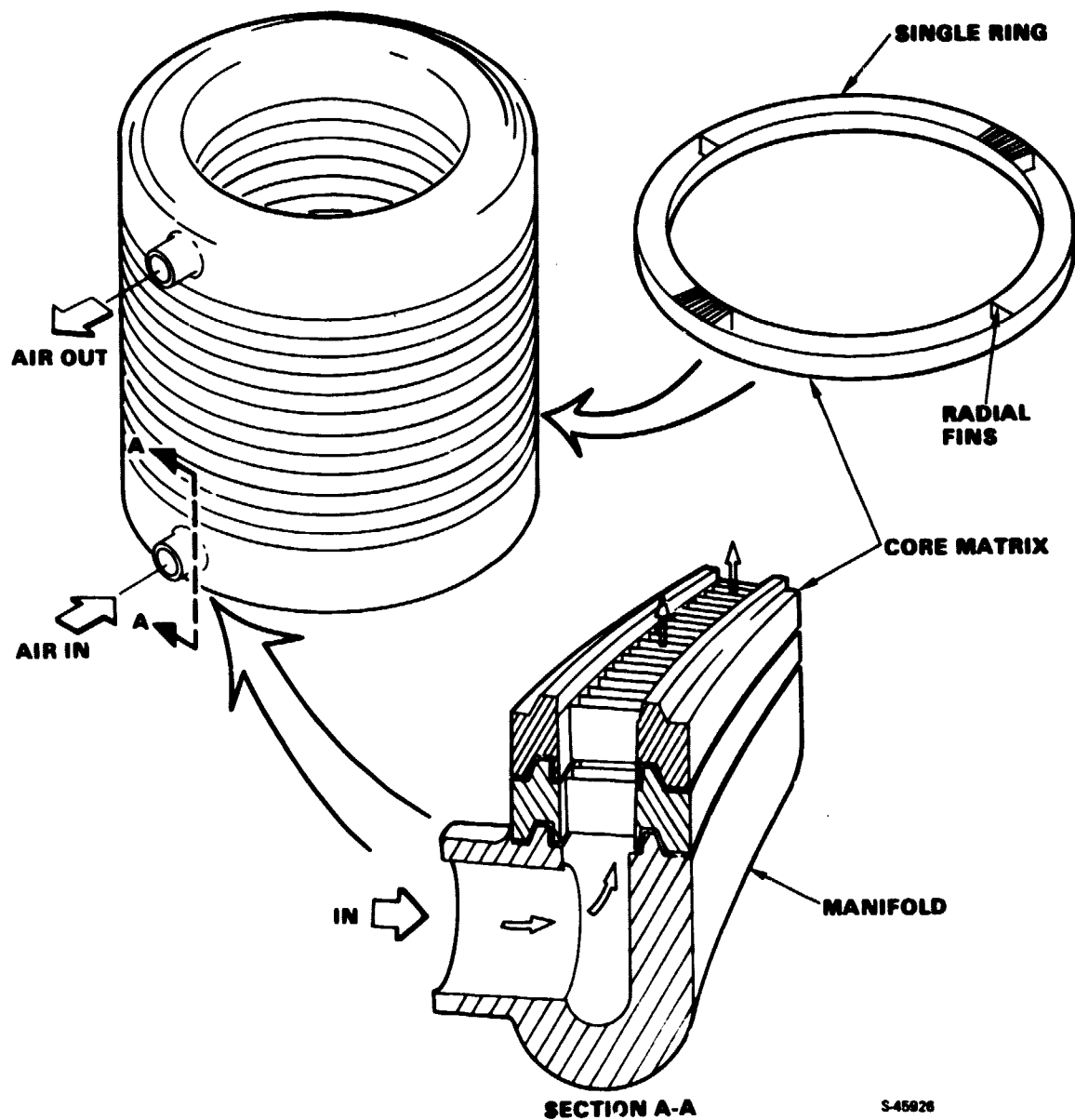
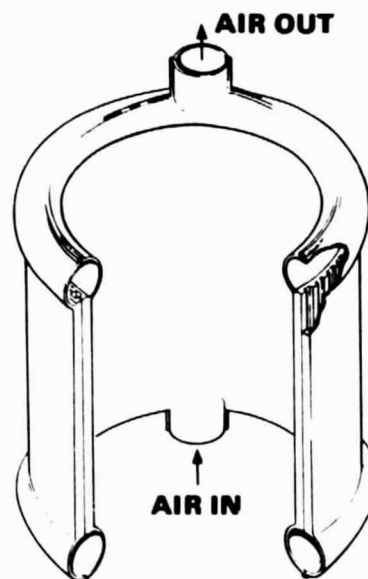
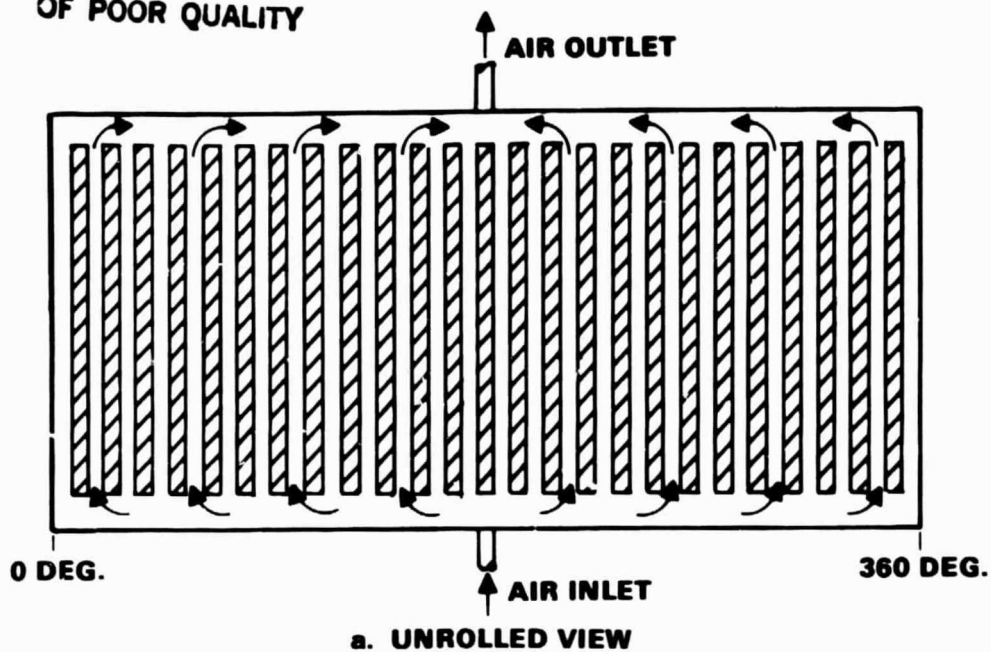


Figure 2-5. Plate-Fin Stacked Ring Concept



ORIGINAL PAGE IS
OF POOR QUALITY



A-23404

Figure 2-6. Concentric Cylinders with Vertical Ribs Concept



AIRESEARCH MANUFACTURING COMPANY

Because the flow is through parallel passages, flow distributing manifolds are required. These can either be cast integrally with the flow passages, as shown in Figure 2-6c, or formed separately and attached to the passages. In either case, the fluid enters the inlet manifold at the bottom of the cylinder, flows upward through the flow passages, and is collected at the top by the outlet manifold. The receiver aperture is at the fluid inlet location.

The heat exchanger is similar in appearance to the continuous plate-fin unit shown in Figure 2-4 (i.e., a series of parallel, smooth flow passages); however, the fin or rib thickness is much greater for the vertical rib concept than for the continuous plate-fin.

4. Dual-Tube Serpentine Flow

This concept is shown in Figure 2-7. This is a concentric cylinder design made by bonding inner and outer cylinders together to form tubular-type flow passages. The fluid enters the heat exchanger through a large inlet tube and flows axially down the cylinder where it is split into two smaller tube paths with half the flow going clockwise and the other half counterclockwise around the cylindrical structure. The flow is essentially axial up and down the cylinder. The flow streams combine and exit the heat exchanger through a large outlet tube. The ducts are at the closed end of the cavity. There are only two flow passages, so there is no need for flow manifolds; problems due to any flow maldistribution would be essentially eliminated.

5. Dual-Tube helical Flow

Instead of having the flow passages axially along the cylinder as in the dual-tube serpentine flow design, the passages could be aligned circumferentially or helically as shown in Figure 2-8. The curvature of the coil increases both heat transfer and pressure drop as compared with a straight tube of similar dimensions. However, there are no wasteful U-bends that utilize pressure drop, but add little to the heat transfer. The air inlet is at the aperture end of the cavity. Since there are only two flow passages, flow maldistribution problems essentially are eliminated. The flow passages are formed by bonding inner and outer concentric cylinders.

6. Single-Tube Helical Flow

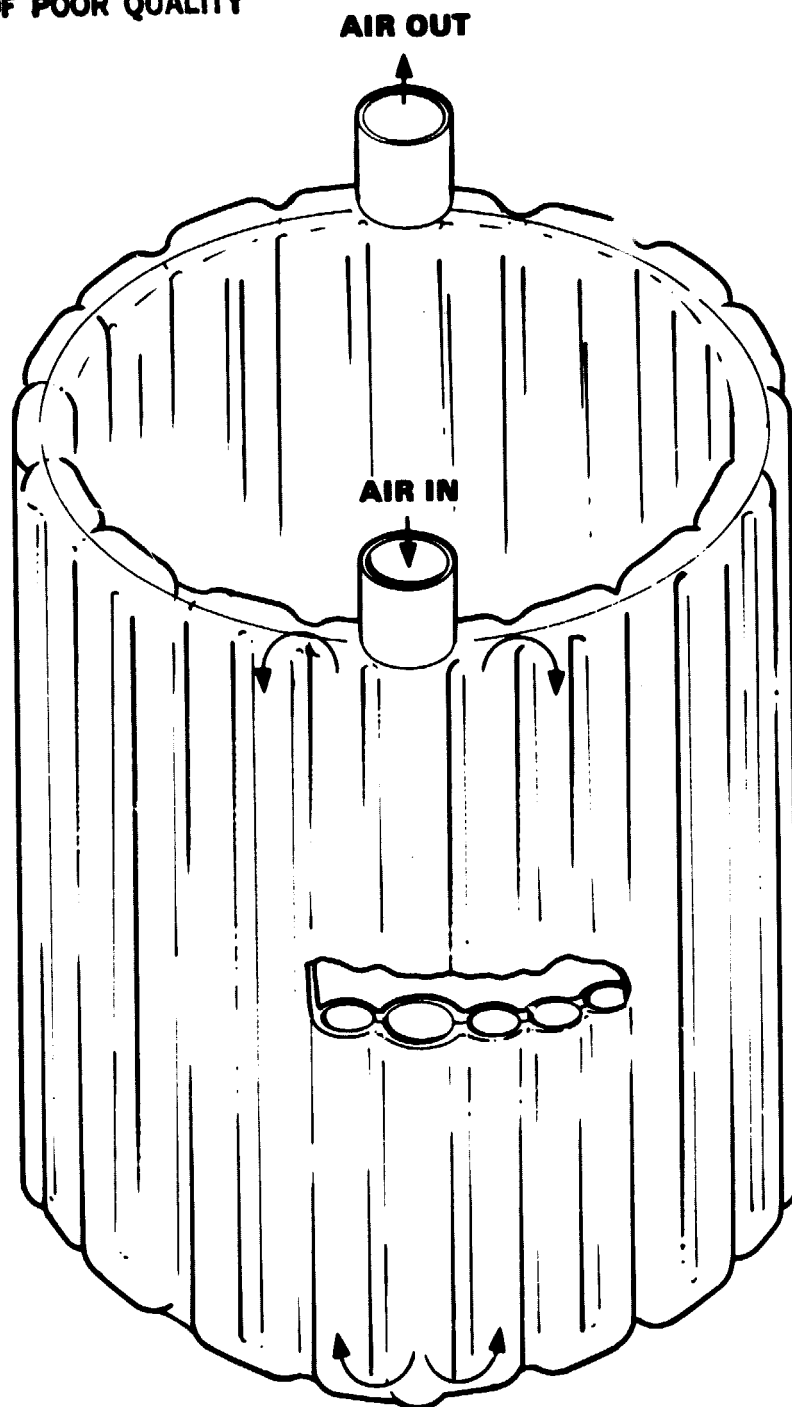
At the expense of a tube diameter larger than that for the dual tube designs, a single-tube helical flow configuration also is feasible. This concept is shown in Figure 2-9. As with the dual-tube configurations, the flow passage is formed by bonding two concentric cylinders. Flow maldistribution problems are totally eliminated since there is only one flow passage. The air inlet is at the aperture end of the cavity.

7. Plate-Fin Stacked Disk

This concept is illustrated in Figure 2-10. It consists of a stack of bonded annular ceramic disks. Each disk is a formed plate-fin passage having both inlet and outlet distribution fins as well as secondary offset fins that are arranged in a circumferential pattern around the disk. Ridges around the



ORIGINAL PAGE IS
OF POOR QUALITY



A-23410

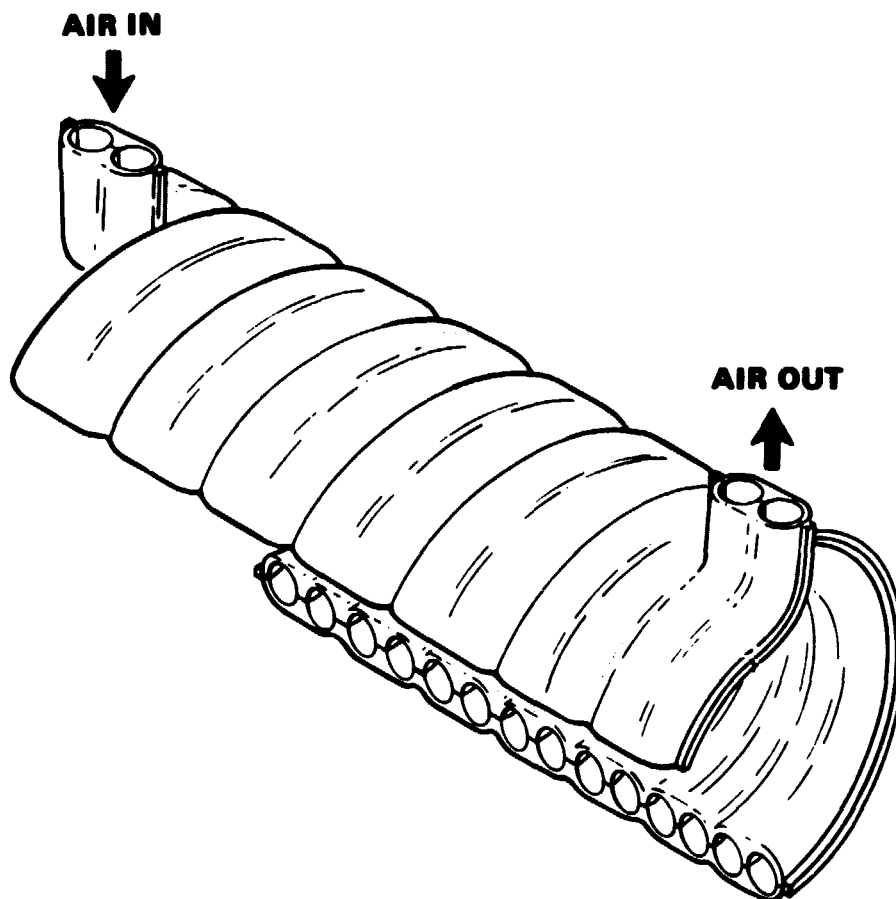
Figure 2-7. Dual-Tube Serpentine Flow Concept



AIRESEARCH MANUFACTURING COMPANY

81-18452
Page 2-10

ORIGINAL PAGE 13
OF POOR QUALITY



A-23415

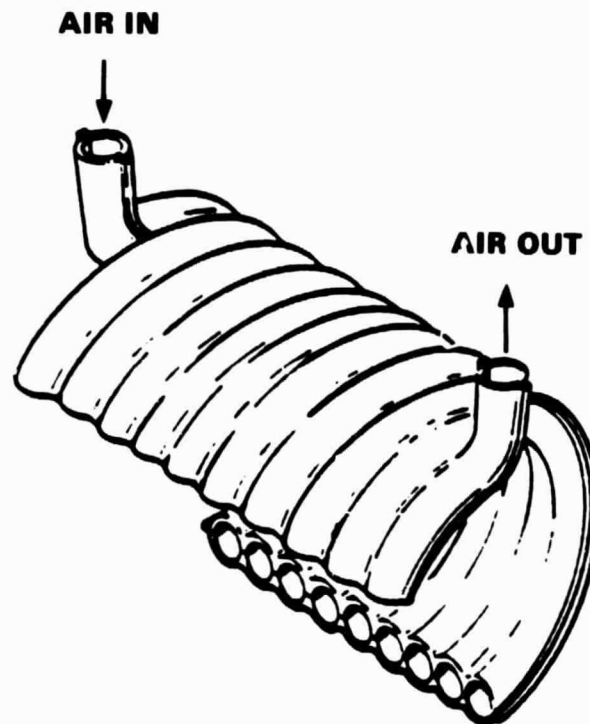
Figure 2-8. Dual-Tube Helical Flow Concept



AIRESEARCH MANUFACTURING COMPANY

81-18452
Page 2-11

ORIGINAL PAGE IS
OF POOR QUALITY



A-23417

Figure 2-9. Single-Tube Helical Flow Concept



ORIGINAL PAGE 13
OF POOR QUALITY

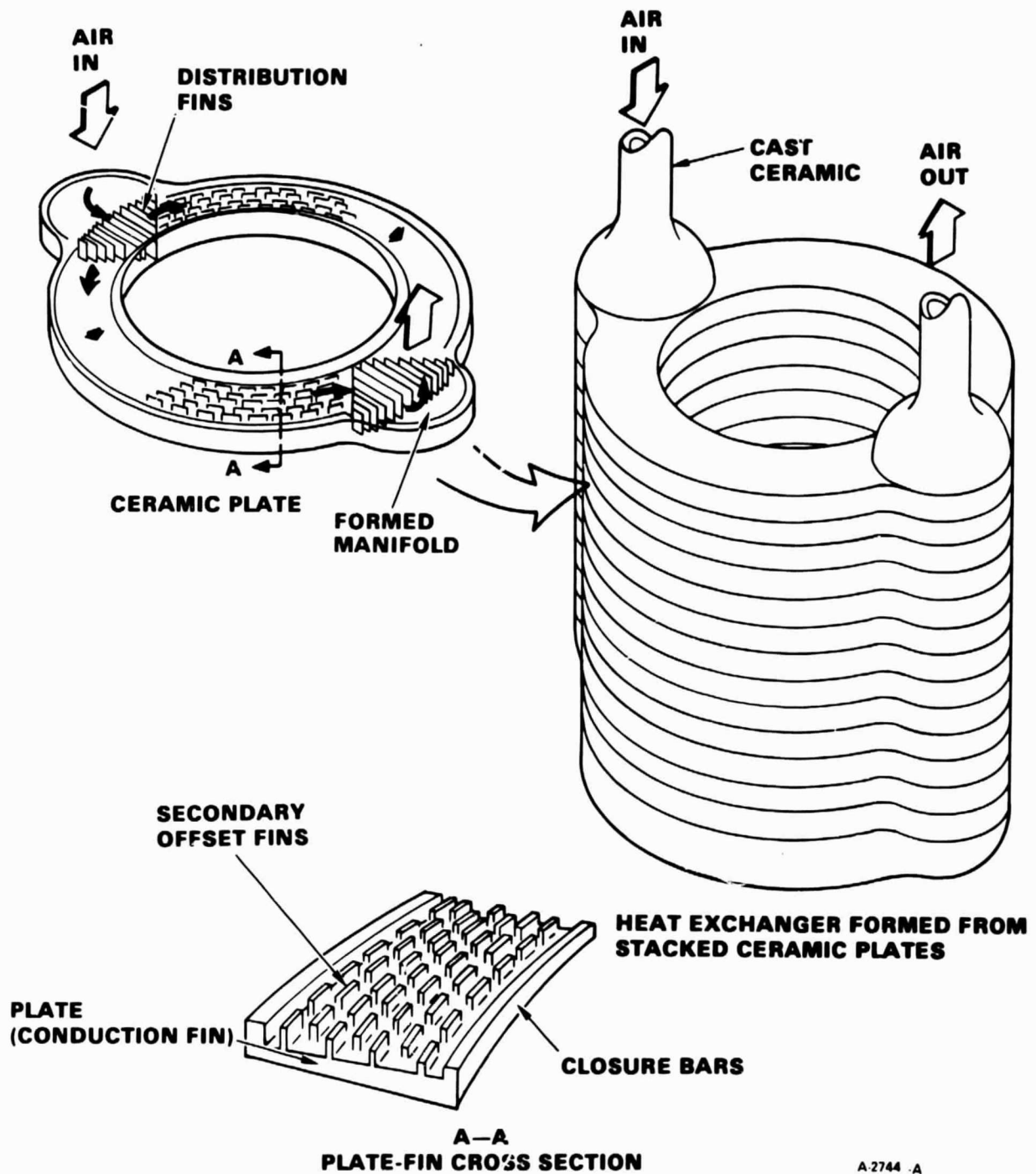


Figure 2-10. Plate-Fin Stacked Disk Concept



inner and outer edges of the disk act as closure bars; when stacked together, they confine the gas to the individual passages. The inlet and outlet manifolds also are formed from ceramic material and are integral with the cylindrical disk so that when the disks are stacked together, the two manifolds are also formed.

The working fluid enters the inlet manifold, where it is distributed to the individual gas passages via the distribution fins. It then flows around the circumference of the cylinder, where it is collected in the outlet manifold via the outlet distribution fins.

A cross section of an individual plate also is illustrated in Figure 2-10. The solar flux is incident on the inner ring of the plate formed by the passage closure bar. The heat is conducted to the interior of the passage by the tapered plate, which acts as a conduction fin, where it is distributed to the secondary gas fins located on the plate surface. The height of the gas fins is set by the passage height and the plate taper; however, the fin density and fin thickness may be varied to achieve desired flow distributions and temperature gradients.

8. Ceramic-Lined Metal Shell

This concept is illustrated in Figure 2-11. For clarity, parts of the outer receiver are shown. These include the ceramic aperture at the open end and a hemispherical closed end. The heat exchanger consists of ceramic fins cast on a ceramic shell that acts as the receiver inner wall. The flow passages are closed with the receiver insulation. Outside the insulation is a metallic outer structure. The inner ceramic structure is attached to the outer metallic structure by an O-ring seal, as shown in Figure 2-11. This assembly acts as a pressure-containing vessel for the working fluid.

As can be seen from Figure 2-11, room is left between the end of the fins and the bottom ceramic plate to act as a flow distribution manifold. The fluid flows up the fins, which may be continued past the cylindrical section into the hemispherical end section. In the end section region, the fin spacing will have to be decreased. It may also be possible to increase the fin height in this section to avoid using too much pressure drop. If necessary, all the fins could be removed in this section. The fluid is collected at the top of the heat exchanger and exits in the outlet duct, which is an internally insulated metallic structure.

Thermal Analysis and Sizing

A great deal of the thermal analysis was conducted using the AiResearch receiver computer program, RECMDL. This program has been described previously in detail.* Briefly, RECMDL is a model generation and performance prediction program. It performs the required conduction, convection, radiation, and

*Eastwood, J. C., Open Cycle Air Brayton Solar Receiver Phase I Final Report, AiResearch Report 79-15677, February 1979.



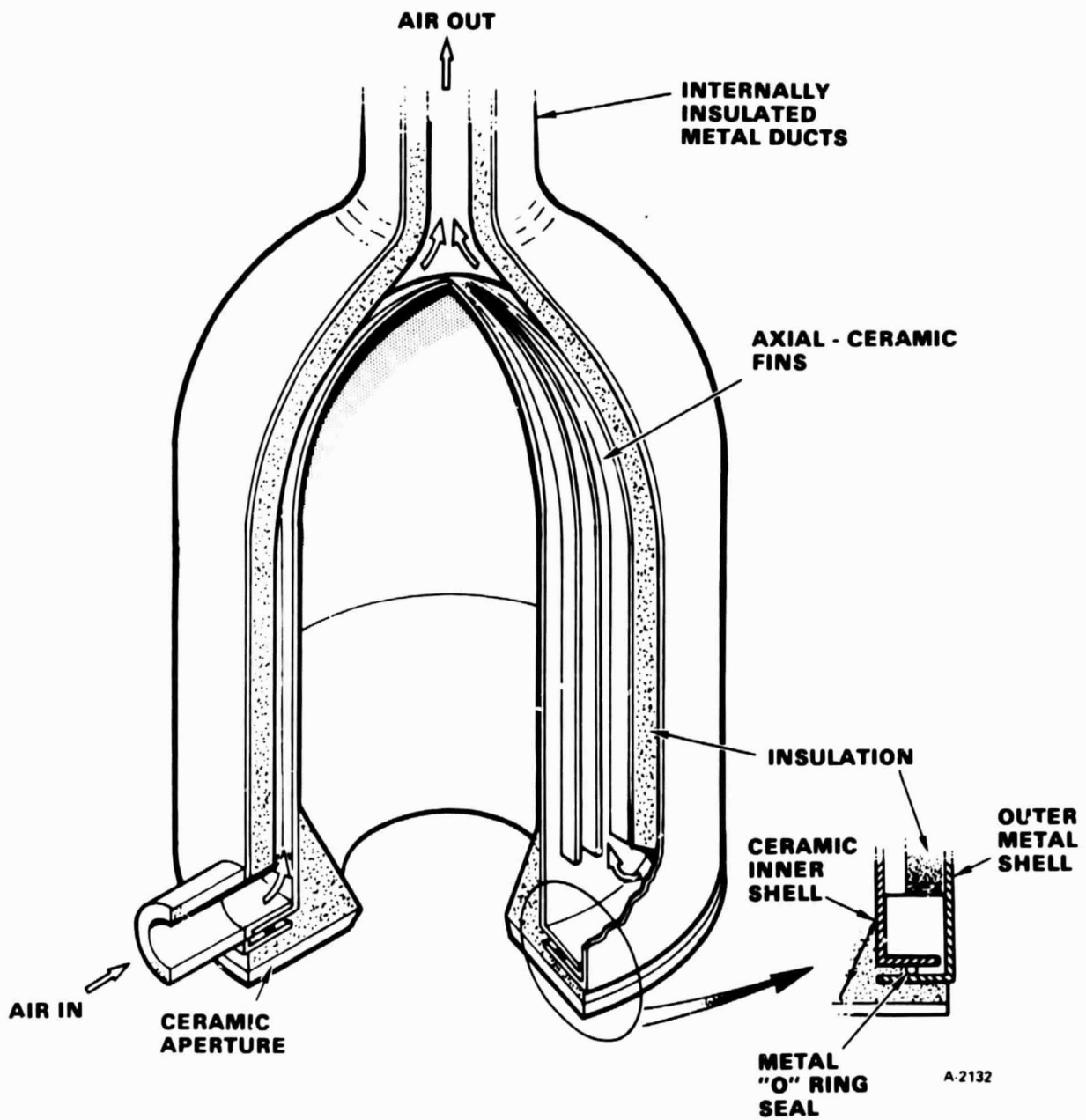


Figure 2-11. Ceramic-Lined Metal Shell Concept

fluid stream heat transfer calculations along with pressure drop calculations to predict the overall cavity efficiency and pressure losses. The program models the receiver as a finite element grid; the output includes a complete nodal temperature map of the receiver (solid and fluid). A typical nodal arrangement is shown in Figures 2-12 and 2-13.

The program has the capability to perform both transient and steady-state calculations; only steady-state calculations were performed for this study. A simplified flow chart for RECMDL is presented in Figure 2-14.

As indicated in Figure 2-14, fixed geometry and inlet conditions are input, with the outlet conditions computed. However, since the problem statement (Table 2-1) specifies input power to the receiver rather than the fluid, the flow rate is not known. Program RECMDL calculates the flow rate by iteration, equating the heat absorbed by the fluid to the product of the power into the receiver and the computed cavity efficiency.

The fin geometry subroutines of RECMDL have been modified to model ceramic-type fins (see Figure 2-3). Previously, the computer code was set up for metallic-type continuous fins.

The computer program models the receiver geometry in two dimensions--axial and radial. Hence, complete circumferential symmetry is assumed for both absorbed flux and surface temperature. For the concepts where the flow is primarily axial, the symmetry assumption is good; however, some of the concepts have flow in the circumferential direction. This would result in a substantial temperature gradient in the circumferential direction as well as an unsymmetrical absorbed radiant flux distribution. The precise analysis of these configurations is beyond the capability of the RECMDL code. An approximate thermal analysis was performed for these concepts using an equivalent thermal conductance approach. This assumes that for a given cavity size, heat exchangers with equal thermal conductances will result in similar wall temperature distributions and cavity efficiencies. Heat exchangers for the unsymmetrical receivers were designed to match the thermal conductances of symmetrical heat exchangers of identical cavity dimensions. The wall temperature distributions were assumed to be similar for the unsymmetrical and symmetrical designs (as determined using RECMDL). The temperature distribution from RECMDL is modified to fit the particular unsymmetrical geometry. For example, Figure 2-15 shows the element locations for the equivalent surface temperature map of the single-tube helical flow configuration. The wall temperatures are particularly important since these temperatures were allowed to approach the nominal NC-430 temperature limit of 2400°F in order to minimize the receiver size.

In the results that follow, the maximum wall temperature represents the maximum predicted surface temperature along the heat exchanger. It does not necessarily occur in the region of maximum fluid temperature (fluid outlet). In fact, for most of the designs the maximum wall temperature occurs closer to the fluid inlet than the fluid outlet. This is due to the nature of the incident flux distribution, which peaks in the region of the maximum wall temperature.



Figure 2-12. Receiver Surface Nodes

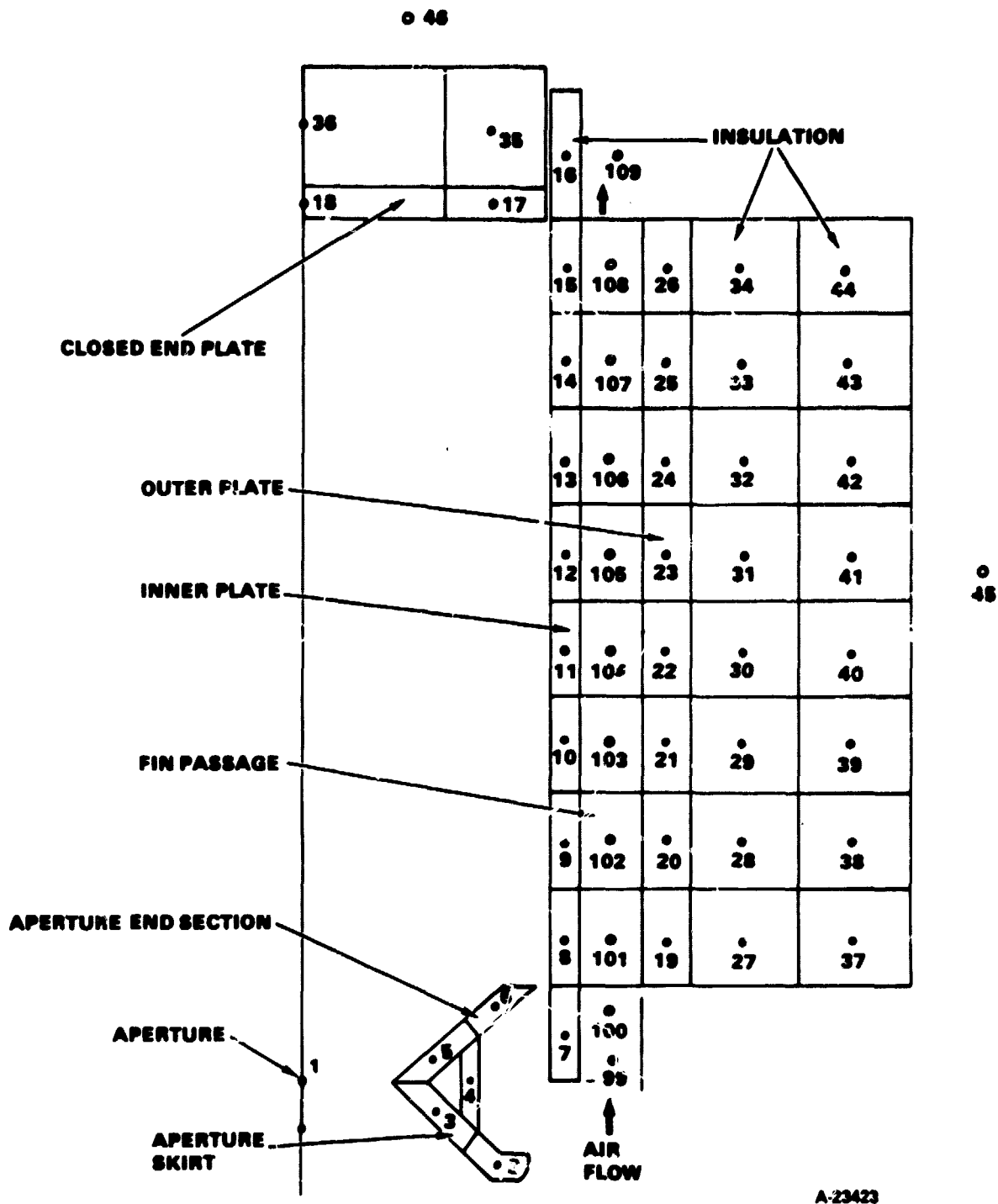
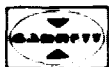
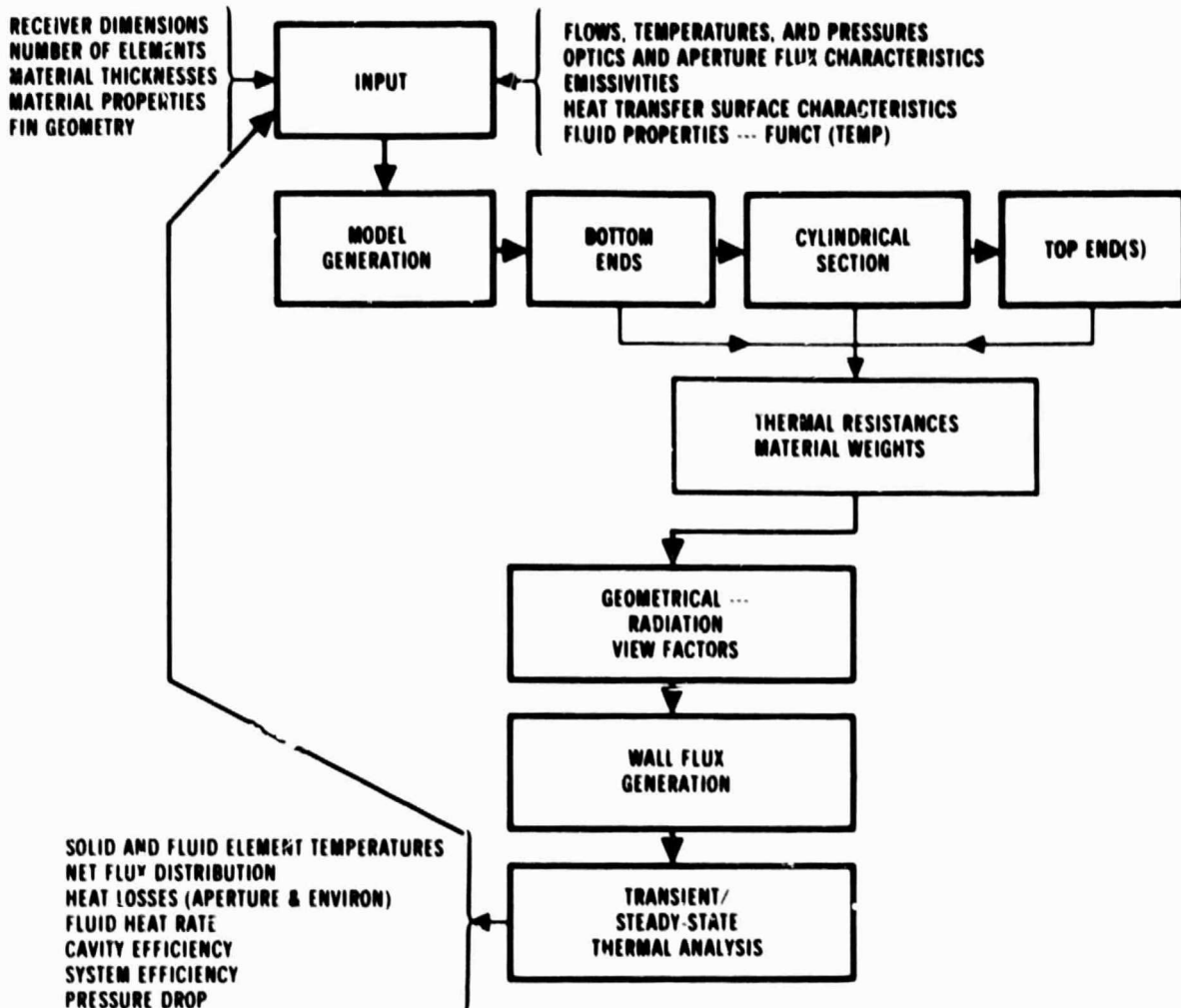


Figure 2-13. Complete Receiver Nodal Model



ORIGINAL PAGE IS
OF POOR QUALITY



A 23408

Figure 2-14. Flow Chart for Solar Receiver Computer Code RECMDL



ORIGINAL PAGE 13
OF POOR QUALITY

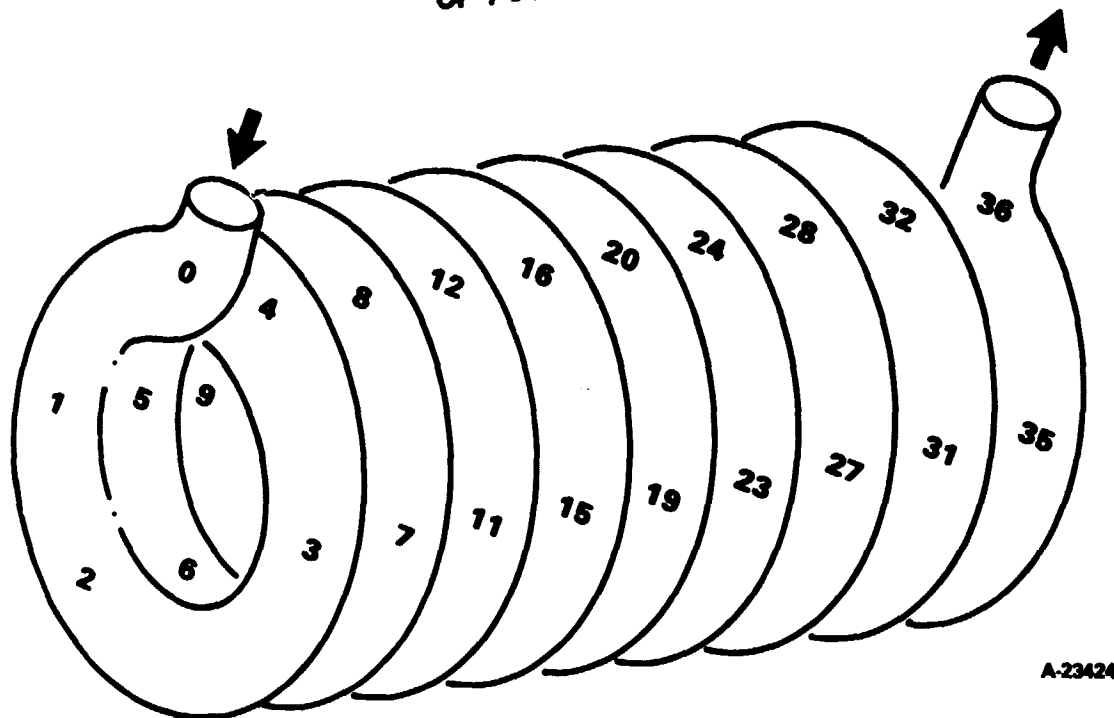


Figure 2-15. Surface Temperature Locations for Single-Tube Helical Flow Configuration

The cavity efficiencies are based on 6-in. insulation around the entire receiver and include all aperture and surface radiation and convection losses. The pressure drops are for the heat exchanger cores only, and do not include manifold or ducting losses.

1. Continuous Plate-Fin

This design, as can be seen from Figure 2-5, has the flow passages aligned axially along the receiver, thus providing the circumferential symmetry necessary for analysis with RECMDL. A fin geometry of 6 fins per in., 0.175 in. high, and 0.010 in. thick (6R-0.175-P-0.010) yielded reasonable designs.

For this fin, various cavity sizes were analyzed for performance. The results of the survey are presented in Table 2-2. Keeping the objectives of maximizing cavity efficiency and minimizing size (while maintaining a maximum wall temperature below 2400°F) in mind, a cavity size of 1.5-ft diameter and 2.5-ft length would appear to be a reasonable selection.

Uniform flow distribution through each of the fin passages is a very important consideration for solar receivers. Passages with restricted flow could run very hot resulting in structural damage. Good flow distribution can be attained at the design point by proper manifold sizing. To ensure good distribution at off-design conditions, large manifolds are indicated. Preliminary investigation suggests that manifold diameters of about 3 in. for the



ORIGINAL PAGE IS
OF POOR QUALITY

TABLE 2-2
CONTINUOUS PLATE-FIN STUDY

Diameter, ft	Length, ft	Maximum Wall Temperature, °F	Pressure Drop, percent	Cavity Efficiency
1.5	1.5	2592	1.19	0.795
1.5	2.0	2457	1.57	0.823
1.5	2.5	2380	1.92	0.833
1.5	3.0	2340	2.25	0.837
1.75	1.5	2547	0.94	0.799
1.75	2.0	2416	1.21	0.827
1.75	2.5	2336	1.49	0.837
1.75	3.0	2293	1.74	0.841
2.0	1.5	2525	0.73	0.798
2.0	2.0	2383	0.96	0.826
2.0	2.5	2313	1.18	0.838
2.0	3.0	2263	1.39	0.841
2.5	1.5	2476	0.54	0.801
2.5	2.0	2349	0.71	0.827
2.5	2.5	2276	0.86	0.837
2.5	3.0	2234	1.02	0.840



inlet and 4 in. for the outlet would be satisfactory for good flow distribution for a wide range of flow rates and temperatures.

2. Plate-Fin Stacked Ring

Thermally, this configuration (Figure 2-5) is similar to the continuous plate-fin design; i.e., a series of parallel rectangular flow passages. One significant difference is that the rings can be staggered, either by placement or by random stacking, to produce an offset fin effect in the flow passages. The offsets continuously break up the fluid boundary layer, thus improving the heat transfer. The pressure drop is also increased.

A parametric study was conducted for this configuration using computer program RECMDL. Based on performance results and manufacturing considerations, a fin geometry of 5 fins per in., 0.25 in. high, and 1/32 in. thick was selected. The ring height (corresponding to the fin offset length) was selected as 0.75 in. Some of the solutions resulting in acceptable pressure drop are presented in Table 2-3 for this fin geometry (5R-0.25-0.75(0)-0.031).

TABLE 2-3
PLATE-FIN STACKED RING STUDY

Diameter, ft	Length, ft	Maximum Wall Temperature, °F	Pressure Drop, percent	Cavity Efficiency
1.5	1.5	2316	1.99	0.848
1.5	2.0	2240	2.69	0.859
1.75	1.5	2308	1.51	0.847
1.75	2.0	2235	2.03	0.860
1.75	2.5	2201	2.54	0.863

As seen in Table 2-3, a cavity size of 1.5-ft diameter and 1.5-ft length is a satisfactory solution. This is considerably smaller than the size required for the continuous plate-fin design (Table 2-2). This is due to the improved heat transfer of the offset fins, which results in a lower maximum wall temperature for a given size heat exchanger. The 1.5-ft length requires 24 stacked rings.

The manifolds for this concept are similar to those for the continuous plate fin. A 3-in. diameter inlet manifold with a 4-in. diameter outlet manifold should be satisfactory.



3. Concentric Cylinders with Vertical Ribs

Thermally, this configuration (Figure 2-6) is similar to the two previous plate-fin designs, i.e., a series of parallel rectangular flow passages. The fins, however, are considerably thicker for this design, assumed here to be 0.125 in., the same as the inner and outer wall thickness. This equivalence was selected to maintain similarity to circular flow passages, where the wall thickness would also be uniform.

A parametric study was conducted for this configuration using the AiResearch computer program RECMDL. Some of the performance results are shown in Table 2-4. A design meeting the pressure drop and temperature limitation requirements is available for a passage size of 0.2 in. The cavity size is 1.5-ft diameter and 2.5-ft long, the same as that for the continuous plate-fin design, but larger than the plate-fin stacked ring design. The required manifolds are the same size as those for the previous plate-fin designs.

TABLE 2-4
CONCENTRIC CYLINDERS WITH VERTICAL RIBS STUDY

Diameter, ft	Length, ft	Passage Size, in.	Maximum Wall Temperature, °F	Pressure Drop, percent	Cavity Efficiency
1.5	2.5	0.150	2237	9.45	0.854
1.5	2.5	0.175	2282	4.93	0.846
1.5	2.5	0.200	2339	2.85	0.837
1.5	2.5	0.225	2391	1.80	0.828
1.5	2.0	0.200	2411	2.33	0.829
1.5	2.0	0.195	2400	2.56	0.831
1.5	2.0	0.190	2389	2.82	0.834
1.5	2.0	0.185	2371	3.18	0.837

4. Dual-Tube Serpentine Flow

Due to the flow configuration of this concept (see Figure 2-7), a substantial circumferential temperature gradient would exist. As previously discussed, this condition requires an approximate analysis in conjunction with RECMDL.



As seen in Figure 2-7, the flow passages are tubular in nature. The thermal conductance was determined by modeling the tubes as modified fins. This reflects the fact that not all of the tube area is "prime" heat transfer surface, but is part prime and part extended (fin) surface.

The overall size of the cavity is 2.3-ft diameter and 3.4-ft long. This large size requirement is due mainly to the U-bends connecting the flow passages. These bends are very wasteful of pressure drop, using up about half of the allowable, while contributing little to the heat transfer. The required tube ID is 2.5 in., with 0.25-in. walls. Both inlet and outlet ducts are 3.5-in. diameter. The maximum wall temperature is less than 2400°F and the pressure drop is 3.5 percent. The large size suggests the elimination of this concept from further consideration.

5. Dual-Tube Helical Flow

This configuration (see Figure 2-8) results in a substantial circumferential temperature gradient. The approximate analysis based on the equivalent thermal conductance approach yields a cavity of 1.5-ft diameter and 2.7-ft length. The flow passage has a 2-in. diameter. The coil has a total of six turns. The maximum wall temperature is predicted to be 2360°F, the pressure drop is 3.5 percent, and the cavity efficiency is 0.835.

6. Single-Tube Helical Flow

This configuration (see Figure 2-9) also results in a large circumferential temperature gradient. The approximate analysis based on the equivalent thermal conductance approach yields a cavity of 1.5-ft diameter and 2.4-ft length. The flow passage has a 2.875-in. diameter. The coil has a total of nine turns. The maximum wall temperature is 2360°F, the pressure drop is 3.5 percent, and the cavity efficiency is 0.835.

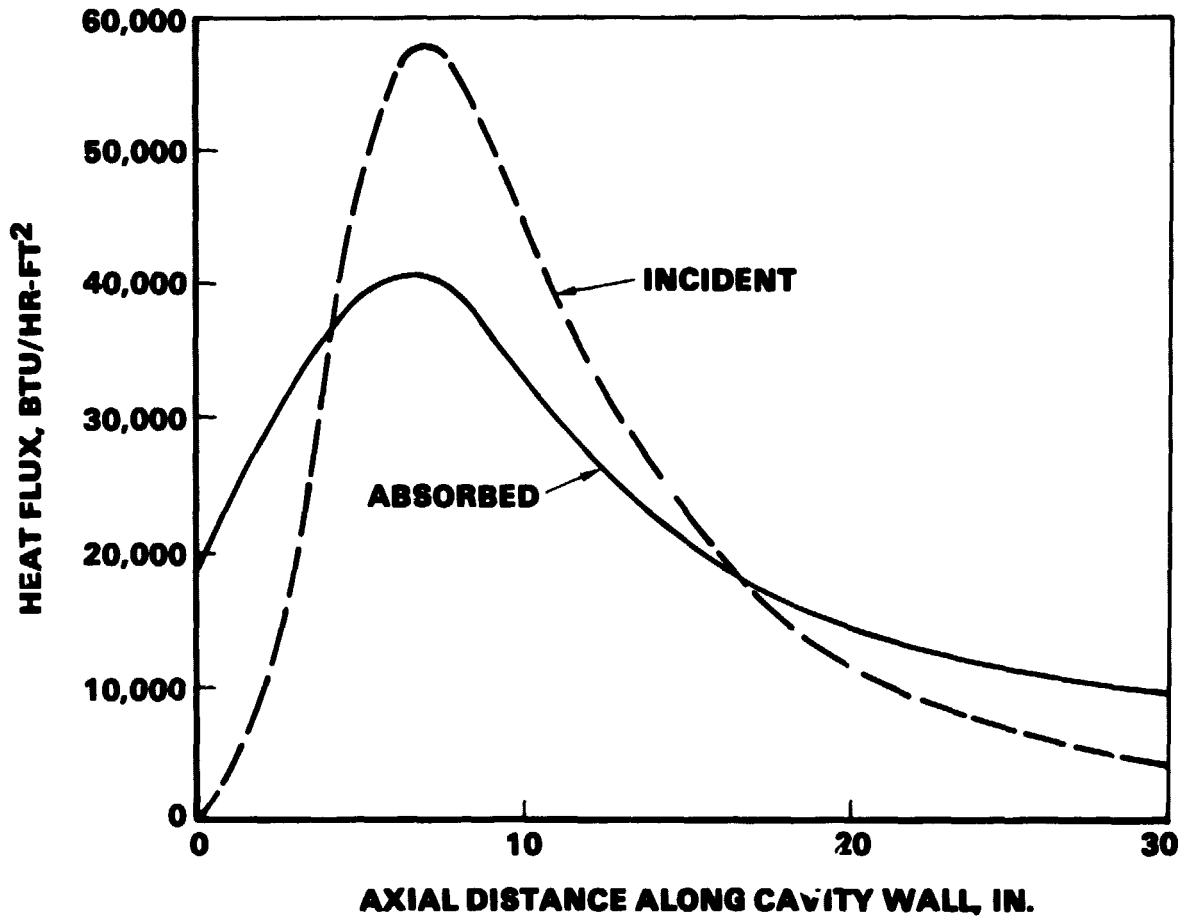
7. Plate-Fin Stacked Disk

The flow configuration for this concept, viz., parallel circumferential paths, is quite different from that of any of the other concepts (see Figure 2-10). The incident solar flux is not uniform in the axial direction of the receiver, thus, each disk layer will transfer a different amount of heat and will have a different outlet temperature. This complicates the manifold flow distribution problem and may require one of the manifolds to have a varying flow area in order to achieve uniform flow for each disk layer.

The thermal analysis of this design is too complex for the AiResearch computer program RECMDL. The following approximate approach was used. In Figure 2-16, typical flux distributions are presented for a symmetrical receiver of 2.5-ft length and 1.5-ft diameter. As can be seen, the peak absorbed flux is considerably greater than the average flux (about 21,400 Btu/hr-sq ft). Although the absorbed flux profile is not directly applicable to the nonsymmetrical stacked disk design, the incident flux profile is still valid for the same size cavity. It is assumed here that the peak absorbed flux will be 50 percent greater than the average flux. This means that one of the disks will absorb



ORIGINAL PAGE IS
OF POOR QUALITY



A-10047

Figure 2-16. Typical Heat Flux Profiles



50 percent more heat than the average disk. A simple calculation indicates that the fluid exit temperature from this disk (assuming uniform flow) would be 2421°F.

The maximum wall temperature, of course, will have to be even higher than 2421°F. To determine the wall temperature, the following design, yielding a 3-percent pressure drop for the secondary offset fins, was assumed. For a 1.5-ft diameter and 2.5-ft long cavity, the fins are 6.5 per in., 0.5 in. high, 0.032 in. thick, with a 0.5 in. offset (6.5R-0.5-0.5(0)-0.032). With a 0.25-in. plate, 40 disks are required. Based on this design, the thermal conductance of the heat exchanger was calculated and the temperature potential required to transfer the heat determined. Assuming a constant wall temperature around the disk, this temperature would be 2480°F.

All of the above assumptions tend to underestimate the maximum wall temperature. Even so, the calculated value considerably exceeds the established limit of 2400°F. Considering this, along with the potential flow maldistribution difficulties, it was decided to eliminate this concept from further consideration.

8. Ceramic-Lined Metal Shell

This design, with its inherent circumferential symmetry (see Figure 2-11), is amenable to analysis with computer program RECMDL. Note that the outer wall of the flow passages is not thermally connected to the inner wall. The fins are assumed to be 5 per in., with an average thickness of 0.075 in. (the actual fins probably will be tapered). The wall thickness is 0.25 in.

The details of the top hemispherical section are not included in the preliminary study. The section was treated as an insulated region, with no fins or heat transfer to the fluid. Considering the cylindrical section only, a parametric study was conducted using RECMDL. Some of the performance results are shown in Table 2-5. The active length is that of the fins in the cylindrical section, and does not include either the hemispherical section or the inlet manifold at the aperture end of the receiver. A design meeting the pressure drop and temperature limitation is available for a fin height of 0.2 in. The cavity size is 1.5-ft diameter and 2.5-ft active length.

The inlet manifold has been sized for good flow distribution using AiResearch computer program H1330. A manifold area of 9 sq in. is sufficient to limit the flow maldistribution to about 4 percent.

Structural Analysis

Based on temperature maps resulting from the thermal analyses of the various concepts, stress analyses were performed. Each concept was modeled using the ANSYS computer code. Based on the limited scope of the Task 1 effort, only the temperature gradients in the receiver radial direction were considered; axial variations and, where applicable, circumferential variations, were not analyzed. Pressure loadings were not included. The dual-tube serpentine flow and the plate-fin stacked disk configurations were not analyzed, because these concepts were eliminated for thermal and size reasons.



TABLE 2-5

CERAMIC-LINED METAL SHELL STUDY

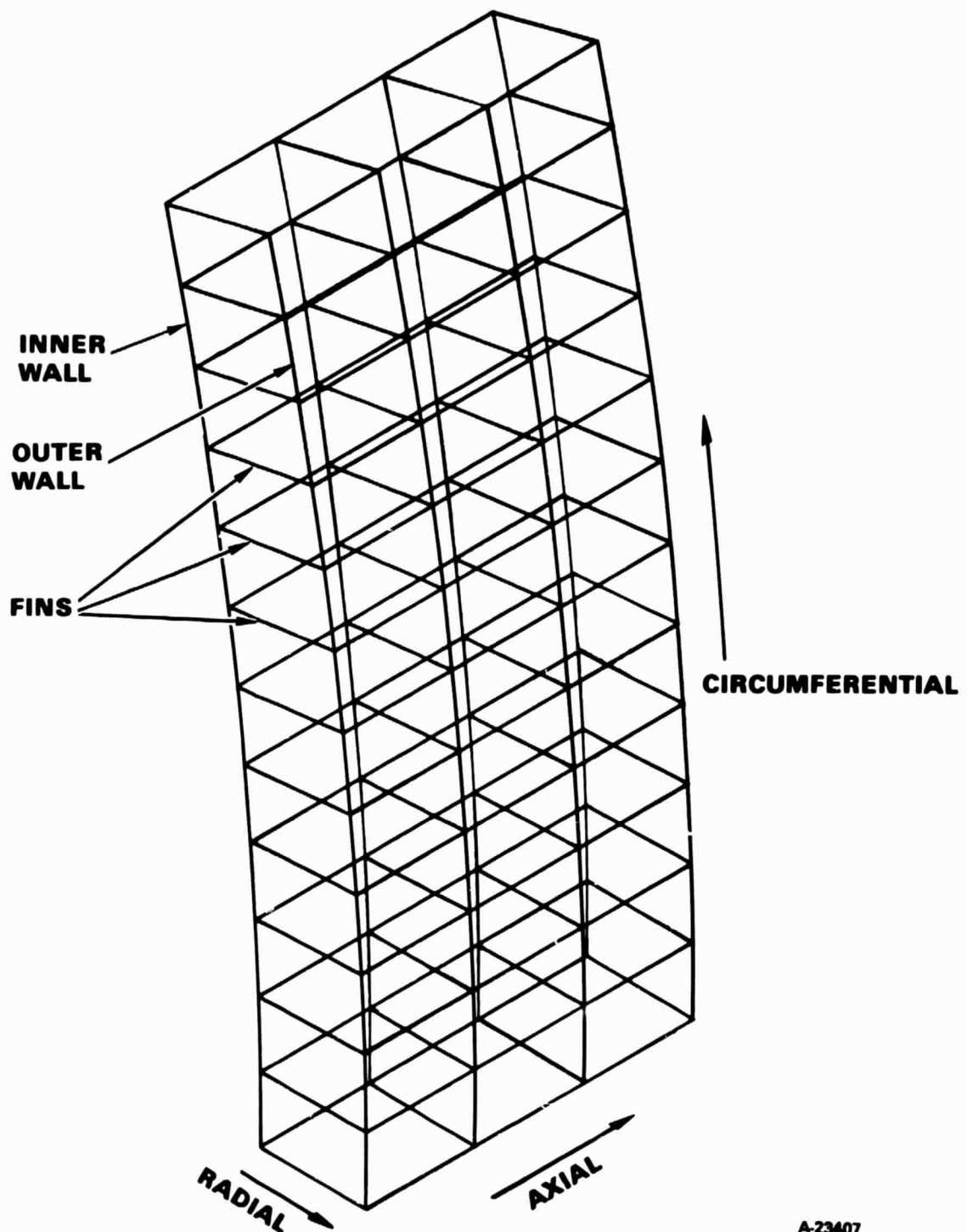
Diameter, ft	Active Length, ft	Fin Height, in.	Maximum Wall Temperature, °F	Pressure Drop, percent	Cavity Efficiency
1.5	2.5	0.24	2392	1.99	0.835
1.5	2.5	0.22	2380	2.46	0.837
1.5	2.5	0.20	2369	3.12	0.838
1.5	2.5	0.19	2363	3.56	0.839
1.5	2.5	0.18	2357	4.09	0.840

The models were essentially of two classes: one represented the multi-passage plate-fin designs and the other represented the single- or dual-passage tubular designs. Due to the smaller dimensions and the flat inner and outer walls, the models required for the plate-fin designs were much simpler than for the tubular designs. The plate-fin concepts were modeled as bodies of revolution consisting of an inner wall, fins, and an outer wall as shown in Figure 2-17. The directional arrows are referenced to the receiver. For the ceramic-lined metal shell, the outer wall is not connected to the fins and is considered a nonstructural member. As a result of this feature, the ceramic-lined metal shell has greatly reduced stress levels caused by radial temperature gradients as compared to the other plate-fin designs with a connected outer wall.

The maximum stresses for the plate-fin designs are listed in Table 2-6. The stress directions are referenced to the receiver. These stresses were calculated for the (axial) location on the receiver wall of maximum temperature. This location was very close to the maximum absorbed heat flux location. Note that positive stress values represent tension while negative values represent compression. Due to the simplified nature of the model, no stresses were generated in the thickness direction of the walls or fins.

For the tubular designs, the models were more complex. The tubes were divided into finite elements along the wall as shown in Figure 2-18. The model is three-dimensional so that stresses were generated in all three directions. The model is similar for the single- or dual-tube helical designs. The temperatures for each element in Figure 2-18 were determined at the location of the maximum surface temperature (modeled in Figure 2-15). This is close to the location of the maximum absorbed heat flux.





A-23407

Figure 2-17. Plate-Fin Stress Model



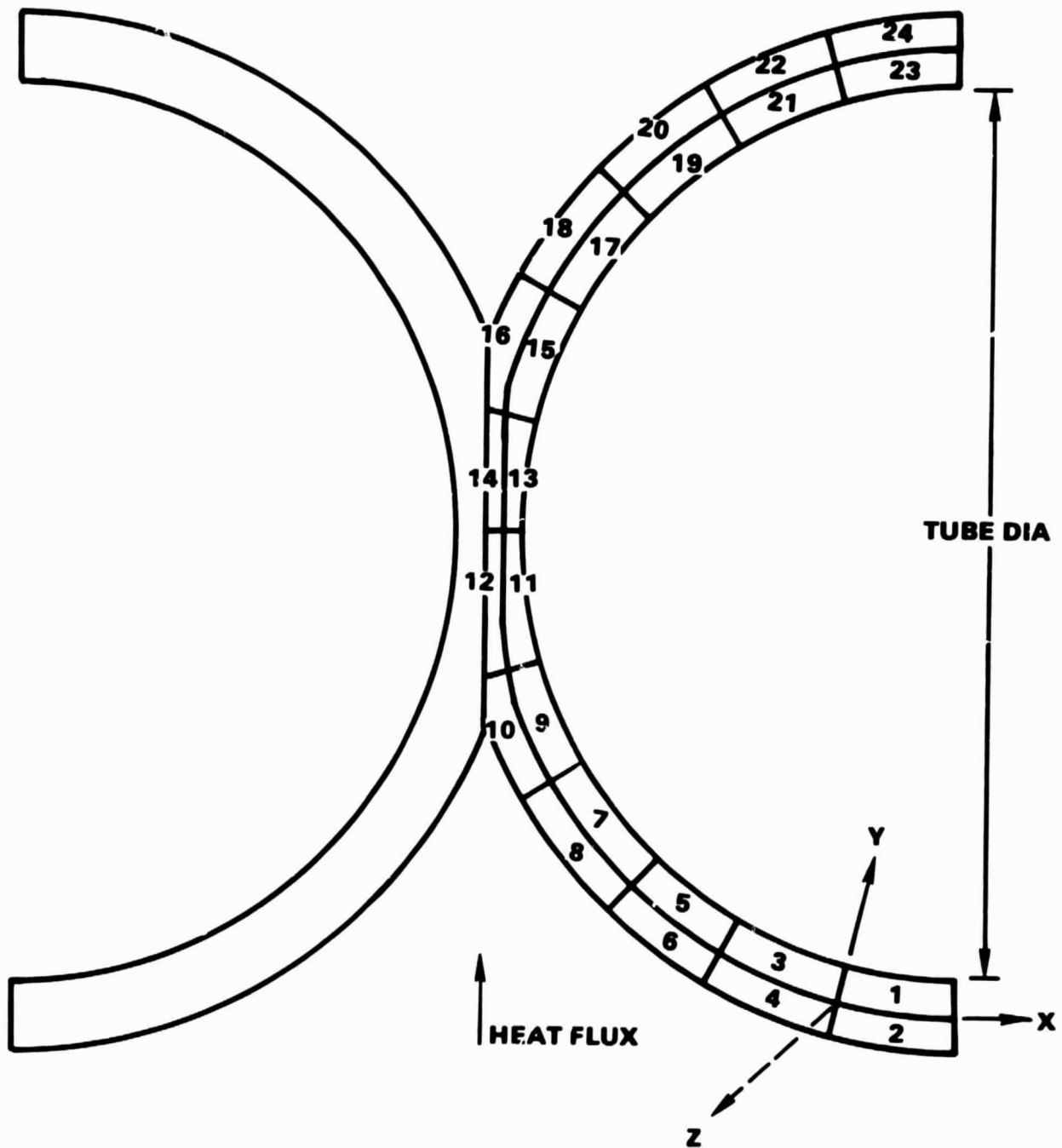
TABLE 2-6

MAXIMUM STRESSES FOR PLATE-FIN DESIGNS, PSI

Plate-Fin Design	Inner Wall			Fins			Outer Wall		
	Axial	Radial	Circumferential	Axial	Radial	Circumferential	Axial	Radial	Circumferential
Continuous Plate-Fin	-13,900	--	-20,400	-360	-6,800	--	+13,900	--	+15,100
Plate-Fin Stacked Ring	-10,500	--	-15,100	+2,100	-2,600	--	+8,500	--	+14,700
Concentric Cylinders with Vertical Ribs	-2,800	--	-5,800	+320	-210	--	+2,300	--	+4,000
Ceramic-Lined Metal Shell	+1,500	--	+230	+1,700	+400	--	--	--	--

ORIGINAL PAGE IS
OF POOR QUALITY

ORIGINAL PAGE 19
OF POOR QUALITY



A-23409

Figure 2-18. Tubular Finite Element Model



The stresses calculated from these temperature profiles are listed in Table 2-7 for the single-tube design and Table 2-8 for the dual-tube design. The stress directions are shown in Figure 2-18; X is the tube circumferential direction, Y is the tube radial direction, and Z is the coil circumferential direction.

A typical deflection map is shown in Figure 2-19. Note that the dashed lines represent the original (ambient temperature) position while the solid lines represent the displaced position. A typical equivalent stress map is shown in Figure 2-20.

Drawings

Sketches for each of the conceptual designs (except for the plate-fin stacked disk) were prepared. These are presented in the following drawings:

<u>Drawing No.</u>	<u>Title</u>
SK52848	Continuous Plate-Fin
SK52849	Plate-Fin Stacked Ring
SK52850	Dual-Tube Helical Flow
SK52851	Single-Tube Helical Flow
SK52852	Dual-Tube Serpentine Flow
SK52853	Ceramic-Lined Metal Shell
SK52854	Concentric Cylinders with Vertical Ribs

Fabrication Analysis

Parallel with the structural analysis of the candidate conceptual designs, the fabrication feasibility of each design was evaluated. Each of the designs was considered with regard to several key processing parameters. Within the guidelines of the contract, only processing techniques that could be scaled up for eventual low-cost, high-volume production were considered. Only NC-430 (siliconized-silicon carbide) was considered as a candidate material for the fabrication analysis. As a further restriction, only state-of-the-art fabrication processes were considered, i.e., no new fabrication techniques were to be developed during the fabrication demonstration. Within these restrictions, the fabrication evaluation of the candidate designs was undertaken with emphasis on the limitations of size, shape, and design detail.



TABLE 2-7

MAXIMUM STRESSES FOR SINGLE-TUBE HELICAL FLOW DESIGN

Element Number	Stresses, psi		
	X-Direction	Y-Direction	Z-Direction
1	-500	+300	-13,300
2	-70	-300	-18,000
3	-1300	-1700	-20,400
4	-2000	+2500	-25,200
5	-7500	-3400	-26,500
6	+2200	+5700	-28,700
7	-9200	-7000	-29,400
8	-500	+6100	-30,800
9	-9100	-6400	-21,100
10	+1900	-1500	-18,600
11	-7700	+700	-1,900
12	-7400	-800	-2,100
13	-5200	+800	+10,300
14	-8500	-1300	+9,400
15	-6300	-4500	+16,800
16	-30	-4100	+17,900
17	-8700	-6400	+20,600
18	+1100	+7700	+25,800
19	-6700	-4400	+22,700
20	+1100	+5600	+26,000
21	-1300	-2300	+22,700
22	-800	+3000	+23,900
23	-80	-300	+20,300
24	+90	+500	+20,400



ORIGINAL PAGE IS
OF POOR QUALITY

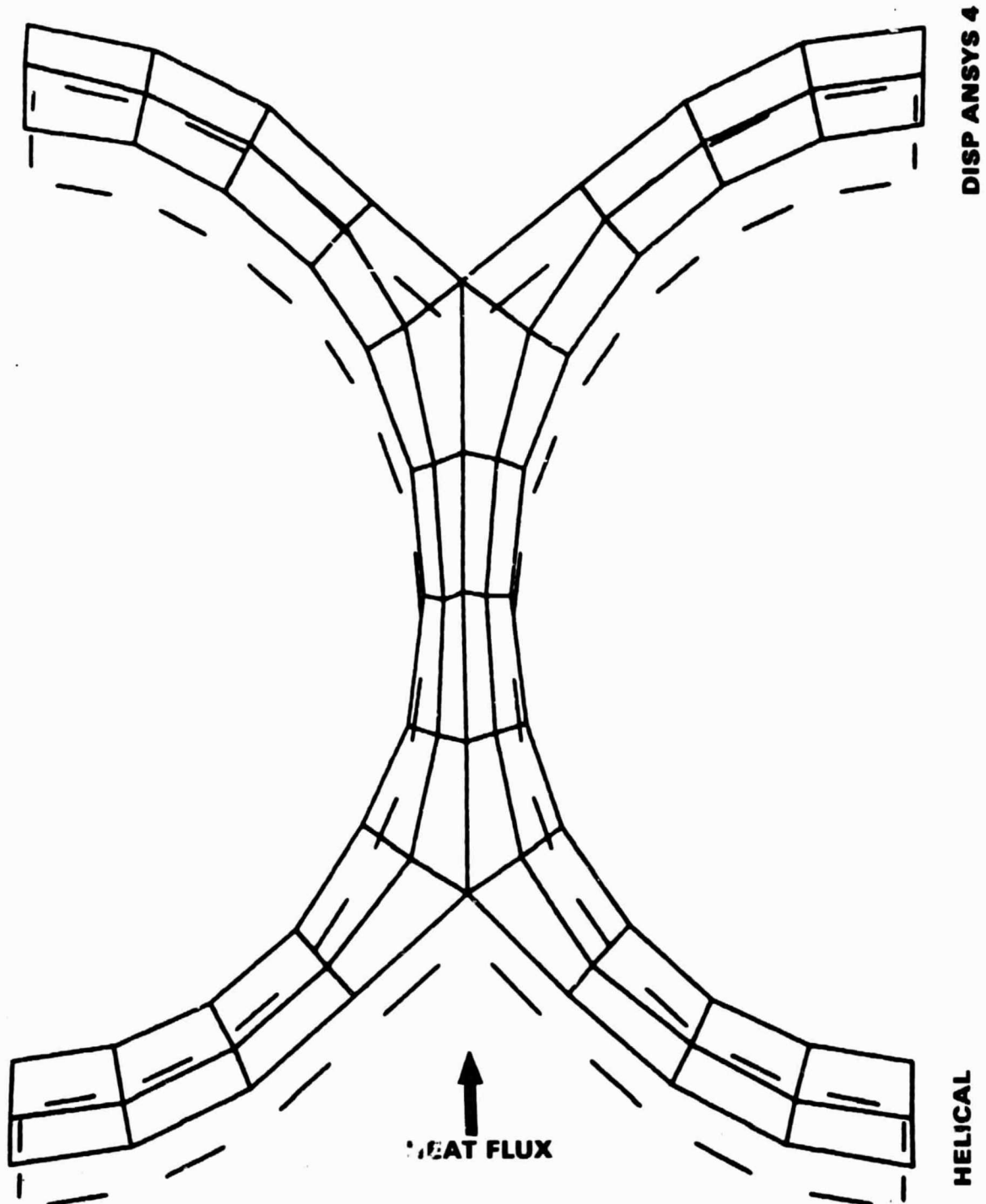
TABLE 2-8

MAXIMUM STRESSES FOR DUAL-TUBE HELICAL FLOW DESIGNS

Element Number	Stresses, psi		
	X-Direction	Y-Direction	Z-Direction
1	-200	+300	-14,900
2	-200	-200	-19,000
3	-1500	-800	-19,200
4	-1100	+1100	-23,200
5	-3800	-2500	-22,800
6	+900	+4100	-25,500
7	-9500	-6400	-26,100
8	+1700	-1800	-27,600
9	-8000	-3200	-18,600
10	+5000	+2600	-15,700
11	-4800	+400	-2,400
12	-5700	-2300	-3,100
13	-3900	-1400	+8,200
14	-5700	-2200	+7,700
15	-5400	-3200	+15,200
16	+5300	+100	+17,600
17	-9700	-5100	+18,900
18	+3200	+2400	+22,600
19	-4000	-2800	+22,200
20	+500	+4100	+24,500
21	-1200	-1300	+22,900
22	-400	+1800	+23,600
23	+100	-200	+22,000
24	+10	+300	+21,900



ORIGINAL PAGE IS
OF POOR QUALITY

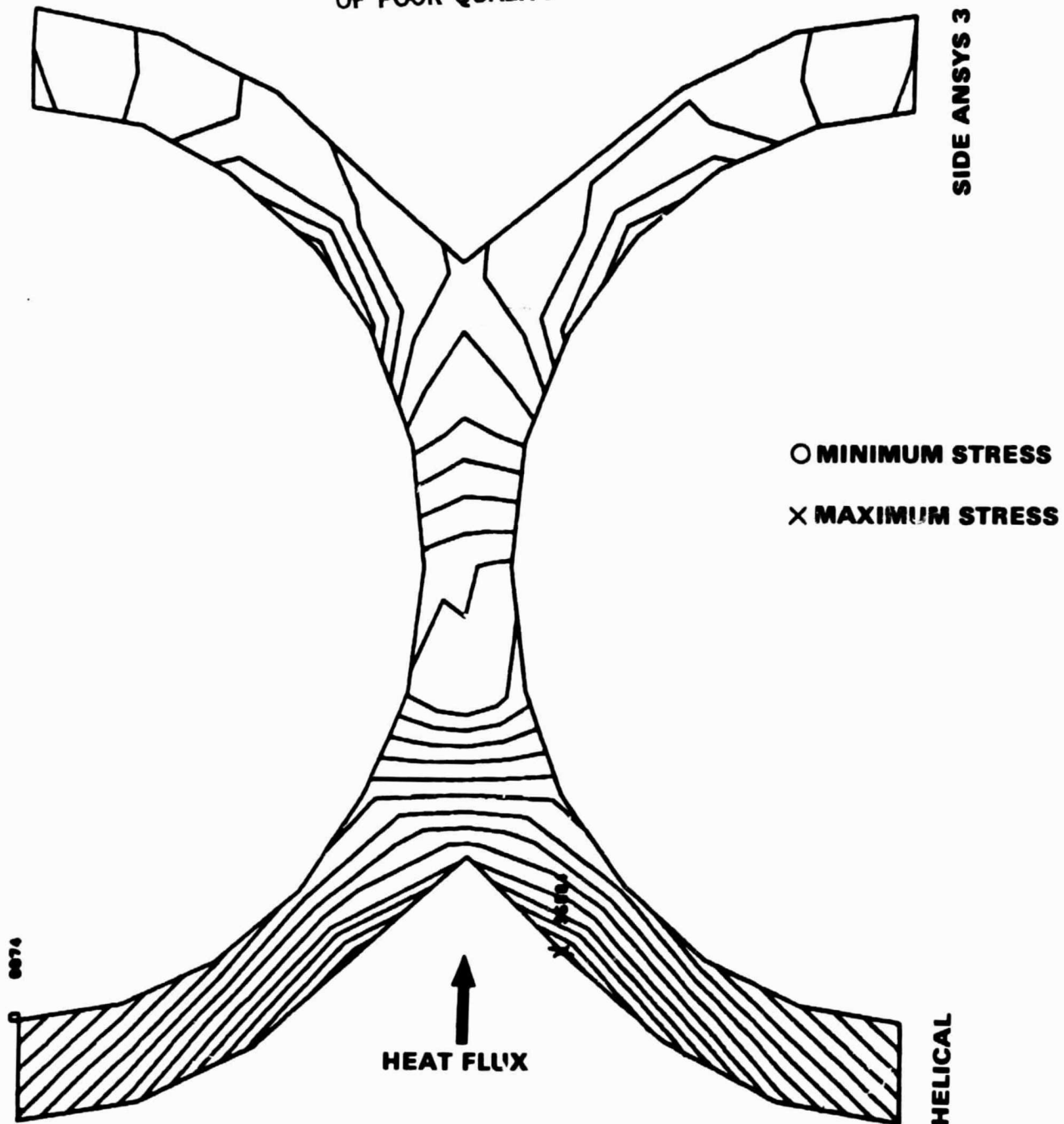


A23413

Figure 2-19. Deflection Map for Tubular Designs



ORIGINAL PAGE IS
OF POOR QUALITY

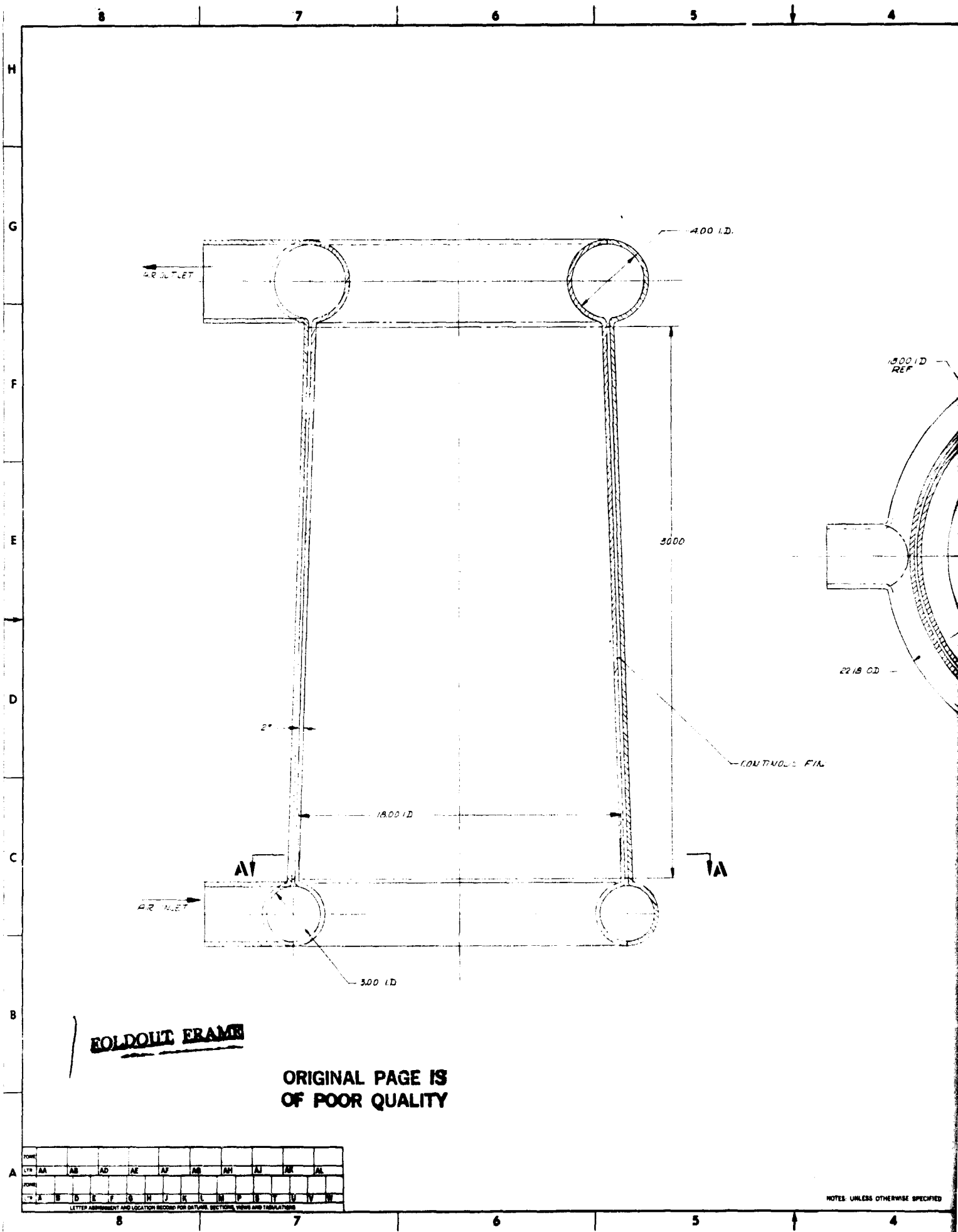


A-23412

Figure 2-20. Equivalent Stress Map for Tubular Designs



SECTION



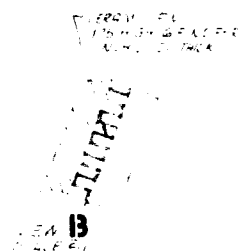
FOLDOUT FRAME

ORIGINAL PAGE IS
OF POOR QUALITY

FORM																							
174	AA	AB	AD	AE	AF	AG	AH	AI	AK	AL													
FORM																							
	A	B	C	D	E	F	G	H	I	J	K	L	M	N	O	P	Q	R	S	T	U	V	W
LETTER ASSIGNMENT AND LOCATION RECORD FOR DATA, SECTION, VIEW AND TABULATIONS																							

NOTES: UNLESS OTHERWISE SPECIFIED

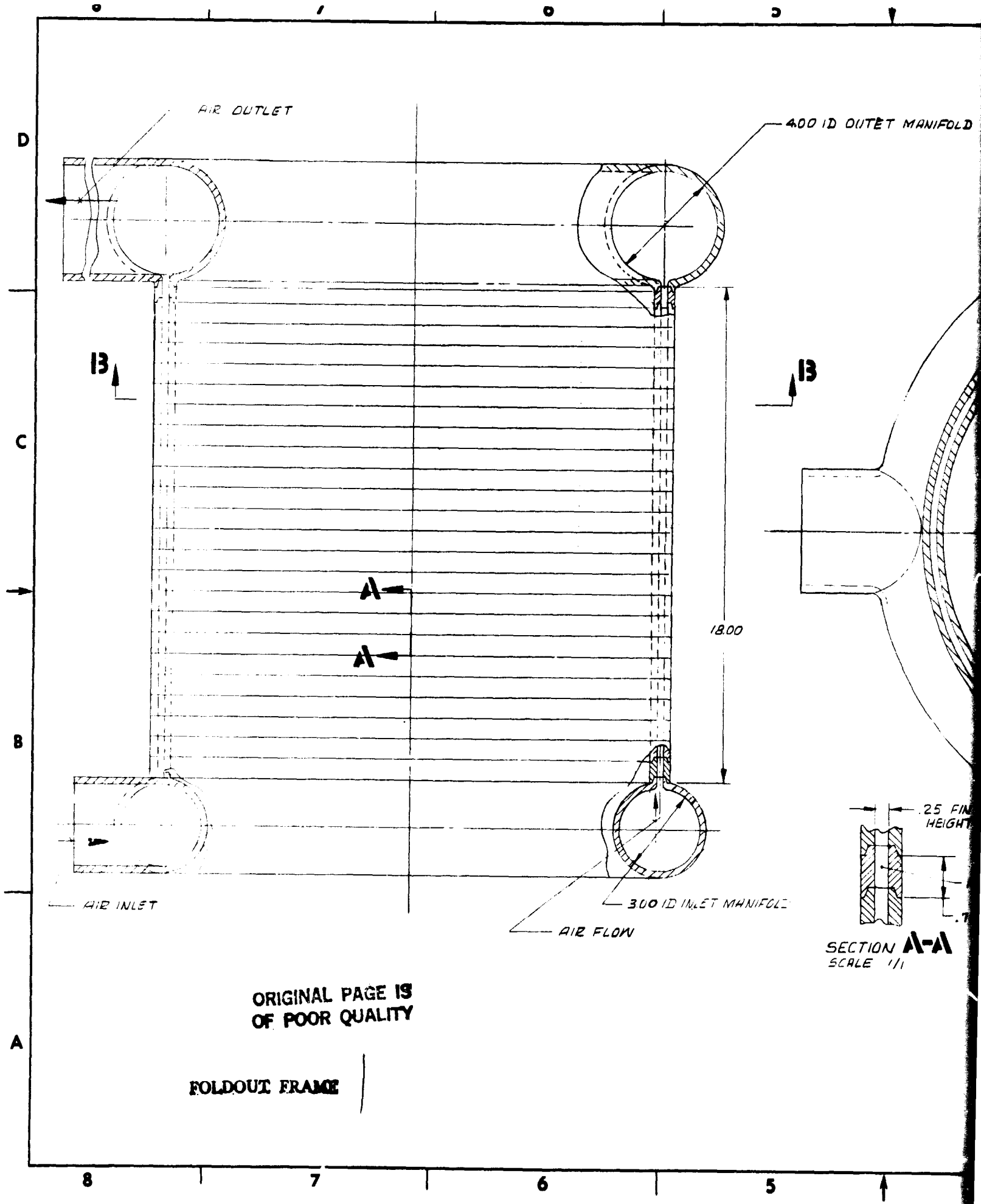
REVISIONS				
DATE	BY	DESCRIPTION	DATE	APPROVED



2 **OLDOUT FRAME**

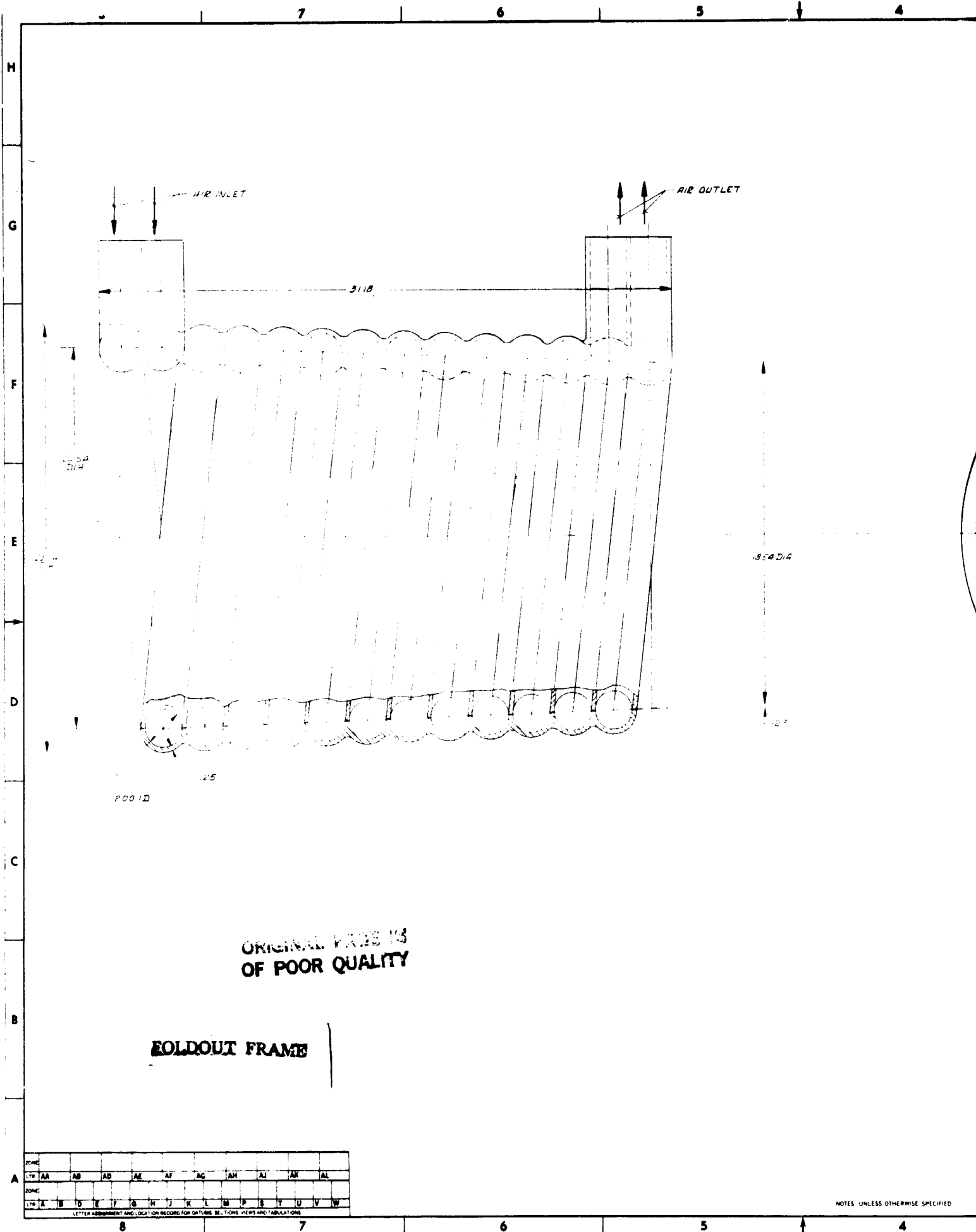
1000 1001 1002 1003 1004 1005 1006 1007 1008 1009 1010 1011 1012 1013 1014 1015 1016 1017 1018 1019 1020 1021 1022 1023 1024 1025 1026 1027 1028 1029 1030 1031 1032 1033 1034 1035 1036 1037 1038 1039 1040 1041 1042 1043 1044 1045 1046 1047 1048 1049 1050 1051 1052 1053 1054 1055 1056 1057 1058 1059 1060 1061 1062 1063 1064 1065 1066 1067 1068 1069 1070 1071 1072 1073 1074 1075 1076 1077 1078 1079 1080 1081 1082 1083 1084 1085 1086 1087 1088 1089 1090 1091 1092 1093 1094 1095 1096 1097 1098 1099 1100 1101 1102 1103 1104 1105 1106 1107 1108 1109 1110 1111 1112 1113 1114 1115 1116 1117 1118 1119 1120 1121 1122 1123 1124 1125 1126 1127 1128 1129 1130 1131 1132 1133 1134 1135 1136 1137 1138 1139 1140 1141 1142 1143 1144 1145 1146 1147 1148 1149 1150 1151 1152 1153 1154 1155 1156 1157 1158 1159 1160 1161 1162 1163 1164 1165 1166 1167 1168 1169 1170 1171 1172 1173 1174 1175 1176 1177 1178 1179 1180 1181 1182 1183 1184 1185 1186 1187 1188 1189 1190 1191 1192 1193 1194 1195 1196 1197 1198 1199 1200 1201 1202 1203 1204 1205 1206 1207 1208 1209 1210 1211 1212 1213 1214 1215 1216 1217 1218 1219 1220 1221 1222 1223 1224 1225 1226 1227 1228 1229 1230 1231 1232 1233 1234 1235 1236 1237 1238 1239 1240 1241 1242 1243 1244 1245 1246 1247 1248 1249 1250 1251 1252 1253 1254 1255 1256 1257 1258 1259 1260 1261 1262 1263 1264 1265 1266 1267 1268 1269 1270 1271 1272 1273 1274 1275 1276 1277 1278 1279 1280 1281 1282 1283 1284 1285 1286 1287 1288 1289 1290 1291 1292 1293 1294 1295 1296 1297 1298 1299 1300 1301 1302 1303 1304 1305 1306 1307 1308 1309 1310 1311 1312 1313 1314 1315 1316 1317 1318 1319 1320 1321 1322 1323 1324 1325 1326 1327 1328 1329 1330 1331 1332 1333 1334 1335 1336 1337 1338 1339 1340 1341 1342 1343 1344 1345 1346 1347 1348 1349 1350 1351 1352 1353 1354 1355 1356 1357 1358 1359 1360 1361 1362 1363 1364 1365 1366 1367 1368 1369 1370 1371 1372 1373 1374 1375 1376 1377 1378 1379 1380 1381 1382 1383 1384 1385 1386 1387 1388 1389 1390 1391 1392 1393 1394 1395 1396 1397 1398 1399 1400 1401 1402 1403 1404 1405 1406 1407 1408 1409 1410 1411 1412 1413 1414 1415 1416 1417 1418 1419 1420 1421 1422 1423 1424 1425 1426 1427 1428 1429 1430 1431 1432 1433 1434 1435 1436 1437 1438 1439 1440 1441 1442 1443 1444 1445 1446 1447 1448 1449 1450 1451 1452 14
--

NOTES UNLESS OTHERWISE SPECIFIED

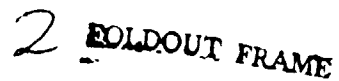


1

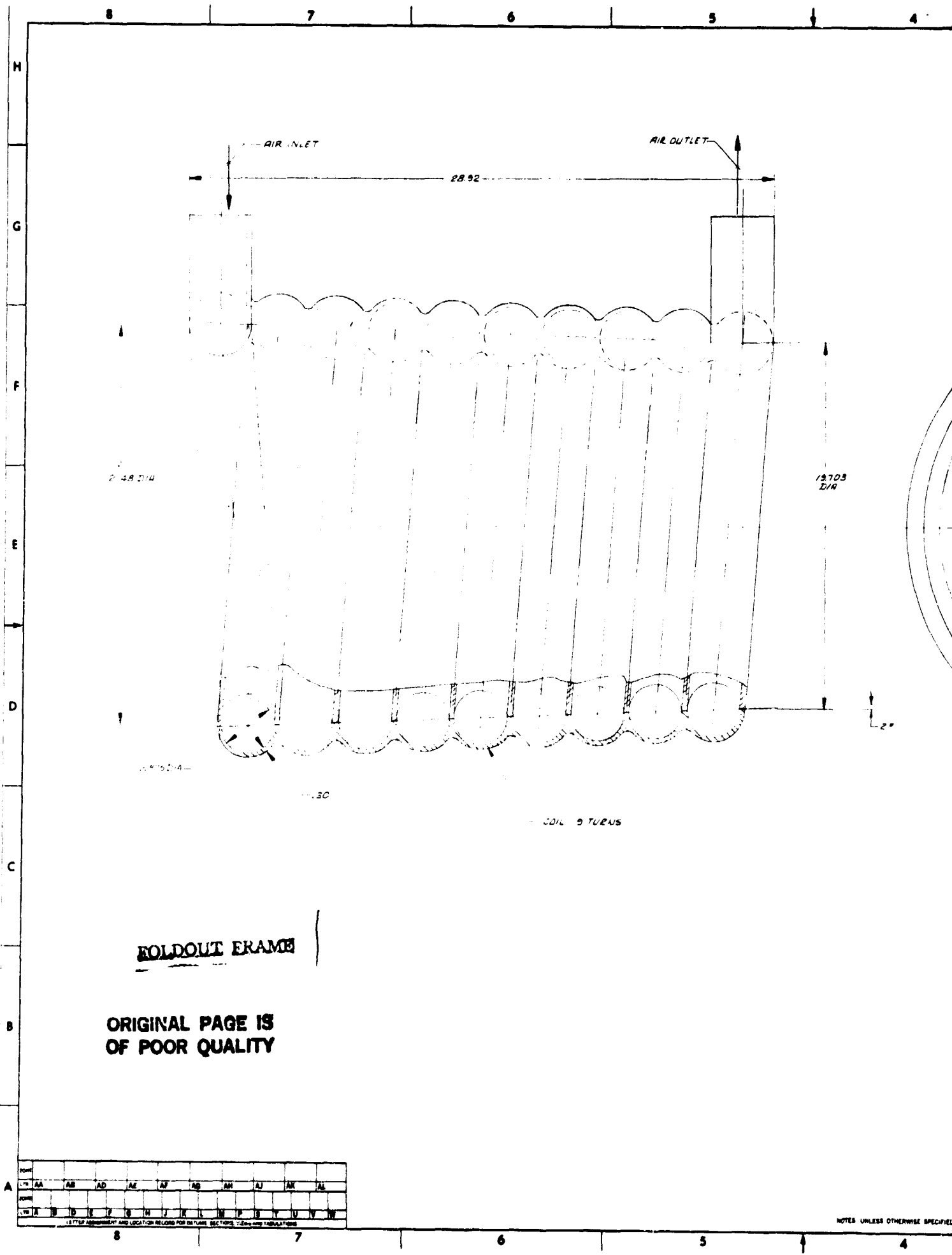
25 20420



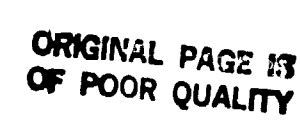
REVISIONS				
NO.	DATE	DESCRIPTION	BY	APPROVED

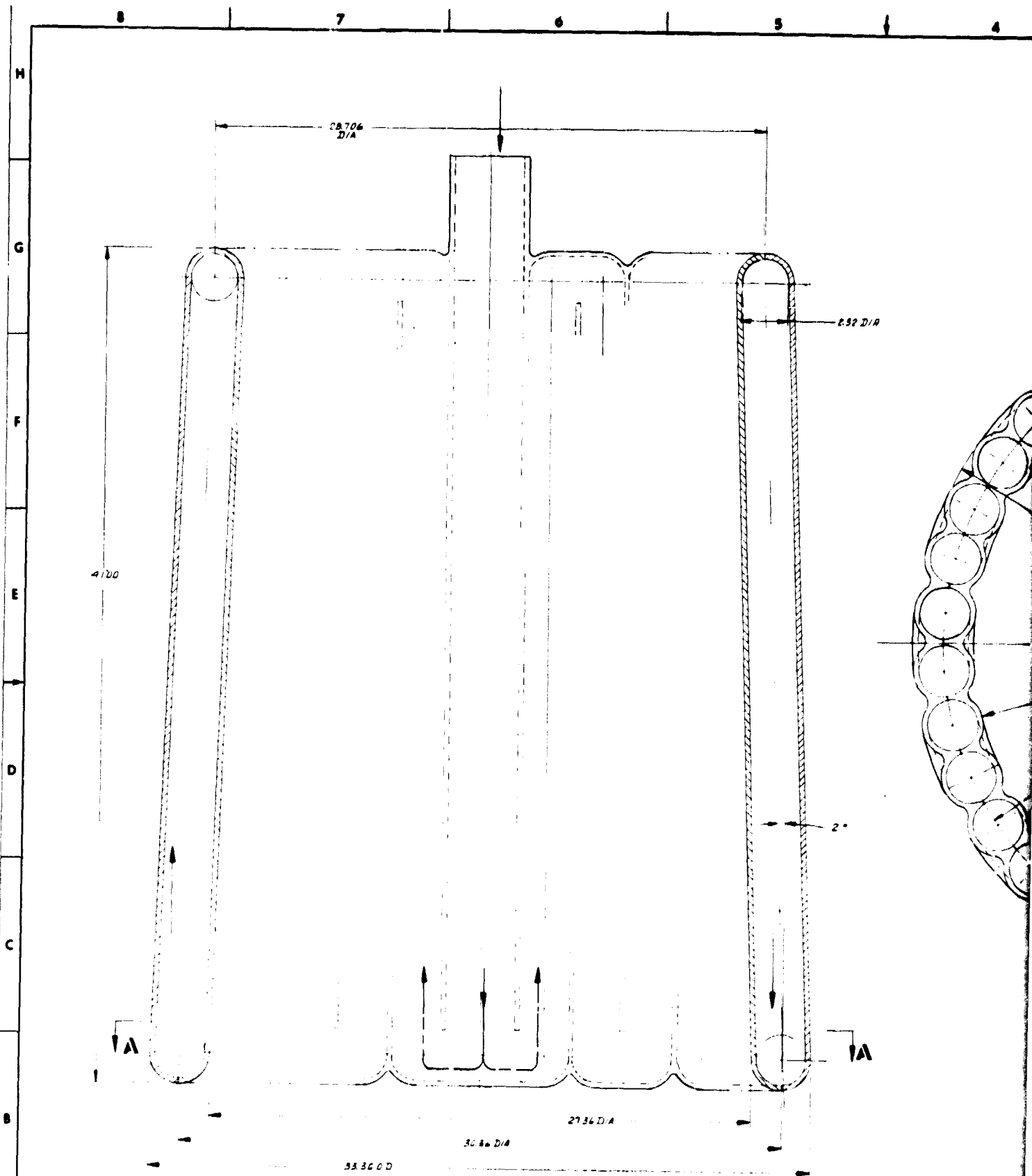
[illegible]

154 2012



REVISIONS				
DATE	BY	DESCRIPTION	DATE	APPROVED

[illegible]



FOLDOUT FRAME

**ORIGINAL PAGE IS
OF POOR QUALITY**

1	2	3	4	5	6	7	8	9	10	11	12	13	14	15	16	17	18	19	20	21	22	23	24	25	26	27	28	29	30	31	32	33	34	35	36	37	38	39	40	41	42	43	44	45	46	47	48	49	50	51	52	53	54	55	56	57	58	59	60	61	62	63	64	65	66	67	68	69	70	71	72	73	74	75	76	77	78	79	80	81	82	83	84	85	86	87	88	89	90	91	92	93	94	95	96	97	98	99	100
---	---	---	---	---	---	---	---	---	----	----	----	----	----	----	----	----	----	----	----	----	----	----	----	----	----	----	----	----	----	----	----	----	----	----	----	----	----	----	----	----	----	----	----	----	----	----	----	----	----	----	----	----	----	----	----	----	----	----	----	----	----	----	----	----	----	----	----	----	----	----	----	----	----	----	----	----	----	----	----	----	----	----	----	----	----	----	----	----	----	----	----	----	----	----	----	----	----	----	-----

NOTES: UNLESS OTHERWISE SPECIFIED

REV	DATE	BY	CHKD	APPD

REVISIONS

H

G

F

E

D

C

B

A

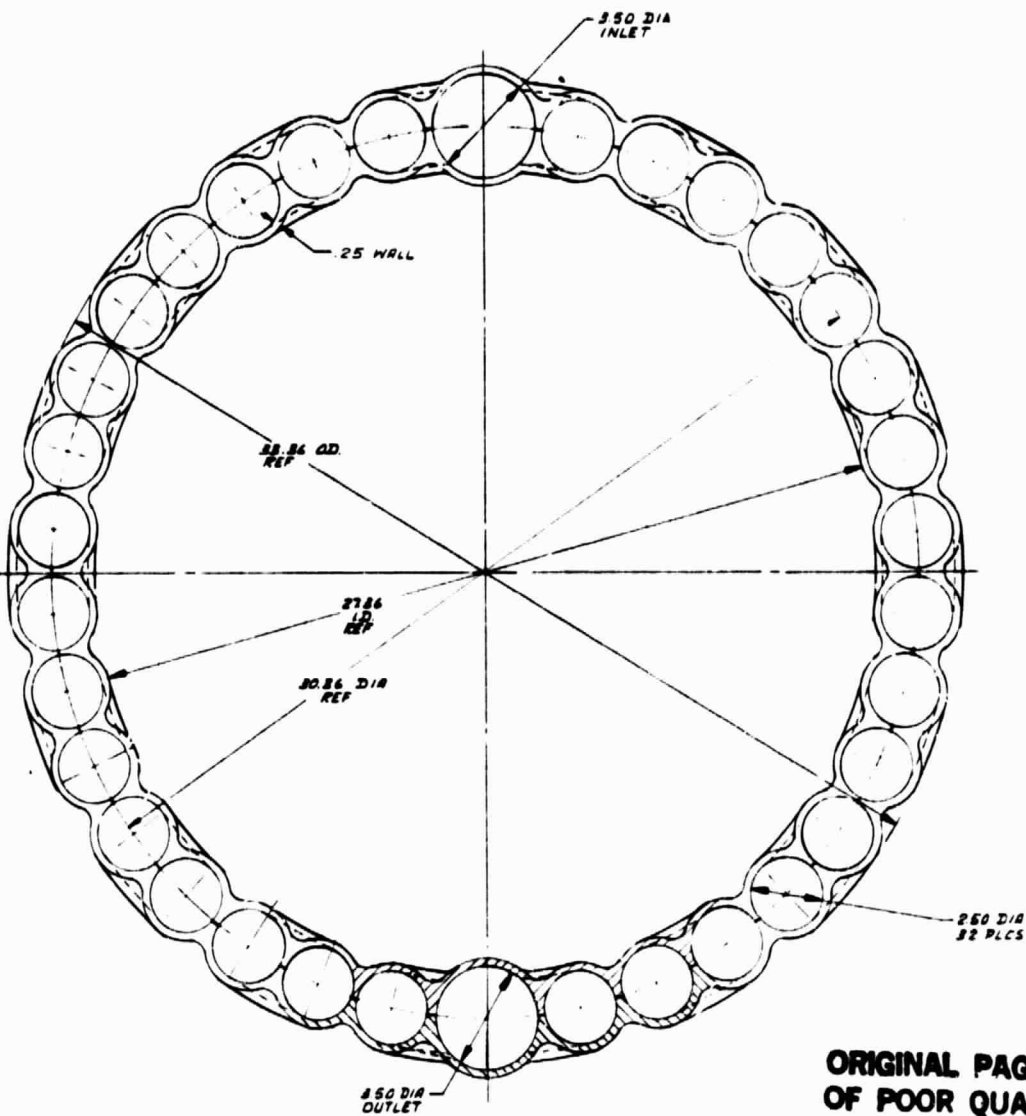
SK 52852

1

2

3

4



ORIGINAL PAGE IS
OF POOR QUALITY

SECTION A-A

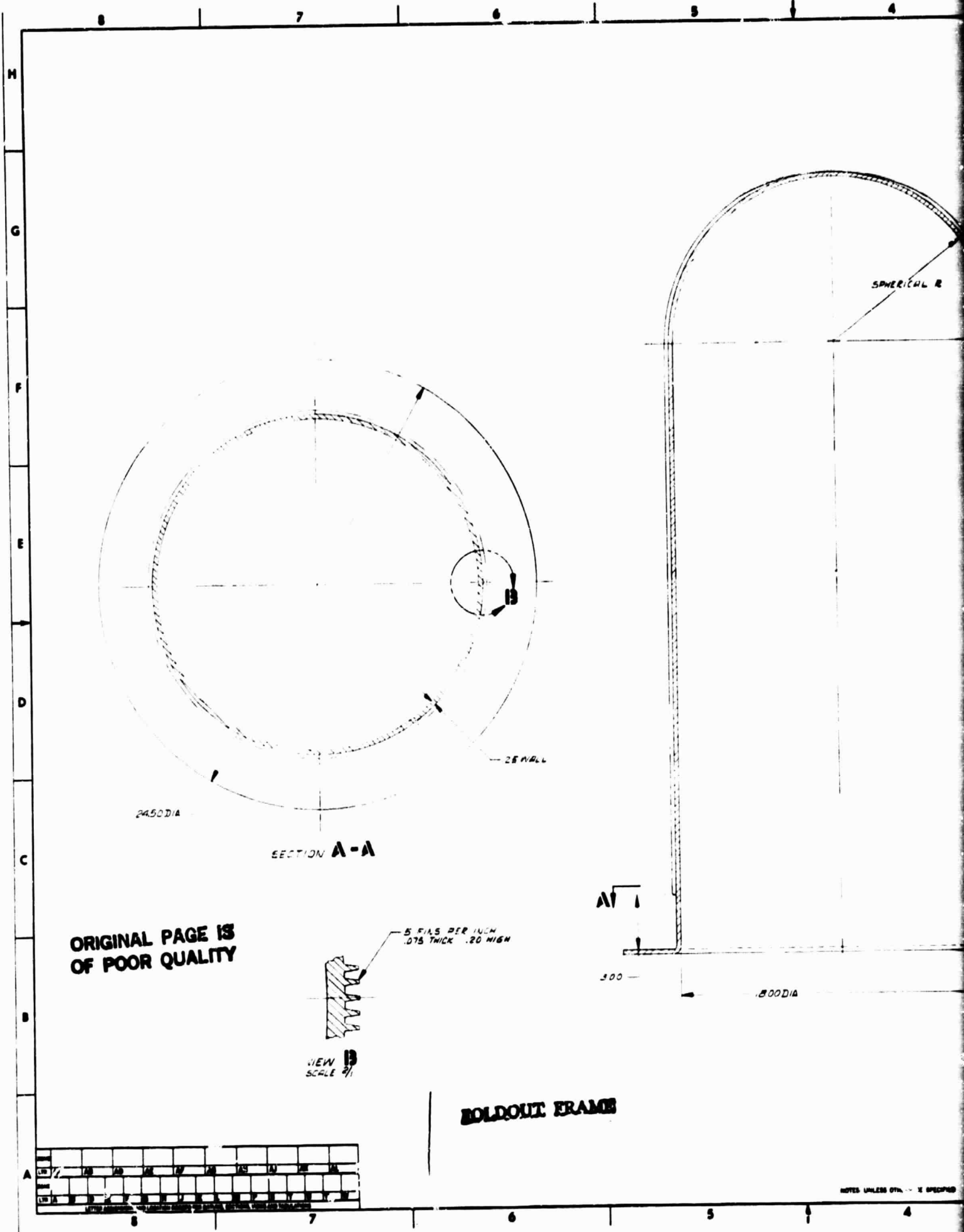
2 FOLDOUT FRAME

PART NO		SK 52852	
DESCRIPTION		SKETCH-CERAMIC HEAT EXCHANGER, DLNL TUBE, SERPENTINE FLOW	
E 70210		SK 52852	
DATE		1964	
BY		JVS	
CHKD		JVS	
APPD		JVS	
APPLICATION		1	

NOTES: UNLESS OTHERWISE SPECIFIED

SK 52852

SEE
PAGE 13



ORIGINAL PAGE IS
OF POOR QUALITY

SECTION A-A

VIEW B
SCALE 2/1


BOLDOUT FRAME

NOTES UNLESS OTHERWISE SPECIFIED

REVISIONS				
NO.	DATE	BY	REASON	APPROVED



FOLDOUT FRAME

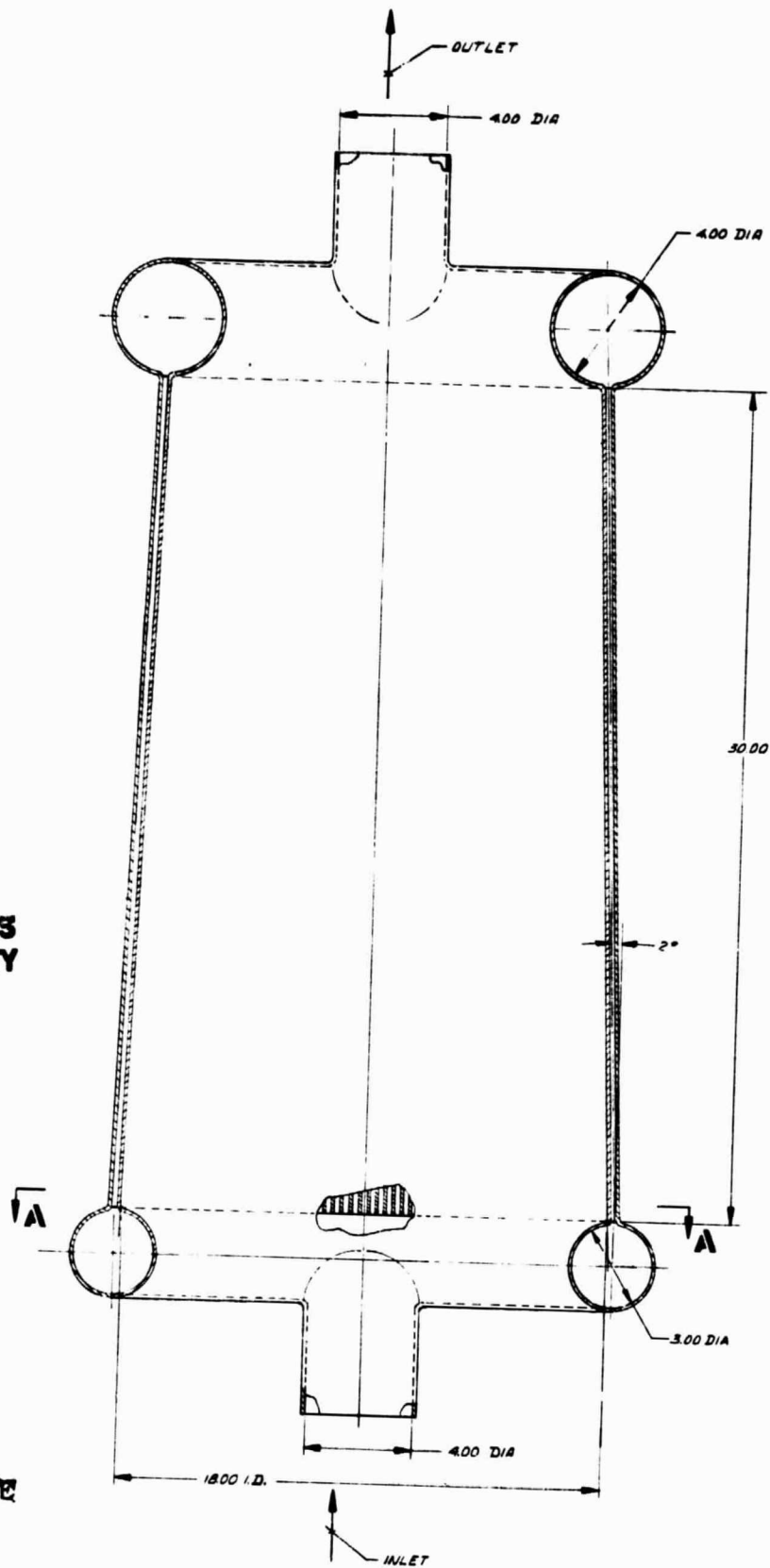
PART		CONTACT NO.		 ARCHEAN MANUFACTURING COMPANY A DIVISION OF THE ARCHEAN CORPORATION WILMINGTON, DELAWARE
ORDER OTHER USE SPECIFIC ORDER CONTROL, FOR ORDER ITS INFORMATION FOR FOR QUOTATION, AT THE END OF THE ORDER		ORDERED BY: <u>W. J. 4-10</u>		
ITEM NO.	QUANTITY	DATE	PRICE	SKETCH-CERAMIC TEST EXCHANGER, METAL SHELL
SHIP TO ADDRESS		QUANTITY	PRICE	E 70210 SK 52853
SHIP TO ADDRESS		QUANTITY	PRICE	SCALE 1/2 SHEET 1 OF 1

NOTES: UNLESS OTHERWISE SPECIFIED

25552

ORIGINAL PAGE IS
OF POOR QUALITY

FOLDOUT FRAME



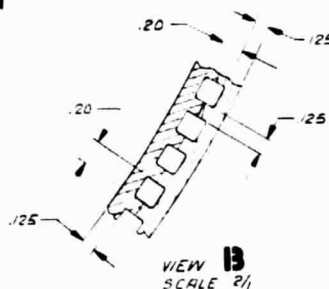
UN	AA	AB	AC	AD	AE	AF	AG	AH	AI	AJ	AK	AL
UN	AM	AN	AO	AP	AQ	AR	AS	AT	AU	AV	AW	AX

LETTER ASSIGNMENT AND NUMBERING SCHEME FOR OTHERS, BEARING, VIEW AND TOLERANCES


NOTES: UNLESS OTHERWISE SPECIFIED

[illegible]

ORIGINAL PAGE IS
OF POOR QUALITY



2 FOLDOUT FRAME

PART NO		SECTION 12		 AEROQUIP MANUFACTURING COMPANY A DIVISION OF THE SHEET METAL WORKS COMPANY, CALIFORNIA	
UNLESS OTHERWISE SPECIFIED: DIMENSIONS ARE IN INCHES ALL DIMENSIONS ARE TO THE NEAREST THOUSAND OF AN INCH		QUANTITY <u>1</u> <u>1/2</u> <u>3/4</u> <u>1/8</u> <u>1/16</u>		SKETCH-CERAMIC -EAT EXCHANGER-REACTOR-1200S VERTICAL-RBS COND-PT	
DRAWING		MATERIAL <u>304</u> FINISH <u>304</u> TOLERANCE <u>304</u> GRADE <u>304</u> SPECIFICATION <u>304</u> QUANTITY <u>304</u> WEIGHT <u>304</u> PRICE <u>304</u> COMMENTS <u>304</u>			
DESIGN		DESIGN <u>304</u> WEIGHT <u>304</u> PRICE <u>304</u> COMMENTS <u>304</u>			
MATERIAL		MATERIAL <u>304</u> FINISH <u>304</u> TOLERANCE <u>304</u> GRADE <u>304</u> SPECIFICATION <u>304</u> QUANTITY <u>304</u> WEIGHT <u>304</u> PRICE <u>304</u> COMMENTS <u>304</u>			
DESIGN <u>304</u> WEIGHT <u>304</u> PRICE <u>304</u> COMMENTS <u>304</u>		DESIGN <u>304</u> WEIGHT <u>304</u> PRICE <u>304</u> COMMENTS <u>304</u>		E 70210 SK52854 SCALE <u>1/2</u> SHEET <u>OF</u>	

NOTES: UNLESS OTHERWISE SPECIFIED

**ORIGINAL PAGE IS
OF POOR QUALITY**

Two state-of-the-art forming techniques, precision casting and slip casting, were considered for NC-430. Figure 2-21 illustrates the precision casting technique. A proprietary mix of raw materials is blended with binders to form a "plastic" mass. This mixture is then pressed or poured into a mold as shown in Figure 2-21a. The binders are allowed to rigidize giving the once plastic mass some "green" (unfired) strength. This allows the mold to be removed, leaving the rigid cast part (Figure 2-21b).

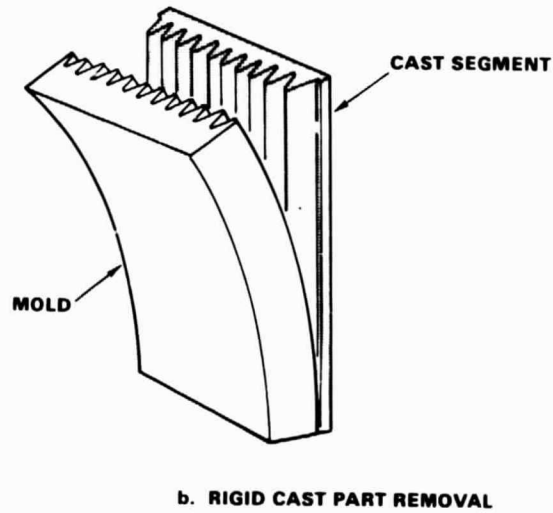
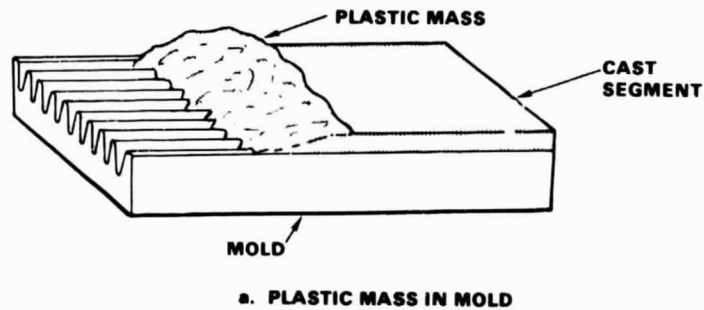
The slip casting process is illustrated in Figure 2-22. Slip casting is the deposition of suspended ceramic particles from an aqueous solution onto the surface of a plaster mold by absorption of the solution into the plaster. In this technique, the suspension of ceramic particles, called slip, is poured into a dry reusable plaster mold as shown in Figure 2-22a. The thickness of particles deposited onto the plaster mold is time dependent. Optimum material properties are obtained for shorter casting times (less than 1 hour) when cast thicknesses are less than 1/4 in. When the desired cast thickness is reached, excess slip is drained from the plaster mold (the name "drain casting" is often used to describe components formed in this way). The mold and cast pieces are allowed to air dry and the casting shrinks slightly, releasing itself from the plaster mold (Figure 2-22b). As the casting continues to dry it develops some green strength which allows removal of the plaster mold without distortion to the cast piece. The green strength is very low and therefore very large pieces are not easily made.

The basic shape of the solar receiver cavity is a cylinder. Many of the conceptual designs require fluid passages that would be formed on the walls of the cylinder. To accommodate these designs, a combination of slip casting and bonding was considered. Figure 2-23 illustrates the conceptual fabrication technique for assembling two concentric tapered cylinders that have fluid passages embossed on the cylinder walls. The taper on the cylinders, shown in Figure 2-23a, would permit easy assembly of the unit with a minimum of fitting problems. The bonding technique to be used has been successfully demonstrated during several research programs where the strength of the bonded material was found to be about 90 percent that of the parent material. The two concentric cylinders would be cast separately and then are bonded together during the final firing process. The fluid passages can be formed in several ways as illustrated in Figure 2-23b. Here, cross sections of the cylinder wall show fluid passages formed by contouring the inside, outside, or both cylinder walls of the cavity.

1. Continuous Plate-Fin

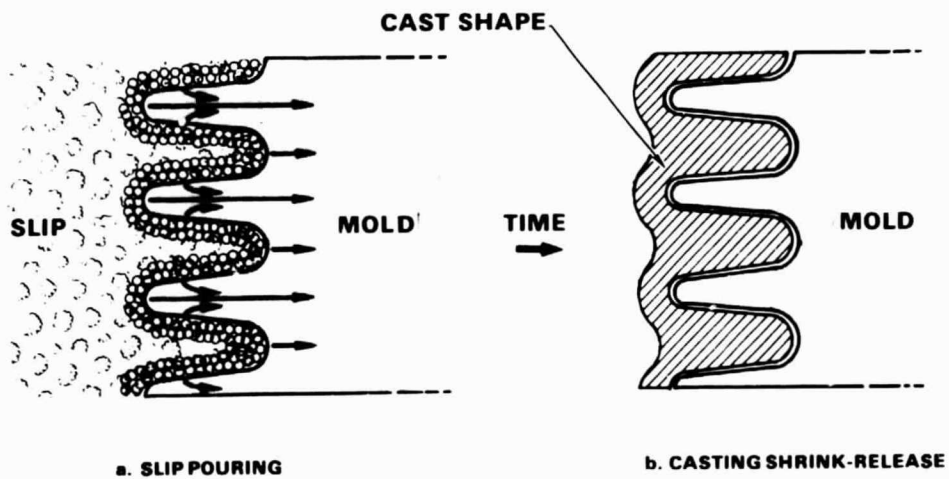
This receiver, illustrated in Figure 2-4, consists of two annular manifolds connected by a cylindrical continuous plate-fin heat transfer matrix. The receiver would be formed in three major sections: inner walls, outer walls, and fin matrix. The receiver walls would be slip cast with half of the integral manifolds at each end. These cylindrical sections would be tapered for easy assembly. The continuous plate-fin matrix would be precision cast and layed up onto the inner receiver wall before assembly of the two slip cast walls. Permanent ceramic bonds would be formed at the fin tips as they touch both the inner and outer walls. Permanent ceramic bonds would also be formed at the joint flange of the inlet and outlet manifolds as indicated in Figure 2-4.





A-23- j

Figure 2-21. Precision Casting



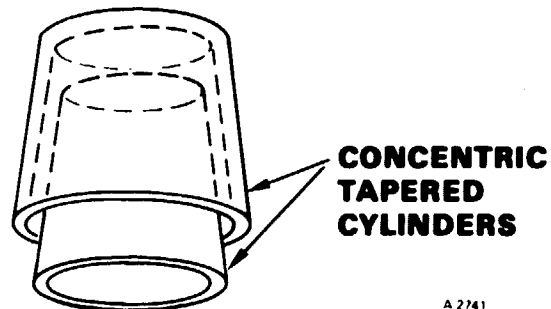
A 234 14

Figure 2-22. Slip Casting

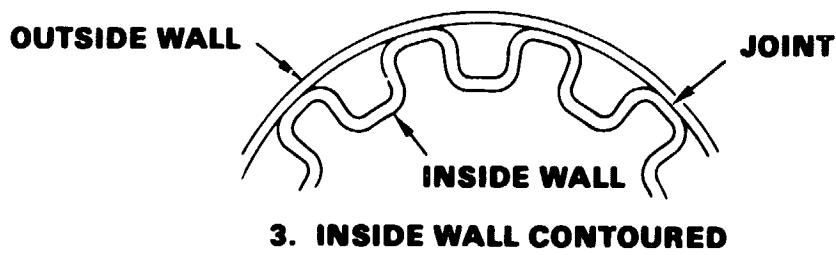
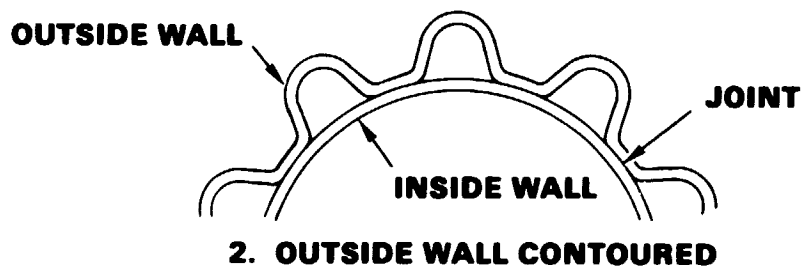
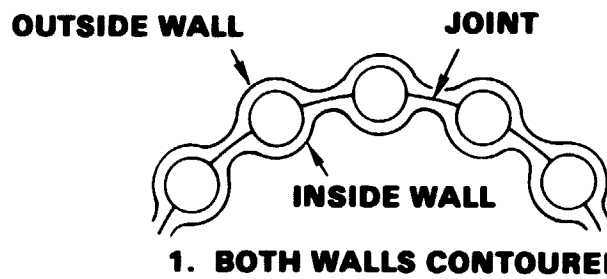
F.36297



ORIGINAL PAGE IS
OF POOR QUALITY



a. CONCENTRIC TAPERED CYLINDER CAVITY WALLS



b. SLIP CAST CONTOURED CAVITY WALLS

A-23419

Figure 2-23. Conceptual Fabrication Technique for Embossed Fluid Passages

This concept presents several problems: the fins are too thin, the receiver unit would probably be too difficult to assemble, and the air passages would probably become clogged with silicon during the final firing. The fin thickness of 0.010 in. for this design would be too difficult to fabricate using either the slip casting or precision casting technique. The fins produced by either forming technique would have extremely low green strength that would not allow the fin structure to be handled for bonding onto the cylinder walls. Assembly of the receiver would require the concentric tapered cylinder technique described in Figure 2-23 with the additional complication of inserting the very fragile fins between the cylinders. During the final firing of siliconized-silicon carbide, the component is fired in an atmosphere of silicon vapor. The vapor penetrates all cavities of the molded part and is wicked into the silicon carbide structure to produce a fully dense part. As the furnace is cooled, silicon vapor condenses over the component, usually in the form of nodules. This excess silicon is generally cleaned off the component by grit blasting. For components like the continuous plate-fin receiver, it would be too difficult to clean the inside surfaces since blasting grit would have to be directed blindly to the wall surfaces with hoses fed through the air inlet and outlet openings. Also, the delicate fin structure would probably not survive the grit blasting required to remove the excess silicon.

2. Plate-Fin Stacked Ring

This receiver, illustrated in Figure 2-5, is made up of two annular manifolds at both ends of a stack of finned rings. Each ring consists of two concentric walls that are joined by radial fins. The concentric walls also have a tongue-and-groove pattern in the axial direction that allows them to be stacked and mated to each other and to the inlet and outlet manifolds. Each ring and manifold would be formed individually by slip casting. Then the rings and manifolds would be stacked up and bonded together to form the receiver cavity. The manifolds do not represent any major difficulty since components of their size and complexity are now produced on a routine basis. The rings are not large, but the fin count and thickness could represent some fabrication problems. The fins might have to be tapered to facilitate removal from the mold.

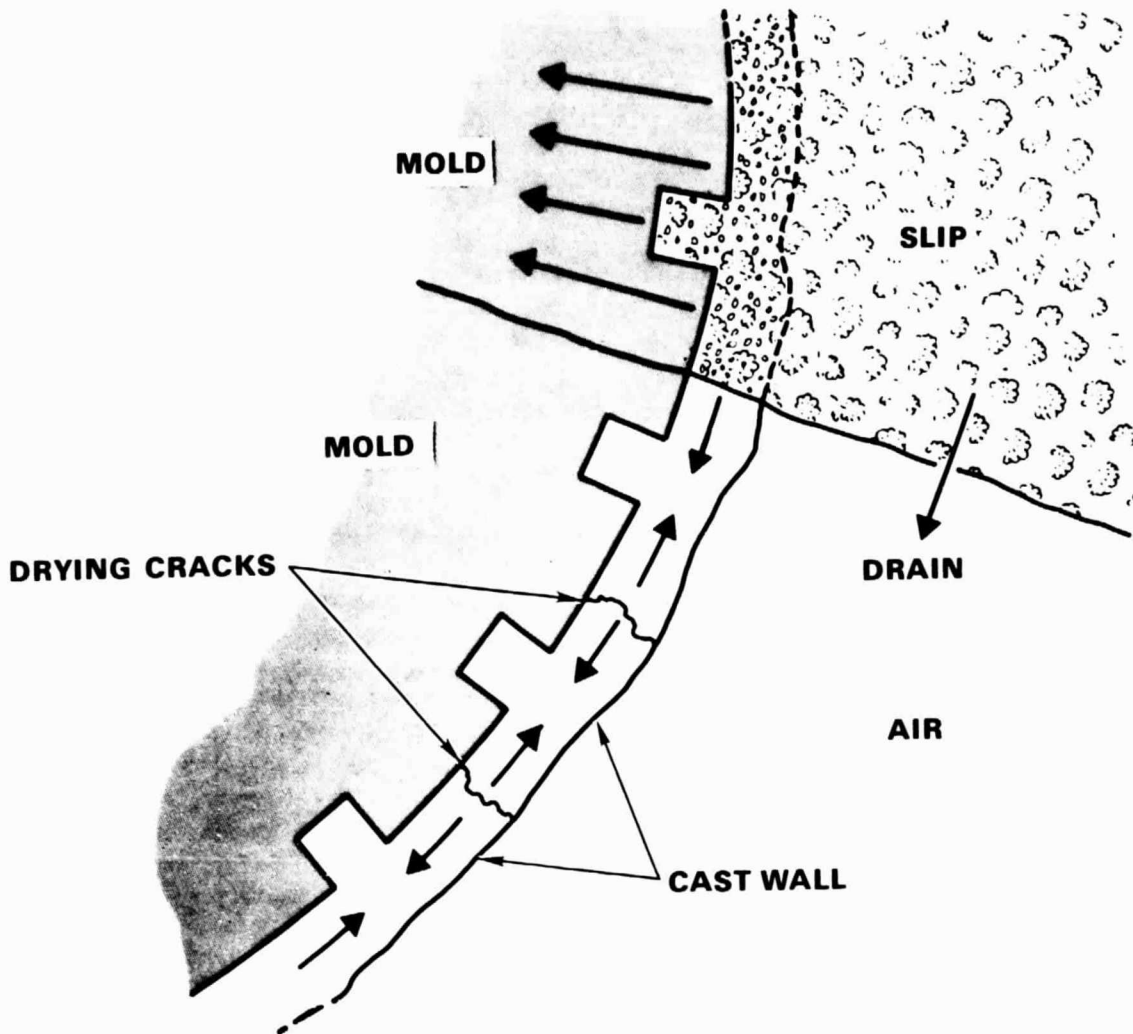
The major problem with this receiver concept is that extensive machining of the rings would be required to obtain good tongue-and-groove stacking. Without machining the tongue-and-groove surfaces, the final stackup would probably not be within acceptable tolerances. Also, the final bonding operation would cause silicon nodules to be formed in the passages, similar to the continuous plate-fin concept, which could not be cleaned without destroying the fins.

3. Concentric Cylinders with Vertical Ribs

This concept, illustrated in Figure 2-6, consists of concentric cylinders with vertical ribs cast integrally with the inner and outer wall surfaces. This concept would be easier to assemble than the continuous plate-fin concept since there are fewer parts and the ribs are not extremely thin and weak. However, the rib pattern on the inside of the outer wall is probably impossible to cast. This problem is illustrated in Figure 2-24. The relation of the



ORIGINAL PAGE IS
OF POOR QUALITY



A-16678

Figure 2-24. Cast Detail on Concave Surface

F-36298



AIRESEARCH MANUFACTURING COMPANY

81-18452
Page 2-47

cast piece to the plaster-of-Paris mold is depicted during the casting and drying processes. As the casting is growing, the mold and cast piece have the same dimensions at the interface. After the cast part has been formed and the excess slip has been drained away, the cast part begins to dry and shrink. As illustrated, if the drying component cannot shrink away from the mold wall due to constraints (like the ribs), drying cracks will develop in the cast piece. For this reason, any concept using the concentric cylinder design that requires embossed detail on the inside surface of the outer cylinder will be impossible to cast without producing drying cracks in the cast piece.

The cross section illustrated in Figure 2-6b shows the split between the inner and outer walls at the center of each rib. An alternate approach was considered to produce the same shape. If the ribs were cast entirely on the inside cylinder, then the mating outside cylinder would not have to be embossed and could be formed with the outside surface in contact with the mold. That is, the outer cylinder would be formed on the inside surface of a cylindrical mold. The outer cylinder drain side would mate to the fins on the inside cylinder.

Several problems would still exist preventing this concept from being produced. The drain side of the outer cylinder may be too rough to allow good contact with all fin surfaces. To ensure good bonding, the outer cylinder mating surface would need to be machined. Also, the bonding process would cause the same silicon blockage referred to previously.

4. Dual-Tube Serpentine Flow

This concept is shown in Figure 2-7. It was designed assuming that this configuration could be fabricated using the concentric/tapered cylinder technique. Since this design requires that the tube pattern be embossed on the inside surface of the outer cylinder, it is not possible to produce this design using state-of-the-art casting techniques. Alternate fabrication techniques were examined. The most reasonable technique would use slip-cast U-tube segments that would be one-half of the cylinder length. These tubes could be bonded into the serpentine configuration. This alternate technique would require extensive machining of the U-tube segments to assure the proper indexing to form the receiver within acceptable tolerances. Extensive bonding would also be required at the U-tube openings and along the length of the U-tubes. Finally, this assembly, sized for the required heat transfer and pressure drop, is too large to be fired in any existing siliconizing furnace at the Norton Company.

5. Dual-Tube Helical Flow

This concept, illustrated in Figure 2-8, was proposed to be formed using the concentric/tapered cylinder scheme. This would require that one-half of the tube configuration be embossed on the inner surface of the outer cylinder. As previously discussed, this appears to be beyond current state-of-the-art slip-casting techniques. Other assembly techniques were considered such as forming each 360-deg tube spiral segment separately and then bonding these segments. This appears to be too complex, however, at least for the dual-tube configuration.

6. Single-Tube Helical Flow

This concept, illustrated in Figure 2-9, was conceived to be produced using the concentric/tapered cylinder assembly technique. However, this design also requires the inside surface of the outer cylinder to be embossed with the tube pattern. This is not possible within the current state of the art as outlined for several of the designs previously discussed. Alternate fabrication techniques were considered to produce the desired configuration. The best alternative would use slip-cast 360-deg spiral tube segments bonded together to form the complete helical flow pattern. Bonds would be formed along the tube surfaces as they were stacked upon each other and at the tube mouth interfaces at each 360-deg segment. This technique would require extensive bonding and machining so that the tube segments would be indexed properly to form a helical configuration within acceptable tolerances.

7. Plate-Fin Stacked Disk

This concept was not evaluated due to the poor results of thermal analysis.

8. Ceramic-Lined Metal Shell

Figure 2-11 is an illustration of the ceramic-lined metal shell concept. The ceramic heat exchanger is a monolithic shape that probably is fabricable within the state-of-the-art slip-casting technology. It consists of axial ceramic fins embossed on the outside surface of the liner. The limiting factor with this design will be the amount of detail that can be produced consistently over the liner surface to form thin, densely packed, high fins. Precision casting techniques may be helpful to achieve the desired configuration. The size of the liner (about 1.5 by 2.5 ft) seems to be within the acceptable limits for forming a monolithic shape.

CONCEPT EVALUATION AND SELECTION

To aid in the selection of the two concepts to be studied in further detail in the Task 2 effort, a summary table, presenting the results of the conceptual design study, was prepared. This summary is shown in Table 2-9. The maximum tensile stress is listed because this is invariably the key stress for ceramic designs. The compression strength of ceramics is many times that under tension.

In fact, the tensile stress limitation effectively eliminates the majority of the conceptual designs. Previous experience with the NC-430 material suggests that tensile stresses should not exceed about 8,000 to 10,000 psi for a highly reliable design. All of the concepts, except for the concentric cylinders with vertical ribs design and the ceramic-lined metal shell design, have stresses exceeding this limit (see Table 2-9). The stresses for the two acceptable configurations were calculated in response to radial temperature gradients only. Stresses caused by axial temperature gradients may be higher, especially for the ceramic-lined metal shell. Since both of the configurations exhibit circumferential symmetry, there should be only small circumferential temperature gradients.



TABLE 2-9
TASK 1 SUMMARY

Concept	Cavity Size, ID by length, ft	Tube Diameter, in.	Maximum Tensile Stress, psi*	Cavity Efficiency	Fabrication Evaluation
Continuous Plate-Fin	1.5 x 2.5	--	15,100	0.833	Not feasible
Plate-Fin Stacked Ring	1.5 x 1.5	--	14,700	0.848	Extensive machining required**
Concentric Cylinders with Vertical Ribs	1.5 x 2.5	--	4,000	0.837	Extensive machining required**
Dual-Tube Serpentine Flow	2.3 x 3.4	2.50	Excessively large cavity	--	Extensive machining and bonding; too large for cur- rent furnace
Dual-Tube Helical Flow	1.5 x 2.7	2.00	24,500	0.835	Not feasible
Single-Tube Helical Flow	1.5 x 2.4	2.87	26,000	0.835	Extensive machining and bonding
Plate-Fin Stacked Disk	1.5 x 2.5	--	Exceeded temperature limitations		Not evaluated
Ceramic-Lined Metal Shell	1.5 x 2.5	--	1,700	0.838	Most feasible

*Radial temperature gradients only

**passage clogging due to free silicon



**ORIGINAL PAGE IS
OF POOR QUALITY**

In addition to the excessive stresses, the rejected concepts all have serious fabrication difficulties. The selected concepts, especially the ceramic-lined metal shell, appear to be the most feasible from a manufacturing point of view.

Of the rejected designs, perhaps the most interesting is the plate-fin stacked ring. This concept might warrant further investigation in the future as manufacturing techniques improve. The offset nature of the heat transfer fins results in a considerably reduced size for this design as compared to the other configurations.



SECTION 3

TASK 2A, PRELIMINARY DESIGNS AND EVALUATIONS

The Norton Company, the proposed ceramic receiver manufacturer, has reviewed the two selected conceptual designs and drawings. From a fabrication point of view, Norton prefers the ceramic-lined metal shell. The concentric cylinders with vertical ribs design was not favored by Norton for a number of reasons. One problem is related to the shrinkage of the molded part with respect to the mold, as discussed previously. To form the outside cylinder with precision details on its inside surface would require the mold on the inside surface. As the molded wall segments dried, they would shrink and crack on the plaster mold which would not change shape (see Figure 2-24). A possible solution would be to mold the entire fin passage on the inside cylinder. The outside cylinder would then be a plain, unribbed cylinder that could be cast with a mold on its outside surface. The drain side of the casting, which usually is rough and uneven, probably would require extensive machining to ensure an accurate mating with the rib tips on the inside cylinder. This would be an expensive procedure, considered by Norton to be economically unattractive.

Another problem involves the inaccessibility of the small flow passages for cleaning after the siliconizing step in the processing of the siliconized-silicon carbide structure. Large quantities of vapor-deposited silicon can build up in the flow passages and must be grit-blasted out, which is a difficult procedure with 0.2-in. passages, 30 in. long. In addition, further silicon deposition will occur during the manifold bonding operation, after which cleaning is impossible.

The ceramic-lined metal shell concept is considered by the Norton Company to be most compatible with current forming and furnacing capabilities, requiring a minimum of bonding in the flange/manifold region. All areas are open for inspection and cleaning after bonding. Since the fin tips do not mate with another ceramic surface, machining would be kept to a minimum.

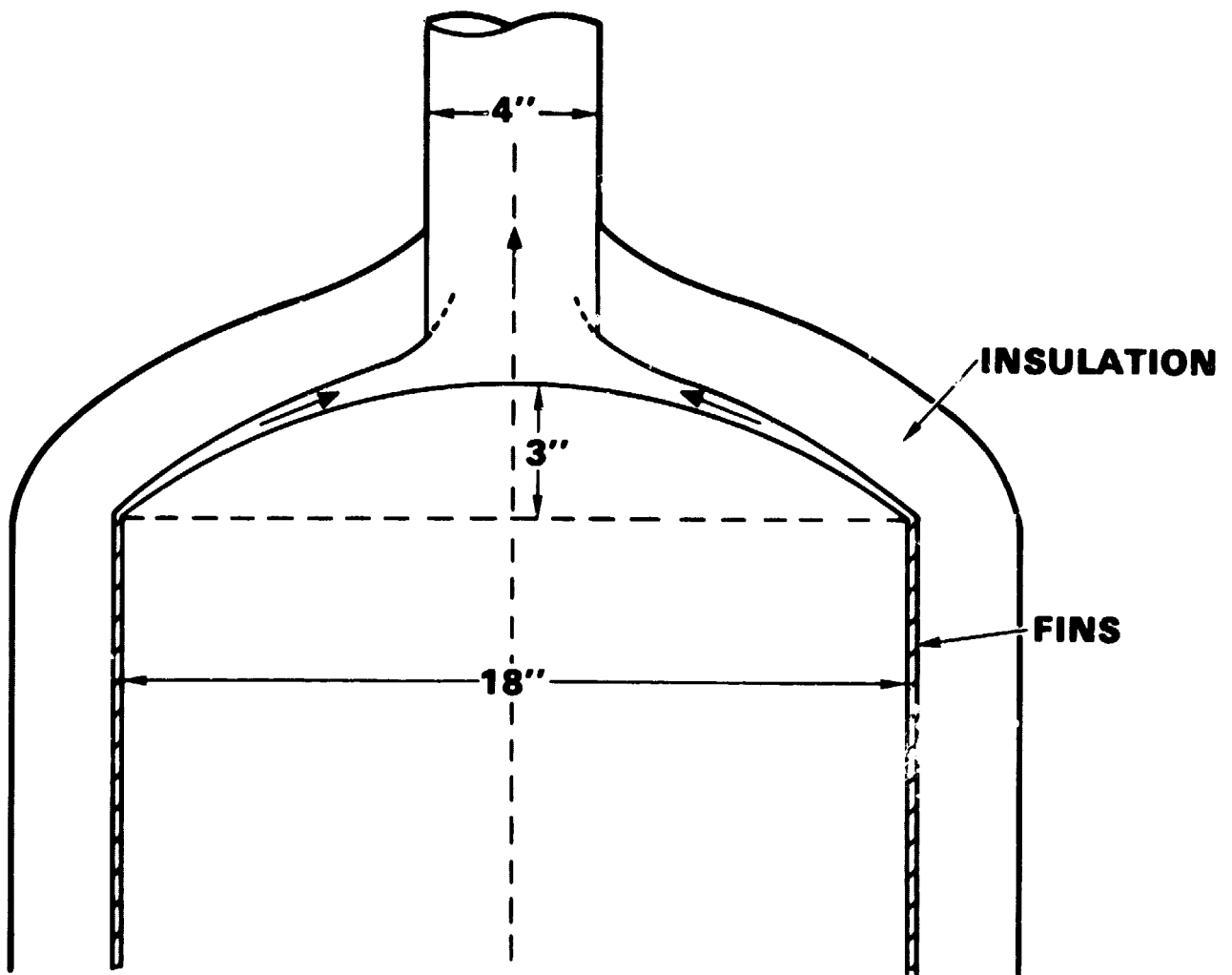
REFINED DESIGN FOR CERAMIC-LINED METAL SHELL

With the Norton opinion in mind, it was decided to prepare a refined design for the ceramic-lined metal shell incorporating a more detailed structural analysis to evaluate the effect of the axial temperature gradients. One change made to the conceptual design was to flatten the top or dome of the receiver. The full hemispherical top of the conceptual design wasted space, with little or no additional heat transfer or pressure drop advantage. The revised shallow top details are shown in Figure 3-1. There are no fins in the top section. Approximately 3 in. of insulation would be required to reduce the temperature sufficiently to enable the use of a carbon steel outer shell. An additional 2 to 3 in. of insulation are required outside the metal shell.

Thermal analyses were performed using the RECMDL computer program. Both plain and offset fins were used. In order to ensure that the temperature and pressure drop limitations (2400°F and 4 percent of the inlet pressure, respectively) would be met, design margins are included in the analyses. Ten-percent

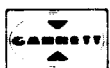


ORIGINAL PAGE IS
OF POOR QUALITY



A-16954

Figure 3-1. Shallow Top Details



**ORIGINAL PAGE IS
OF POOR QUALITY**

margins for both friction factor and heat transfer coefficient were used for the plain fin designs and margins of 15 percent for the offset fins designs. The larger margins for the offset fins reflect the lower level of accuracy in the friction factor and heat transfer coefficient data used.

Some of the performance results are presented in Table 3-1. The active length is that of the fins in the cylindrical section, and does not include either the closed dome section or the inlet manifold at the aperture end of the receiver. The dome and manifold are expected to add about 3 in. each to the overall length. The fin geometry is designated as $nR-b-l(0)-t$, where nR is the number of rectangular fins per inch, b is the fin height, $l(0)$ is the offset length, and t is the mean fin thickness (see Figure 2-3). An offset length designation of P indicates plain fin passages.

It can be seen from Table 3-1 that the offset fin designs result in substantially smaller receiver sizes than the plain fin designs, at least for the assumed maximum fin count of five per inch. Drawings of typical designs are presented in Drawing SK52855 for plain fins and Drawing SK52856 for offset fins.

Previous stress analyses performed during Task 1 indicated very low stress due to radial temperature gradients. The refined analyses for Task 2A include the axial temperature gradients. The entire ceramic shell was considered, including the dome and the flange/manifold sections. Both a full hemispherical dome and the shallow, 3-in.-high dome were analyzed. A typical temperature profile for a plain-fin receiver, 1.5 ft diameter and 2.5 ft long, was assumed. The two-dimensional ANSYS model, with the input temperatures, is shown in Figure 3-2. The model includes both pressure and temperature loading. Because the stresses due to radial temperature gradients are very low, these gradients are neglected, i.e., only the axial temperature gradients are considered.

The manifold/flange region is not modeled in RECMDL; hence, no surface temperatures were predicted. For the ANSYS model, the flange temperature was assumed to be that of the inlet air while the unfinned cylinder surface (manifold wall) was assumed to be at a temperature intermediate between that of the flange and the first finned element. To effect such a temperature distribution, it will be necessary to reduce the insulation thickness in the manifold region to permit some fluid heating. This will enable the cylinder wall to be at a temperature higher than the fluid temperature, as required for the assumed distribution.

The results of the stress analyses for an external pressure loading of 25 psig (39.7 psia) are presented in Table 3-2. The directions are referenced to the receiver. Since the model was two-dimensional, no radial (wall thickness) stresses were generated.

As shown in Table 3-2, the maximum tensile stresses are in the flange region, and are about the same for the two dome types.

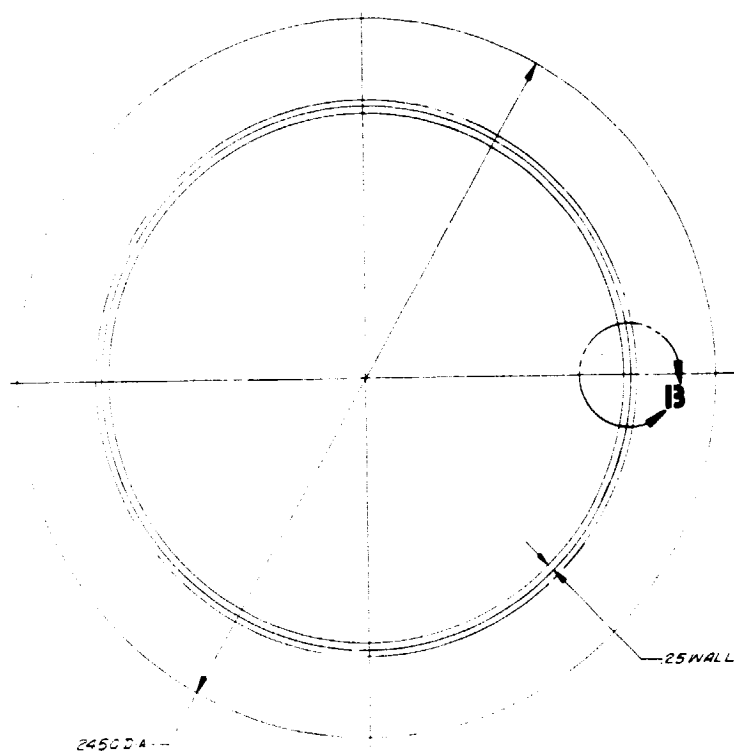


ORIGINAL PAGE IS
OF POOR QUALITY

TABLE 3-1
REFINED CERAMIC-LINED METAL SHELL DESIGNS

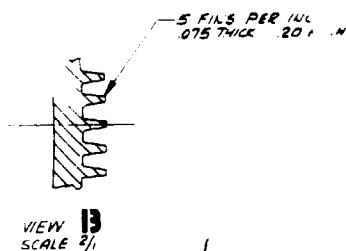
Diameter, ft	Active Length, ft	Fin Designation	Maximum Wall Temperature, °F	Pressure Drop, Percent	Cavity Efficiency
1.5	2.0	3R-0.25-0.7(0)-0.050	2446	2.93	0.836
1.5	2.0	5R-0.375-0.6(0)-0.040	2388	1.87	0.852
1.5	2.0	5R-0.375-0.5(0)-0.040	2382	2.15	0.854
1.5	2.0	5R-0.375-0.375(0)-0.040	2373	2.70	0.856
1.5	2.0	5R-0.35-0.5(0)-0.040	2380	2.51	0.854
1.5	2.0	5R-0.32-0.5(0)-0.040	2378	3.06	0.854
1.5	2.5	5R-0.18-P-0.075	2415	4.29	0.831
1.5	2.5	5R-0.20-P-0.075	2423	3.27	0.829
1.5	2.5	5R-0.22-P-0.075	30	2.57	0.827
1.5	2.5	5R-0.14-P-0.040	2440	4.20	0.825
1.5	2.5	5R-0.16-P-0.040	2454	2.95	0.821
1.667	2.5	5R-0.16-P-0.075	2402	4.68	0.834
1.667	2.5	5R-0.18-P-0.075	2412	3.44	0.832
1.667	2.5	5R-0.20-P-0.075	2419	2.66	0.831
1.5	2.75	5R-0.20-P-0.075	2382	3.56	0.832
1.5	2.75	5R-0.22-P-0.075	2392	2.80	0.830
1.5	2.25	8R-0.21-P-0.040	2404	3.05	0.841
1.5	2.5	8R-0.22-P-0.040	2360	3.06	0.841
1.5	2.333	8R-0.21-P-0.040	2388	3.16	0.842
1.5	2.333	8R-0.25-P-0.040	2390	2.21	0.841
1.5	2.333	8R-0.27-P-0.040	2388	1.92	0.842



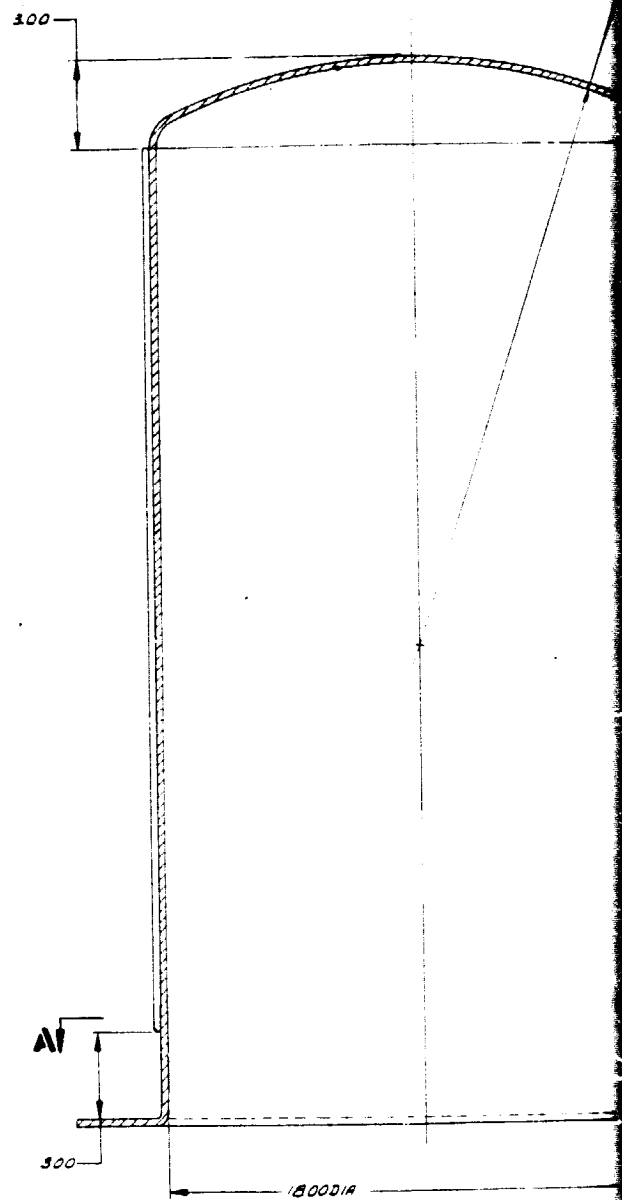


SECTION A-A

ORIGINAL PAGE IS
OF POOR QUALITY



FOLDOUT FRAME



LINE	AA	AB	AC	AD	AE	AF	AG	AH	AI	AJ	AK	AL
LINE	BA	BB	BC	BD	BE	BF	BG	BH	BI	BJ	BK	BL
LINE	CA	CB	CC	CD	CE	CF	CG	CH	CI	CJ	CK	CL

NOTES: UNLESS OTHERWISE SPECIFIED

REVISIONS				
DATE	TIME	DESCRIPTION	DATE	APPROVED

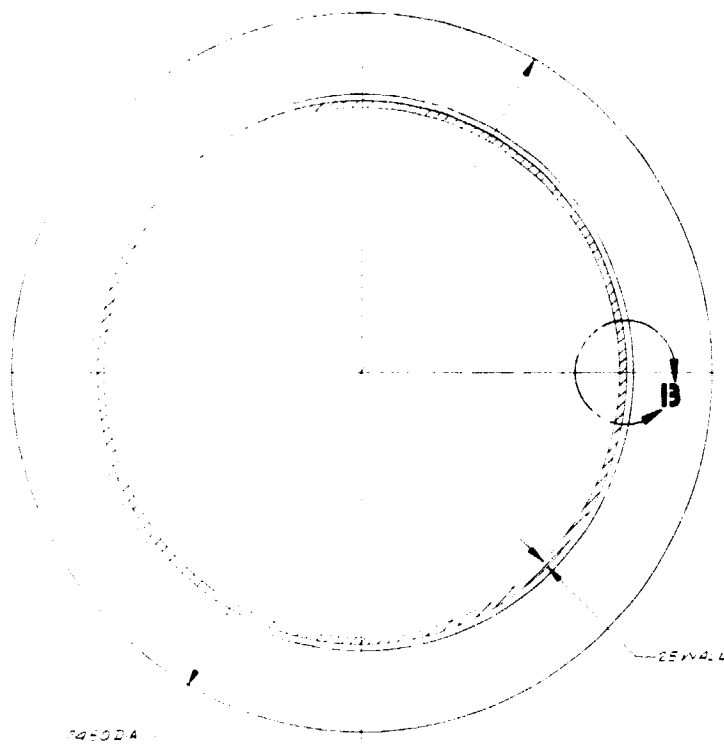


2 FOLDOUT FRAME

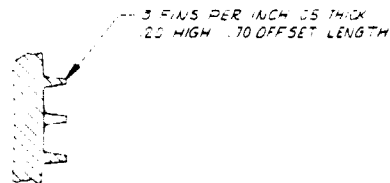
[illegible]

ORIGINAL PAGE IS
OF POOR QUALITY

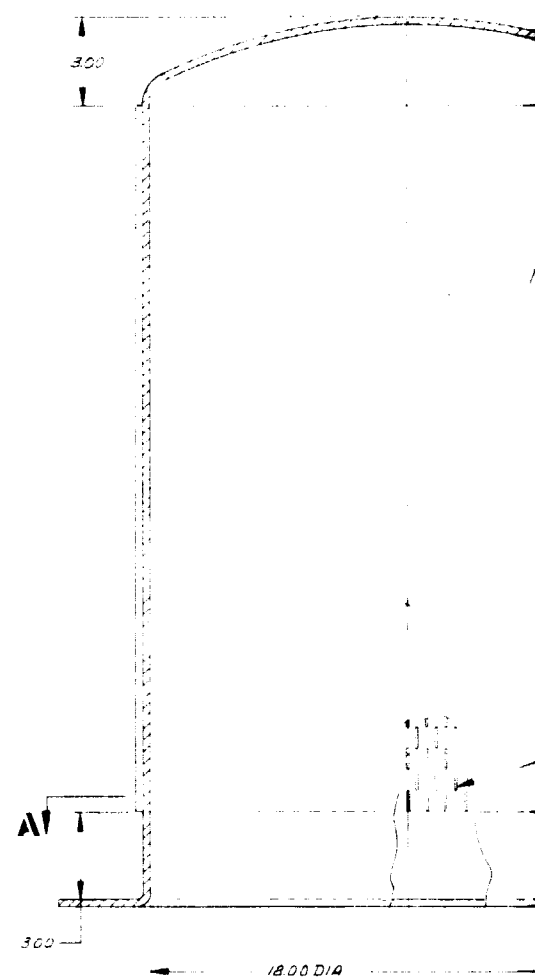
FOLDOUT FRAME



SECTION A-A



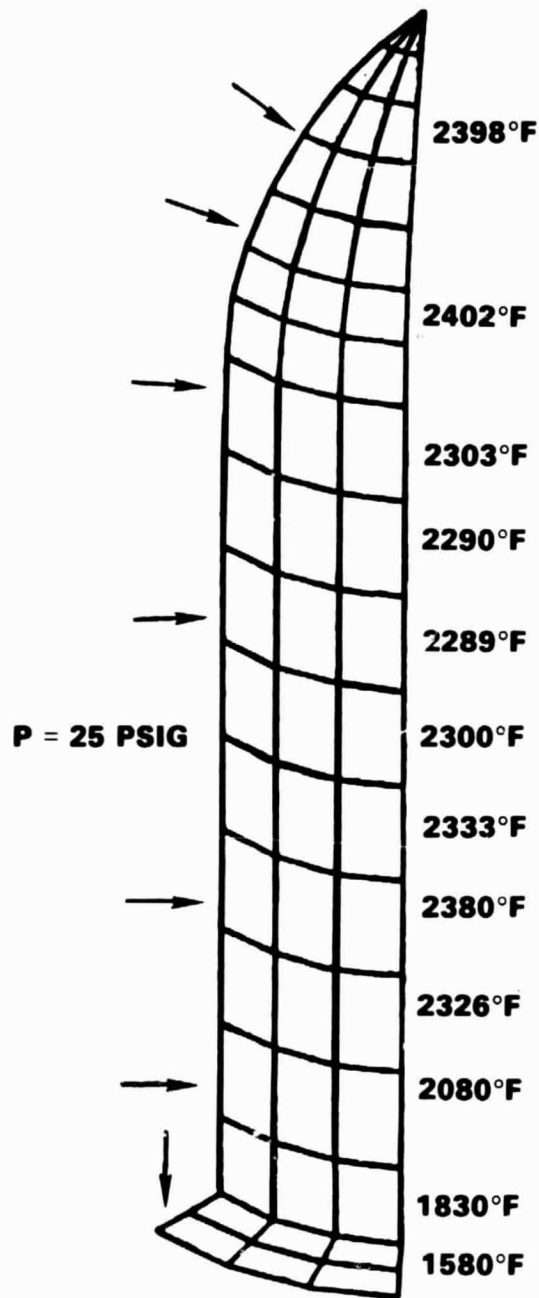
VIEW 13
SCALE 2/1



ZONE	AA	AB	AC	AD	AE	AF	AG	AH	AI	AJ	AK	AL
LET	A	B	C	D	E	F	G	H	I	J	K	L
ZONE	MA	MB	MC	MD	ME	MF	MG	MH	MI	MJ	MK	ML
LET	M	N	O	P	Q	R	S	T	U	V	W	X

NOTES: UNLESS OTHERWISE SPECIFIED

ORIGINAL PAGE 19
OF POOR QUALITY



A-23408

Figure 3-2. Ceramic-Lined Metal Shell Two-Dimensional AYSYS Model



AIRESEARCH MANUFACTURING COMPANY

TABLE 3-2

REFINED DESIGN MAXIMUM TENSILE STRESSES, PSI

Section	Hemispherical Top		Shallow Top	
	Tangential	Axial	Tangential	Axial
Dome	250	958	147	1745
Cylinder	573	3272	2343	3272
Flange	7541	3979	7541	3979

CONCEPT SELECTION

The maximum stress levels shown in Table 3-2 are somewhat on the high side, but are probably within the acceptable region for the material system. It is expected that stress levels could be lowered with detailed design effort. It is felt that based on essentially state-of-the-art fabrication techniques, the ceramic-lined metal shell has a greater probability of success than the concentric cylinders with vertical ribs. Thus, this configuration has been selected for further design effort. A summary comparison of the two concepts is presented in Table 3-3.

TABLE 3-3

CONCEPT SELECTION

Concentric Cylinders With Vertical Ribs	Ceramic-Lined Metal Shell
Stress level acceptable.*	Stress level acceptable.
Performance and pressure drop acceptable.	Performance and pressure drop acceptable.
Possible cracking of ceramic due to shrinkage if mold on inside surface of outer cylinder.	Mold on outside of cylinder only.
If mold placed on outside surface of outer cylinder, extensive machining necessary.	Minimal machining since fins do not have to mate to another surface.
Silicon nodules accumulating in flow passages cannot be removed easily.	Deposited silicon removed readily by grit blasting.
	Minimum volume of ceramic material involved.

*Based on radial temperature gradients only.



FABRICATION OPTIONS

Several fabrication options were devised based on discussions held with the Norton Company. These options were formulated on the desire to achieve the highest, most closely spaced, thinnest fins possible to minimize the receiver size, and to develop a design that was just within the current fabrication state of the art. The design options presented below are the result of several iterations with Norton. The dimensional limitations quoted represent the best estimate of current fabrication capabilities.

The first option is illustrated in Figure 3-3. The ceramic liner would be slip cast in three separate parts consisting of the cap, cylinder, and flange. These parts would be bonded together during the final firing to form one monolithic structure. These components have a thickness of about 0.25 in. The cap and flange are simple pieces to fabricate and do not represent any special problems. Of the three components, the cylinder is the most difficult to produce. Norton feels that the limitations on fins for the cylinder would be less than 5 fins per in., a minimum thickness of 0.075 in., and a maximum height of 0.375 in. The minimum fin thickness is measured at mid-height since the fins are slightly tapered to facilitate mold removal.

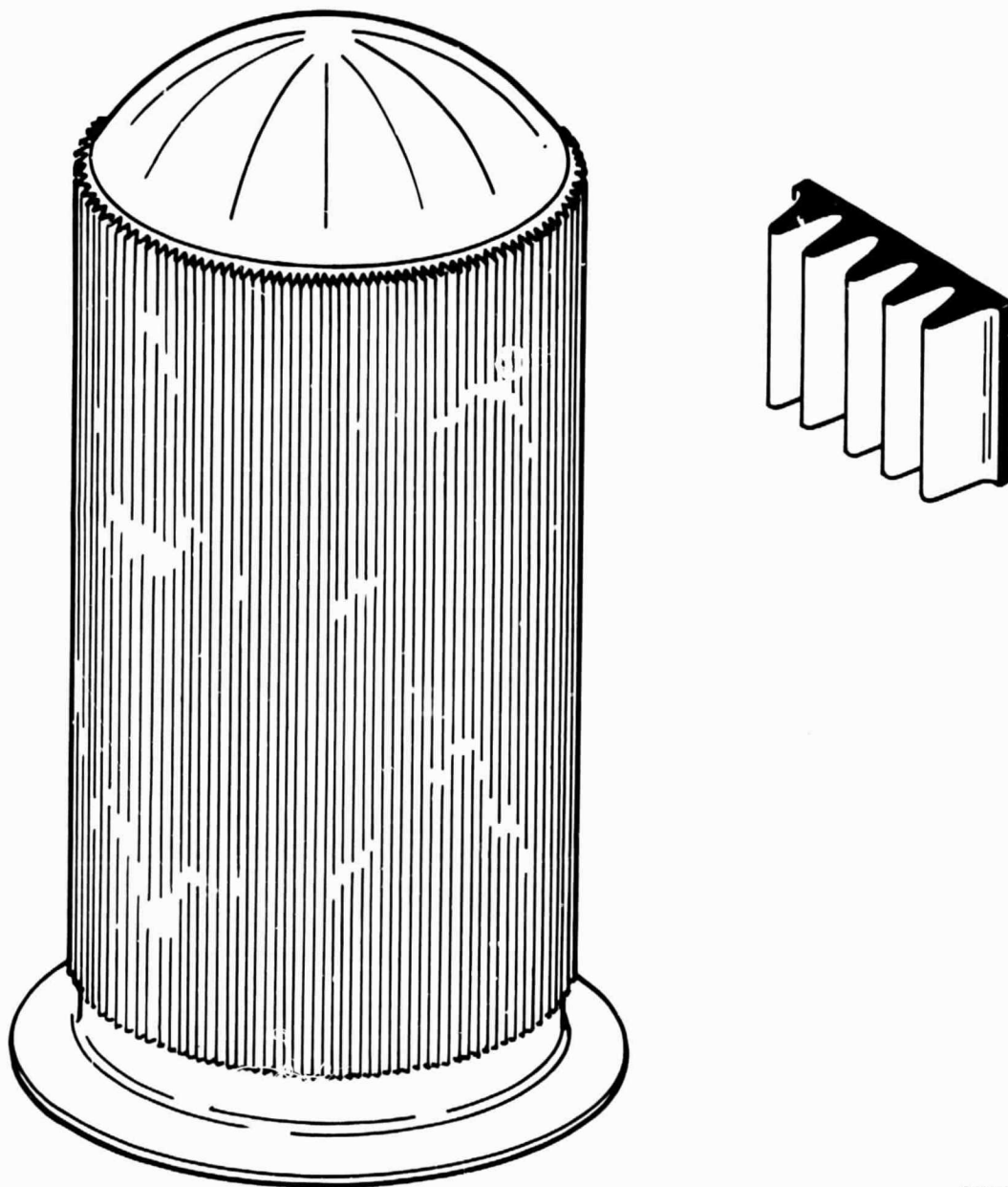
To form these fins as the cylinder outer surface, a minimum 50-piece mold would be needed. These mold segments would be axial strips that would be removed radially. Each strip would form only a few axial continuous fins. The large number of mold segments is required so that fins are not broken in the mold removal process. The large number of mold segments also complicates the fabrication process because the removal must be done quickly to prevent uneven drying of the green cast piece.

A second option, illustrated in Figure 3-4, is similar to the first option, except that the cylinder is now faceted with 12 to 20 flat, finned faces. The liner consists of three parts: cap, cylinder, and flange, which are bonded together during the final firing. The faceted cylinder was conceived in an attempt to reduce the number of mold segments required to make the cylinder. Figure 3-4 illustrates how each mold segment forms one of the liner facets. Two mold pieces may be required for each facet. Thus, the maximum number of mold segments required would be about two times the number of facets. This would be considerably less than the number of mold segments needed for the cylindrical slip-cast design (Figure 3-3). The fin limitations for this option are identical to the cylindrical slip-cast option: less than 5 fins per in., a minimum 0.075 in. thickness, and a 0.375 in. maximum height.

A third option combines precision-cast and slip-cast components. Figure 3-5 illustrates the technique. The basic shape of the receiver cavity ceramic liner is slip cast in two parts. The cap and cylinder are cast as one piece with the cylinder having between 12 and 20 facets. The outside of the cylinder and dome are smooth, as-cast surfaces. The flange is cast as a separate piece and is bonded to the faceted cylinder. Precision-cast plates of fins are cast in separate molds. These precision castings are made to fit the width of the facets on the slip-cast cylinder. It may be necessary to make several segments of fins to cover the length of each facet. The slip-cast and precision-cast parts are processed separately through the siliconizing steps. Then the finned



ORIGINAL PAGE 13
OF POOR QUALITY

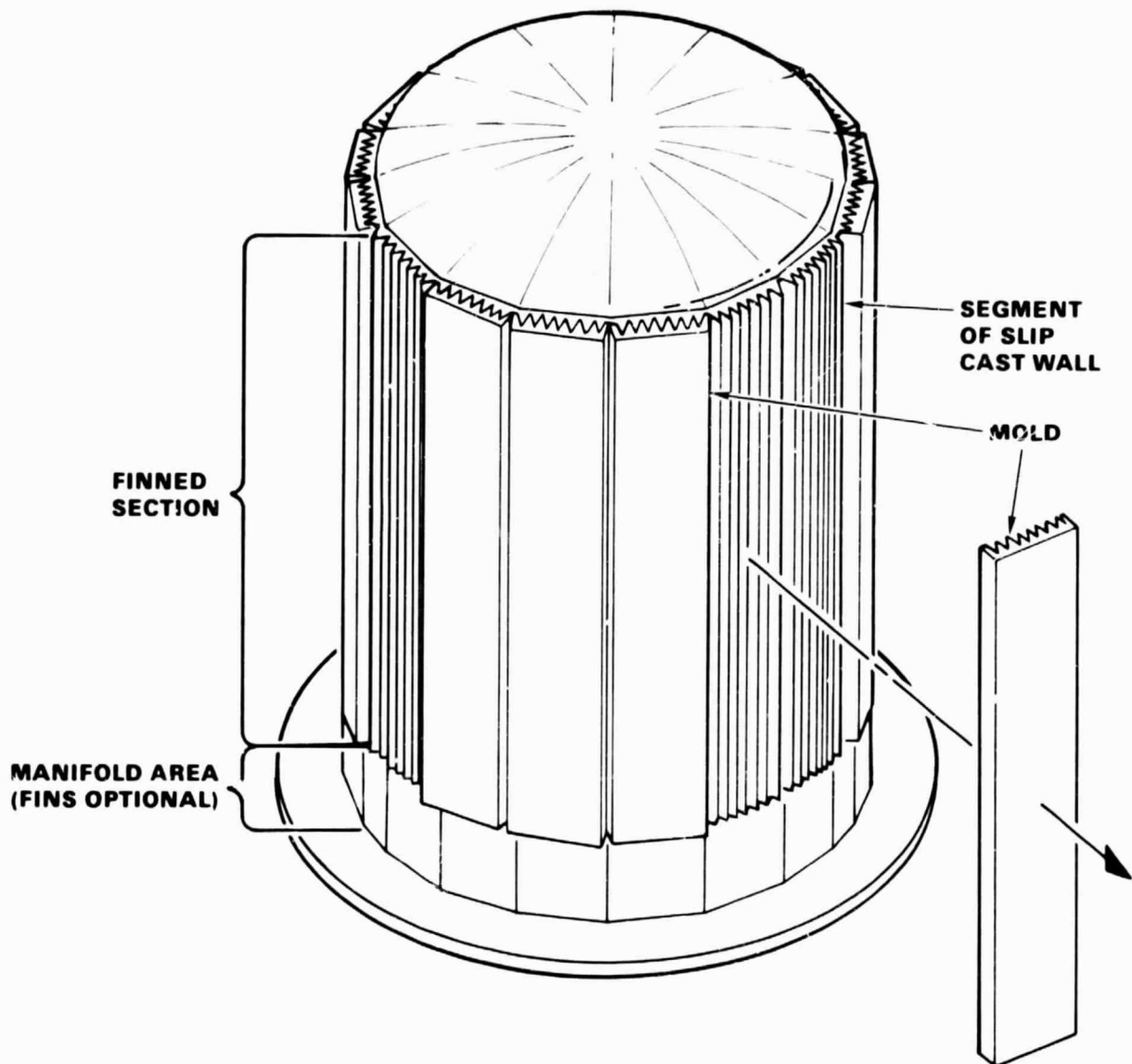


A-24366

Figure 3-3. Cylindrical Slip-Cast Ceramic Liner



ORIGINAL PAGE 13
OF POOR QUALITY

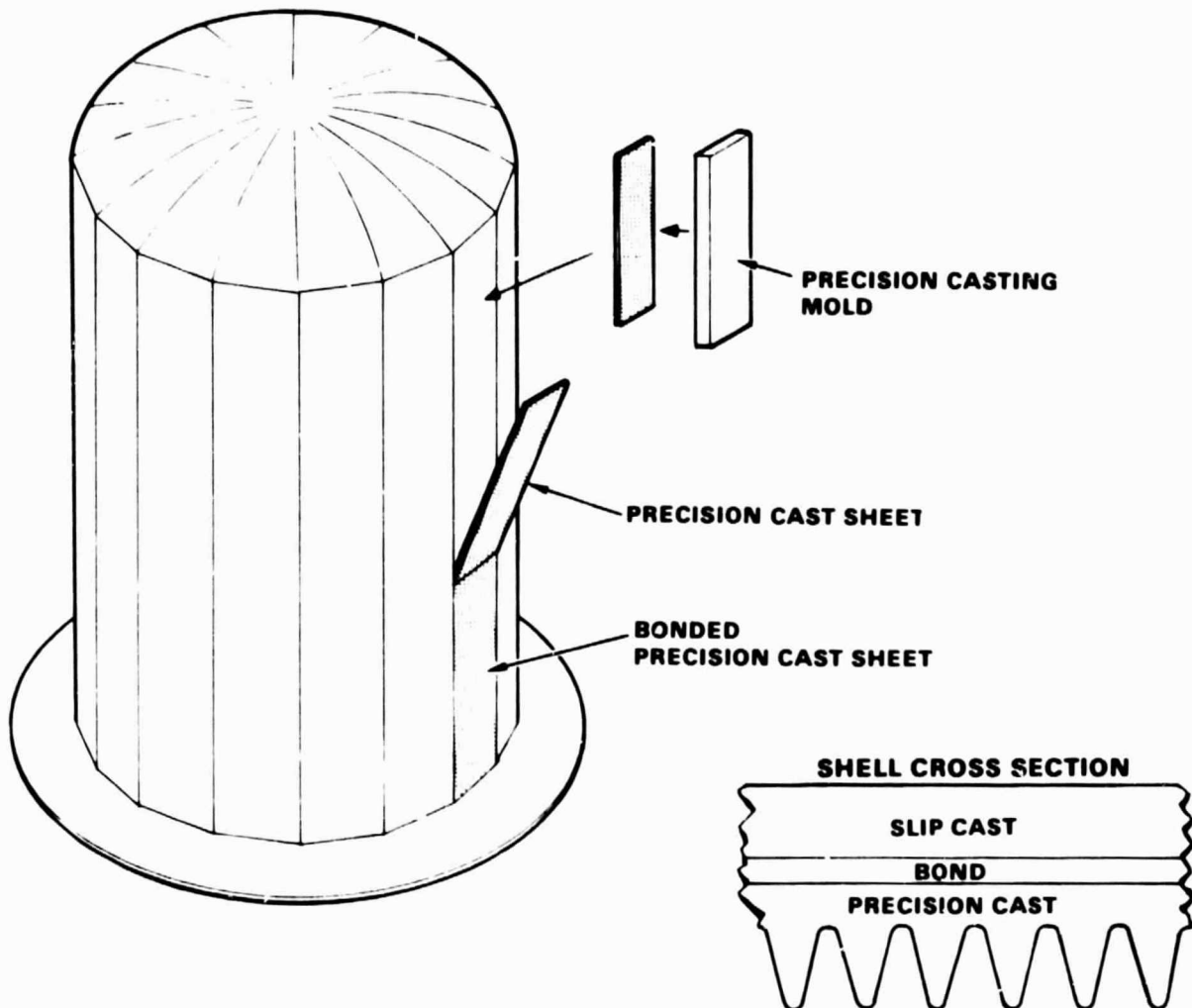


A 16687 - A

Figure 3-4. Faceted Slip-Cast Ceramic Liner



ORIGINAL PAGE IS
OF POOR QUALITY



A 16756

Figure 3-5. Precision/Slip-Cast Ceramic Liner



plates are bonded to the facets of the slip-cast cylinder to form the completed receiver cavity. The precision casting of the finned plates allows greater control of the quality of fins on the completed receiver cavity because miscast and improperly processed segments can be eliminated before they are bonded to the cavity wall.

The fins can be either offset or plain. A schematic of an offset fin plate is shown in Figure 3-6. The fin limitations are: a maximum of 5 fins per in., a minimum fin thickness of 0.040 in. (at mid-height), and a maximum fin height of 0.375 in. A plain fin schematic is shown in Figure 3-7. The fin limitations are: a maximum of 8 fins per in., a minimum fin thickness of 0.040 in. (at mid-height), and a maximum fin height of 0.375 in. The reduced complexity of fabricating plain fins allows for a higher fin count than for offset fins.

The combined precision/slip-cast approach was considered to have the best chance for success because a large number of mold segments are not needed to form any of the individual components. For the other options, a large number of mold segments must be used simultaneously to cast the finned cylinder. Mold removal becomes a problem because the green cast component dries rapidly in the area where the mold is removed. If the mold segments are not removed quickly from the entire piece, differential drying would probably occur causing cracking of the cast piece. For this reason, the precision/slip-cast technique was selected as the most feasible based on fabrication considerations.

PRELIMINARY DESIGNS

Preliminary designs were prepared for each of the potential fabrication techniques, using fin geometry limitations in accordance with manufacturing capabilities of the Norton Company. The designs presented in Table 3-4 are based on the analytical solutions from Table 3-1. Note that the receiver outside diameters are listed in Table 3-4; previous tables gave inside diameters, which are more appropriate for parametric evaluations. The outside diameter includes the wall and plate thickness, and the fin height. The overall length includes the manifold/flange region, the shallow top, and the wall thickness.

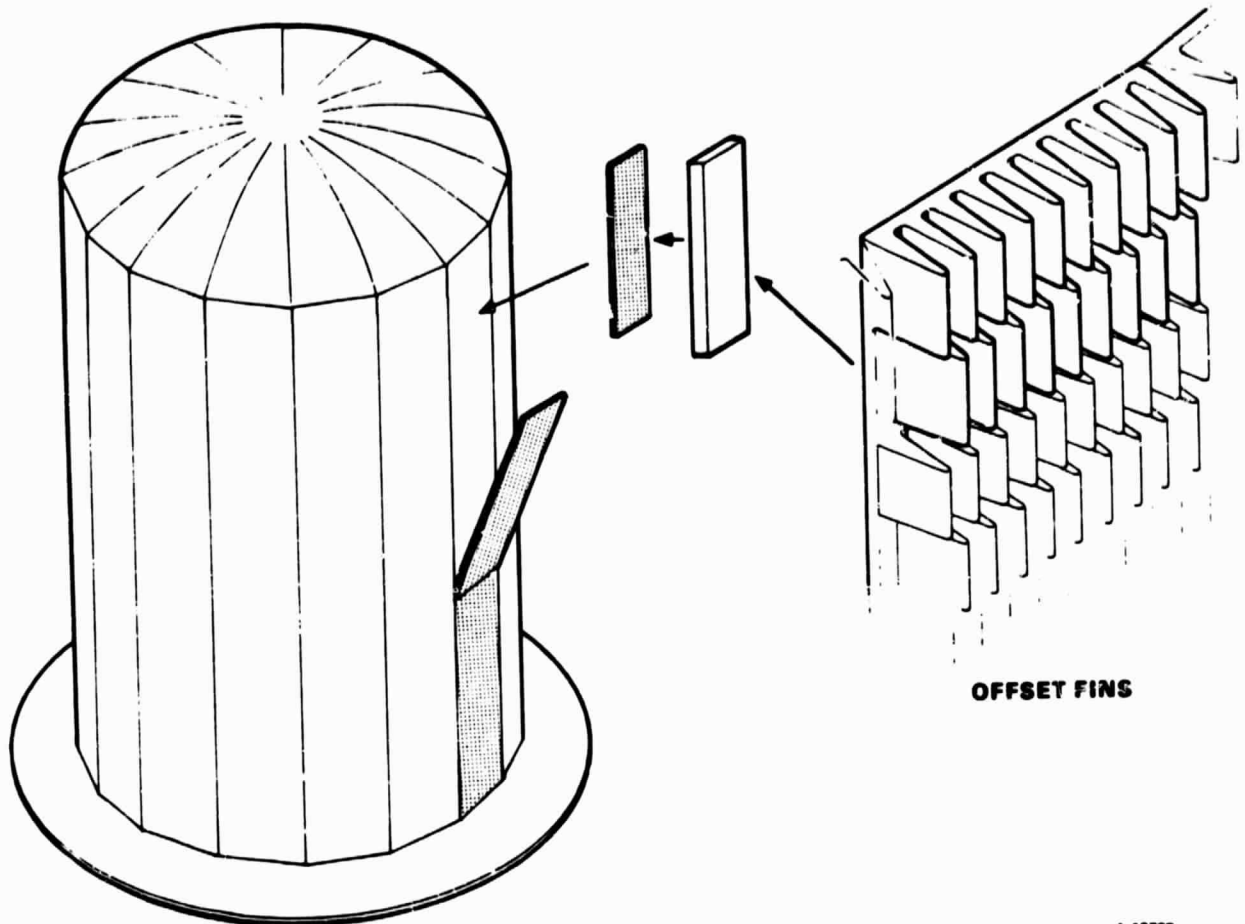
FINAL DESIGN CONFIGURATION

The mixed precision/slip-cast configuration appears to be both the smallest size and the most feasible from a manufacturing point of view. Either plain or offset fins could be used on the fin sheets, with the offset fins affording a size advantage. The selected fin is the offset fin listed in Table 3-4, 5R-0.375-0.6(0)-0.040. A schematic of the final design configuration is shown in Figure 3-8.

As shown in Figure 3-8, the fins are in the cylindrical section of the shell. There are no fins in the top or flange regions. The outer boundary of the flow passages is defined by the insulation, which is expected to be of two types. The inner portion forming the flow passages is an air-setting coating cement, which hardens to form a rigid, nonporous boundary. The outer insulation is a high-temperature, blanket-type alumina-silica product. The insulation also forms the boundary of the outlet duct, as shown in Figure 3-8.



ORIGINAL PAGE IS
OF POOR QUALITY



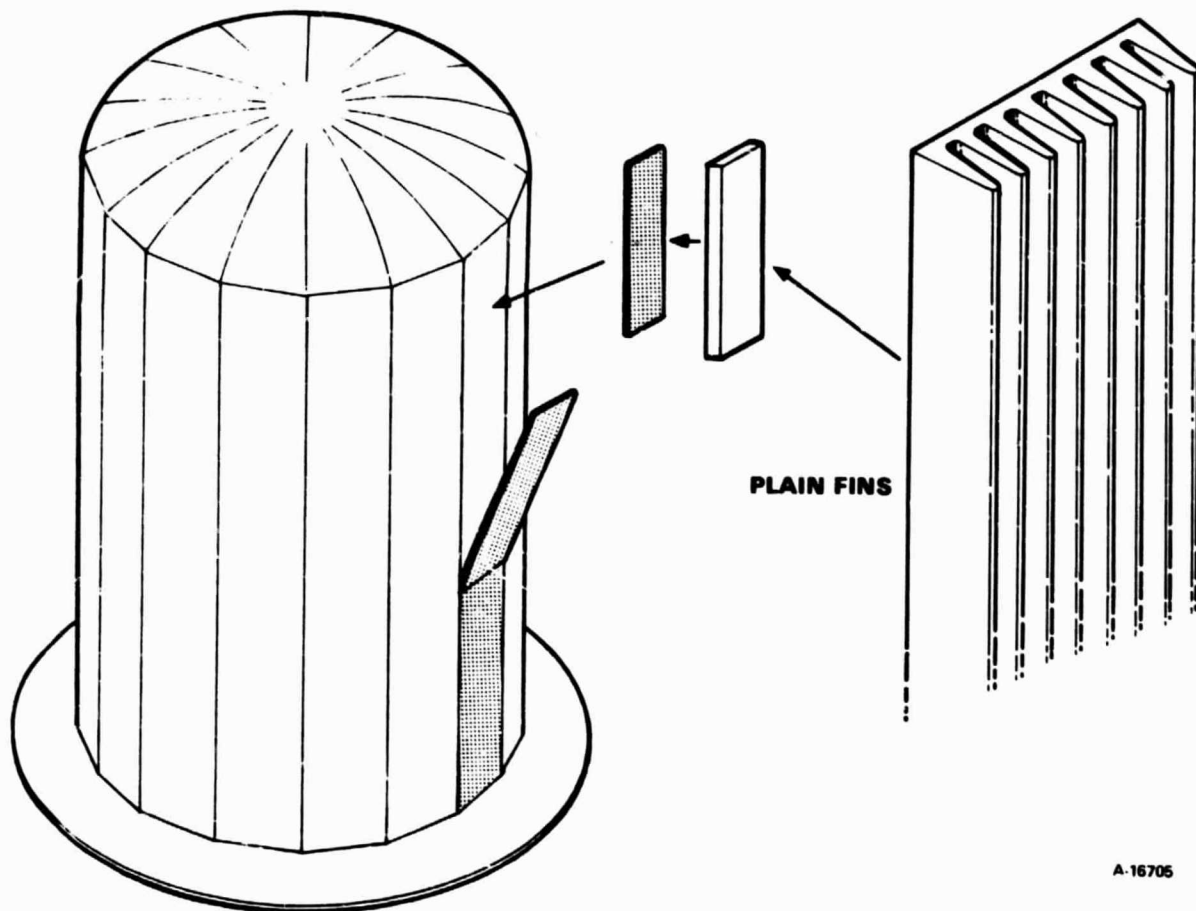
A-18708

Figure 3-6. Precision/Slip-Cast With Offset Fins



AIRESEARCH MANUFACTURING COMPANY

ORIGINAL PAGE IS
OF POOR QUALITY



A-16705

Figure 3-7. Precision/Slip-Cast With Plain Fins

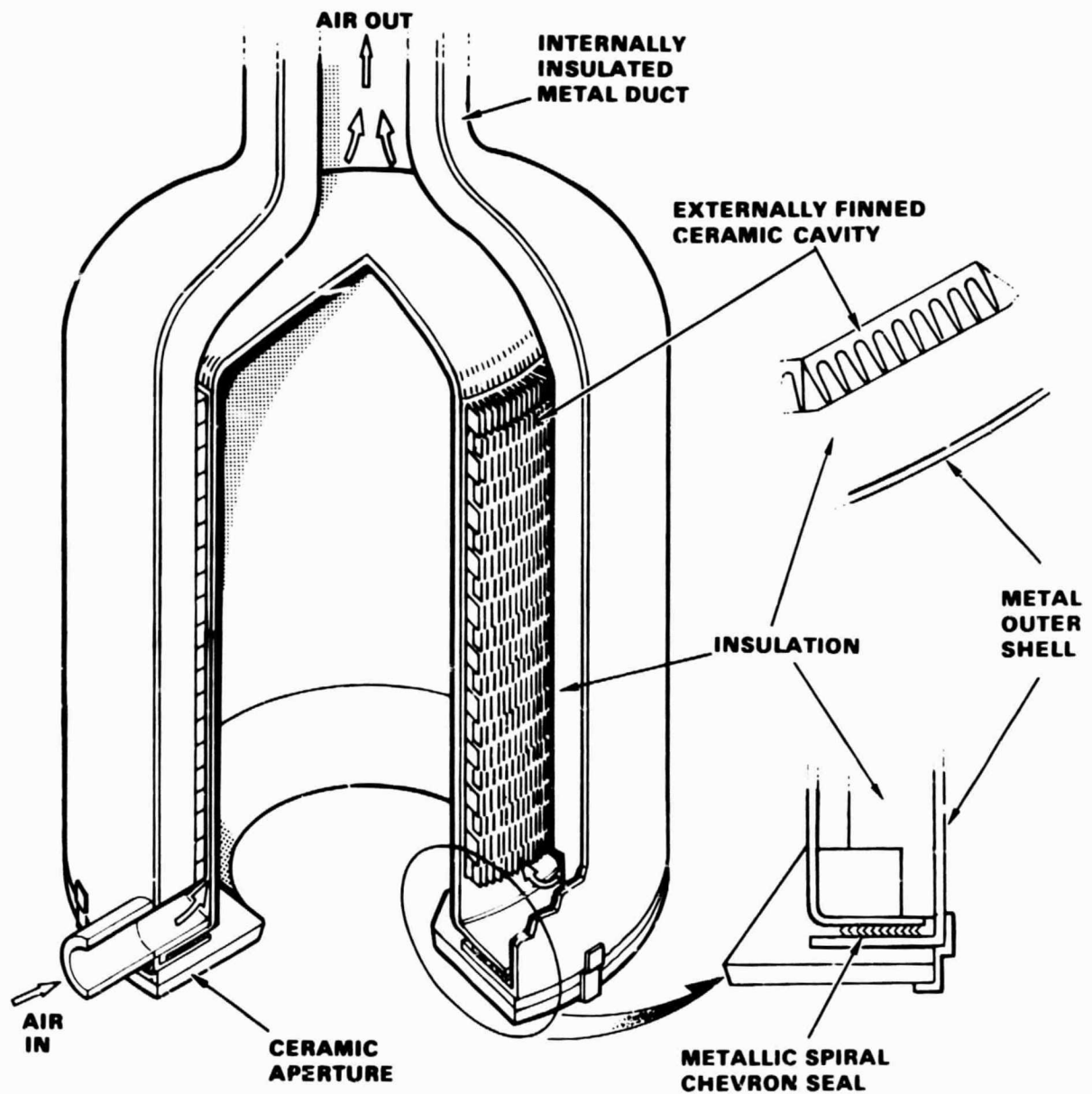


TABLE 3-4
PRELIMINARY DESIGNS

	Faceted Slip Cast	Cylindrical Slip Cast	Precision/Slip Cast	
			Plain Fins	Offset Fins
Outside diameter, in.	19.1	19.1	19.1	19.3
Active length, in.	33.0	33.0	28.0	24.0
Overall length, in.	39.5	39.5	34.5	30.5
Fin geometry	5R-0.22-P-0.075	5R-0.22-P-0.075	8R-0.25-P-0.040	5R-0.375-0.6(0)-0.040
Wall thickness, in.	0.25	0.25	0.25	0.25
Pressure drop, percent	2.80	2.80	2.21	1.87
Cavity efficiency	0.830	0.830	0.841	0.852
Maximum wall temperature °F	2392	2392	2390	2388



ORIGINAL PAGE IS
OF POOR QUALITY



A-22351

Figure 3-8. Ceramic Finned Shell Solar Receiver



Outside the insulation is the metallic outer shell (continuing into the outlet duct region). The metallic structure is sealed to the ceramic shell using a "Flexitallic" chevron seal between the metallic and ceramic flanges. The seal consists of a spirally wound strip of metal and ceramic filler on a metallic mandrel. This type of seal is under development in another AiResearch program, Electric Power Research Institute (EPRI) Project 545-2, "High Temperature Ceramic Heat Exchanger." The sealed ceramic and metallic shells form an assembly that acts as a pressure-containing vessel for the working fluid. The pressure loading acts in the direction to improve the seal. Note that the insulation is not pressure-loaded and does not act as a structural member.

Stress Levels

A stress analysis was performed for the selected design using the ANSYS computer code and the predicted axial temperature profile. A three-dimensional model was constructed as shown in Figure 3-9. This detail is desirable if the stresses are used for probabilistic reliability analysis, as discussed in the next section. The directional arrows are referenced to the receiver. Also shown in Figure 3-9 is the input axial temperature profile.

The calculated maximum tensile stresses in Table 3-5 are for the cap, cylinder, and flange sections of the receiver. The axial locations of the maximum stress levels in the cylinder section are indicated. The maximum predicted stress, about 7300 psi, is on the high end of the acceptable region. It should be possible to lower the stress level by varying the wall thickness in the flange region or altering the temperature profile by selective insulation.

TABLE 3-5

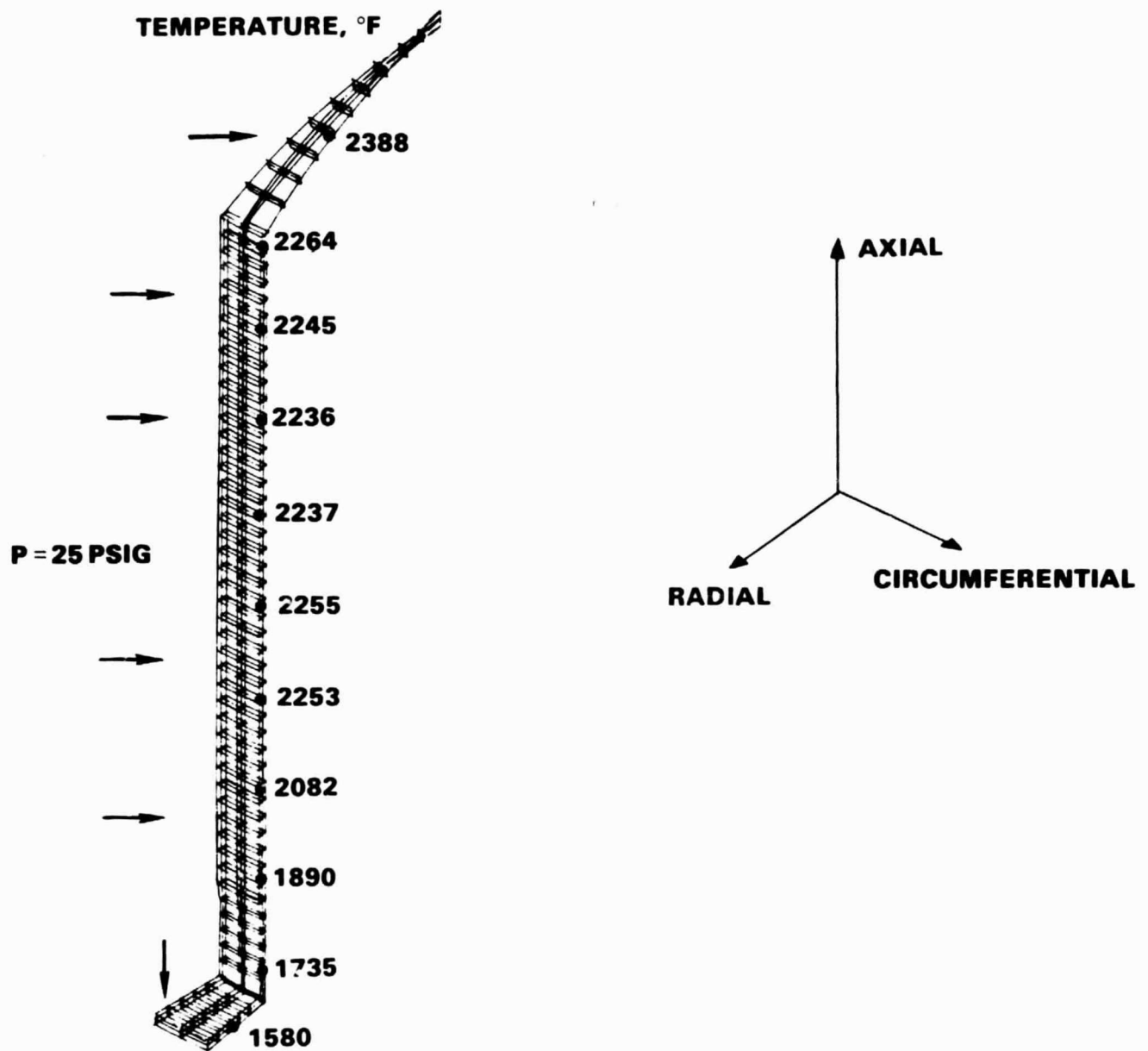
FINAL DESIGN CONFIGURATION
MAXIMUM TENSILE STRESSES, PSI

Section	Circumferential	Axial	Radial
Cap	120	560	1800
Cylinder	5900 ¹	2800 ²	1100 ³
Flange	7300	960	2700

- 1 At top, near cap
- 2 Near center
- 3 At bottom, near flange



ORIGINAL PAGE IS
OF POOR QUALITY



A-23406

Figure 3-9. Ceramic-Lin. Metal Shell Three-Dimensional, SYS Model



AIRRESEARCH MANUFACTURING COMPANY

Component Reliability

Estimates of ceramic component reliability can be calculated when an accurate, statistically significant description of the candidate material mechanical strength properties are known at the anticipated operating conditions. The brittle nature of ceramic materials precludes the use of standard design techniques. A statistical approach to design of ceramic components has been used successfully at AiResearch and elsewhere. The method used to estimate a statistical description of a ceramic engineering material and a detailed description of the probabilistic design methodology used at AiResearch can be found in the Electric Power Research Institute report High-Temperature Ceramic Heat Exchanger, EPRI FP-1127, July 1979, available from Research Reports Center (RRC), Box 50490, Palo Alto, CA 94303, (415)961-9043. Briefly, the report describes how statistical design parameters (Weibull parameters) are derived from basic material data, and how these parameters are applied to finite element stress models (mechanical and thermal) to derive an estimated component reliability. These design criteria, embodying aspects of a deterministic technique, and utilizing a probabilistic basis built into the analytical tools on an individual finite-element volume and surface area basis, are considered to provide the best approach to effective design with ceramics. In the presence of adequate materials and component test data, this approach is valid; even with a lower level of materials data, it provides a realistic method of comparing designs. This approach is being employed currently by AiResearch in the analysis of all ceramic designs including turbine and heat exchanger components. Test results, when compared with prior predictions, have been very encouraging thus far. Appendix B, "Design with Ceramic Materials," describes the design methodology and other important considerations.

For components made of NC-430, a large data base exists at a variety of temperatures and surface conditions, which enables a reasonable estimate of material properties to be made. When care is taken in the production of NC-430 components, it is possible to achieve a Weibull modulus, m , of 10 or greater and a characteristic stress, σ_0 , of 30 ksi (refer to EPRI Project 545-2 Final Report, to be published). These values were used to calculate an estimate of the ceramic liner reliability based on both a volume and surface failure assumption. The survival probability of the ceramic liner at steady-state operating conditions is estimated to be 96.5 percent based on volume probability, and 99.9 percent based on surface probability.

The reliability of each receiver liner can be increased further by proof testing the component. With NC-430, slow crack growth is not observed, therefore, the material does not exhibit time-dependent failure. For this reason, a simple over-stress proof test can be used to prove the reliability of the component. To be useful, however, the proof test stress should be greater in magnitude and duplicate the stress pattern in the component and its application.



TASK 2B, FABRICATION DEMONSTRATION

The fabrication of a prototype half-scale solar receiver ceramic liner was performed by the Norton Company. The combined slip/precision-cast technique described previously was used for the fabrication. Design Drawing 193921 and the schematic in Figure 4-1 show the demonstration model. Note that a 16-sided cylinder is specified. To demonstrate fabrication capability, full-size fins were used with the reduced size cylinder.

The fabrication program was structured in the following sequence:

1. Fabrication of the finned plates
2. Fabrication of the cylinder/flange unit
3. Assembly of the finned plates to the cylinder/flange unit
4. Siliconization/bonding of the assembly

The following paragraphs present a chronological description of the fabrication effort.

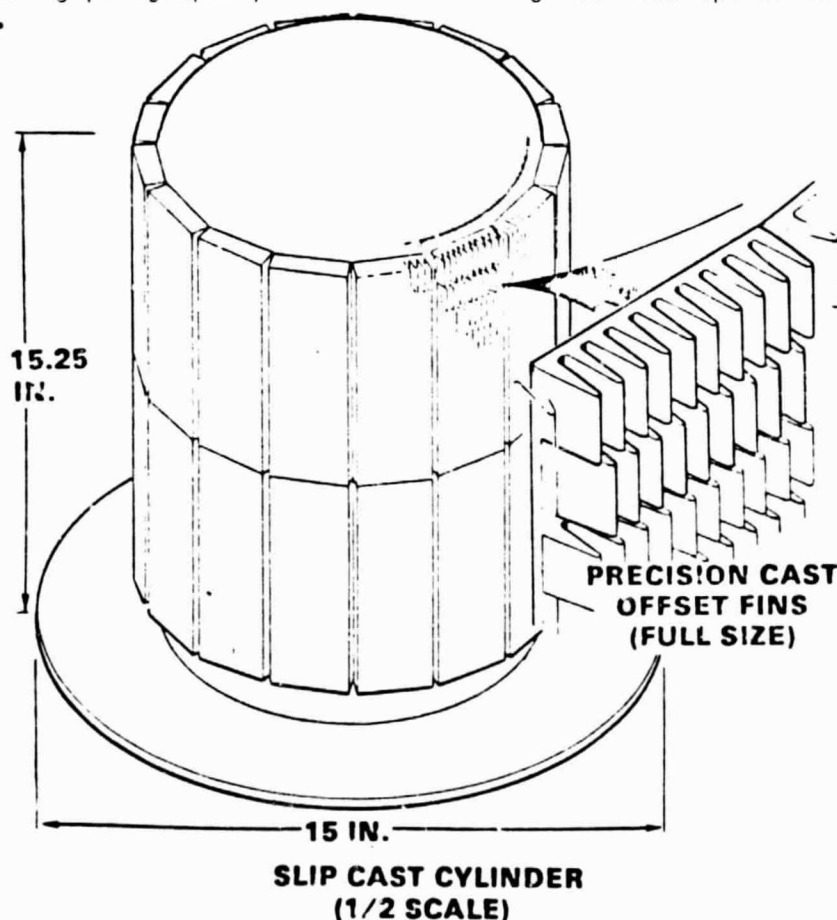
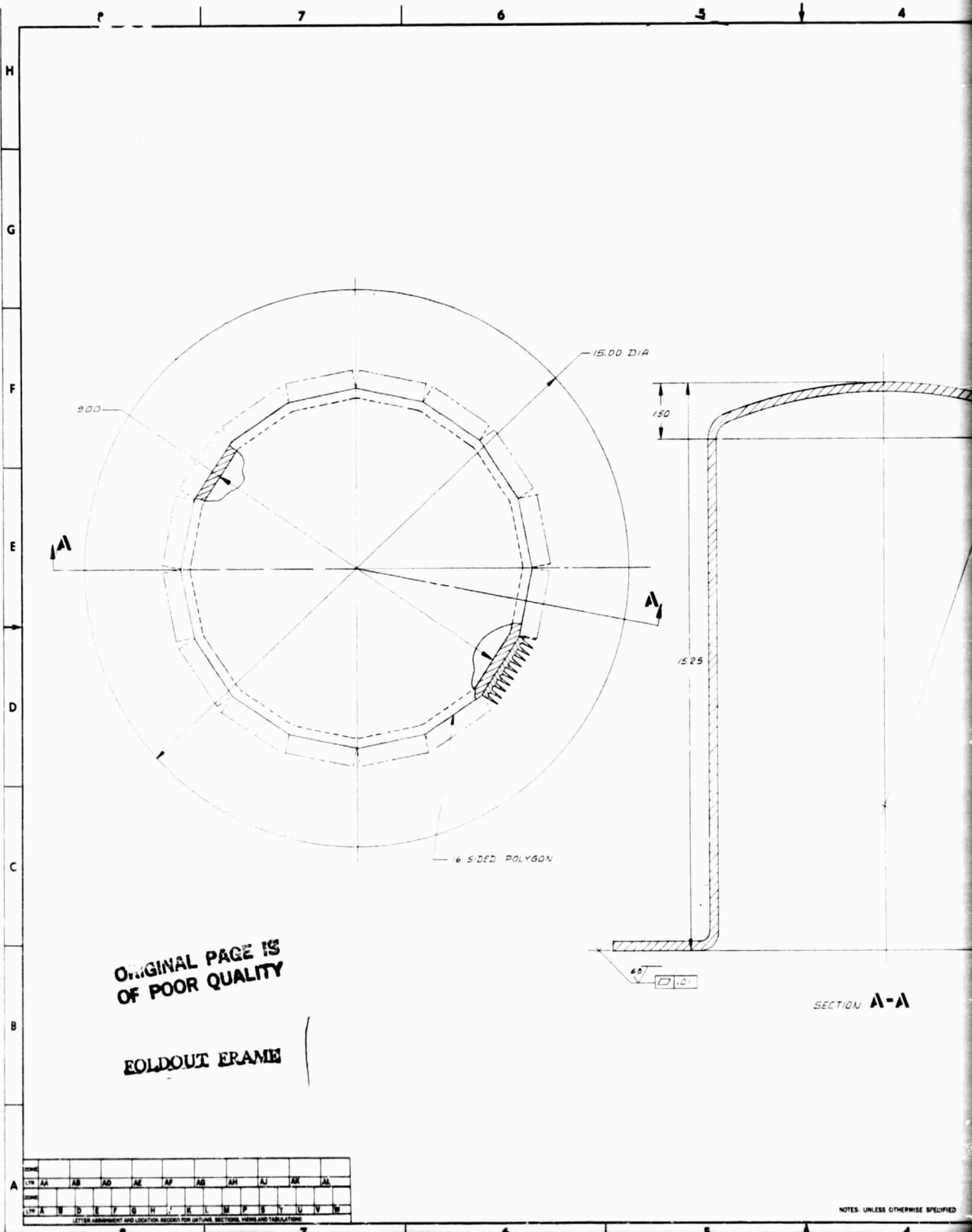


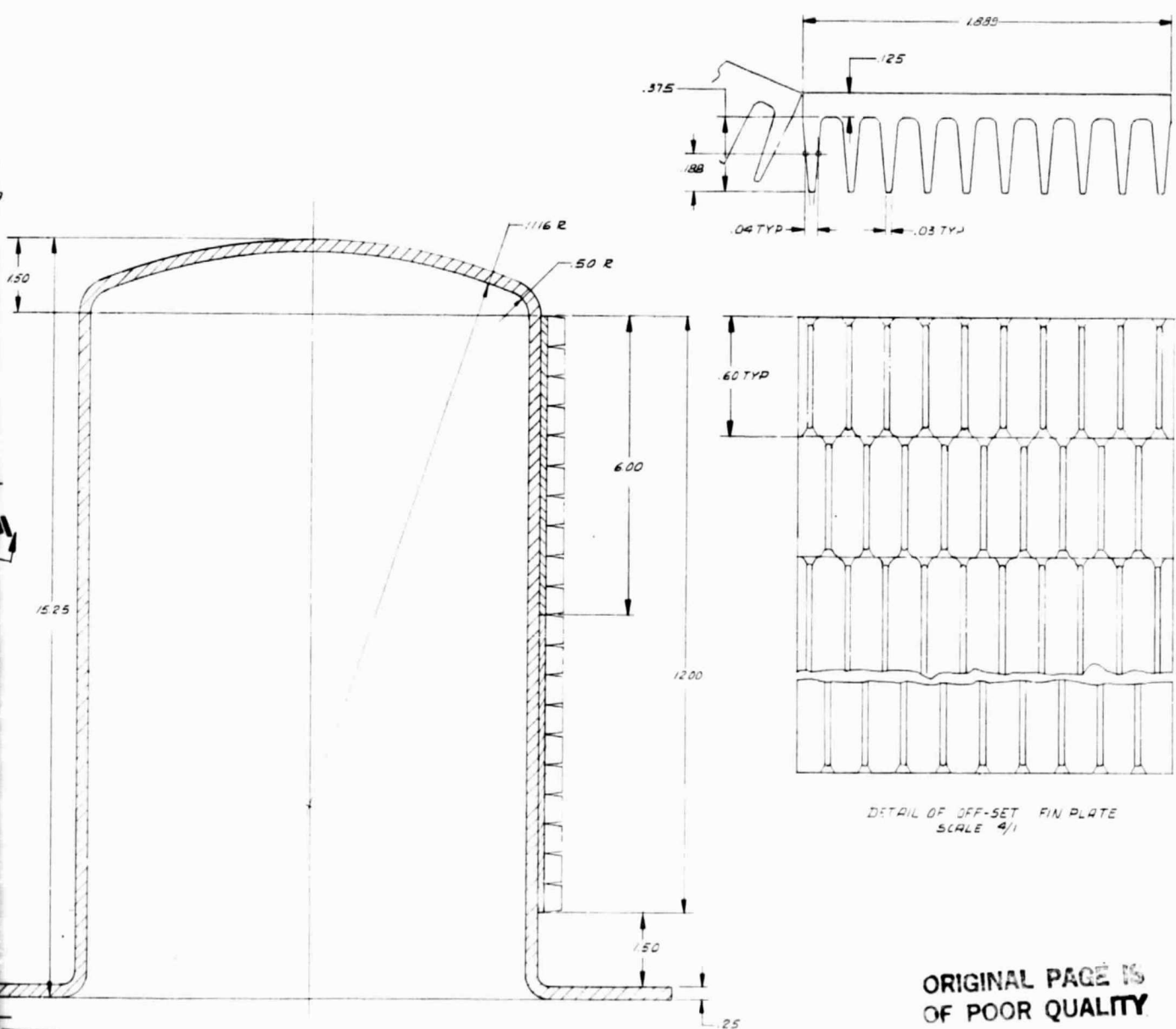
Figure 4-1. Fabrication Demonstration Model





REVISIONS		DATE	APPROVED
ZONE	LTN		

KEY STATUS



DETAIL OF OFF-SET FIN PLATE
SCALE 4/1

ORIGINAL PAGE IS
OF POOR QUALITY

2 FOLDOUT FRAME

SECTION A-A

NOTES: UNLESS OTHERWISE SPECIFIED

PART NO. 193921-1		CONTRACT NO.		AIRESEARCH MANUFACTURING COMPANY A S. 1-1000 OF THE SUBBETT CORPORATION TOMER LAKE, CALIFORNIA	
UNLESS OTHERWISE SPECIFIED: SURF CONTROL PER SC800 FIT INTERPRETATION PER ASME IDENTIFICATION MARKING PER METS		PROPERTY BY <i>2-10-1968</i>		CERAMIC LINER, PRECISION SLIP CAST	
MATERIAL CERAMIC		FINISH FALUT ENGR		E 70210 193921	
TOLERANCES FRACTIONAL		SPECIFIC SPECIFICATIONS MATERIAL SPECIFICATIONS		SCALE 1/1	
RECORD NEXT ASBY USED ON APPLICATION		DESIGNER'S SIGNATURE		SHEET 1 OF 1	

FABRICATION OF THE FINNED PLATES

An aluminum pattern of the full-size offset fin plate was machined. This is shown in Figure 4-2. The 12-in. long pattern was actually made in two 6-in. sections because it was not known whether a 12-in. ceramic plate could be precision-cast and stripped from the mold.

Closed and open molds of the 6-in. aluminum panels were made and casting trials showed that 6-in. ceramic plates could be precision-cast successfully. Casting of the full 12-in. length plate proved to be more difficult. The base of the plate was only 0.125 in. thick and tended to fracture during stripping. Alternate stripping techniques were tried to minimize the bending stresses placed on the plate during stripping. After numerous attempts a satisfactory stripping technique was arrived at which allowed successful stripping of 90 percent of the cast plates.

After solving the stripping problems, attention was turned to the problem of incomplete formation of the tips and corners of the fins. Initial castings of finned plates had areas where the fins were only partially formed due to incomplete filling of the mold, air entrapment in the plastic mass, and premature drying of the mass prior to complete filling of the mold. Deairing of the plastic mass, open mold casting, and vibration were evaluated and found to be helpful in minimizing the problem. Figure 4-3 shows a close-up view of a row of fins that had incomplete corner filling. As Figure 4-3 shows, the portion of missing fin is minimal and only causes the corner to appear chamfered.

A series of 12-in. long plates were fabricated. Some of these are shown in Figure 4-4 awaiting assembly with the cylinder section.

FABRICATION OF THE CYLINDER/FLANGE UNIT

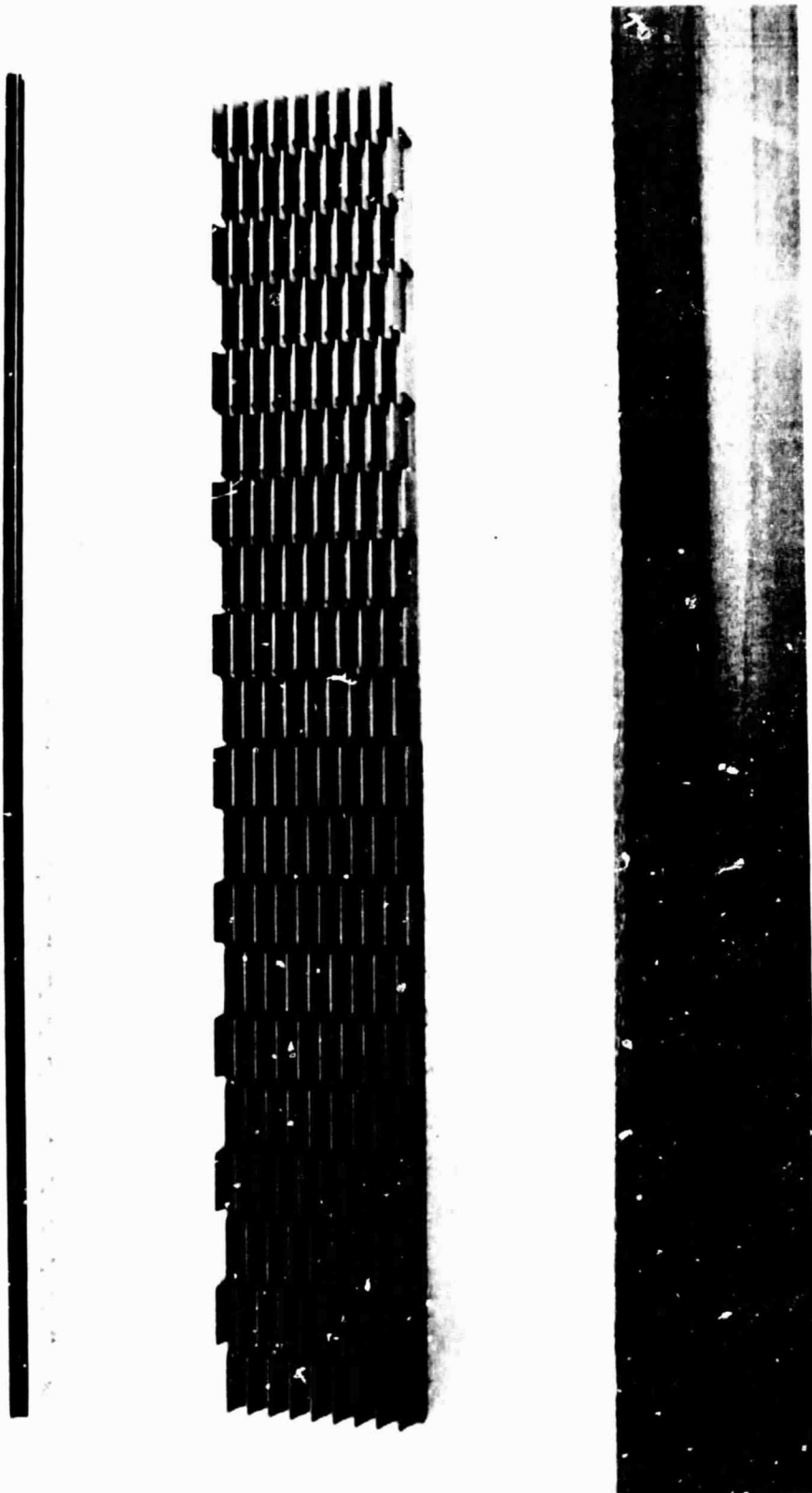
Figure 4-5 shows the wooden pattern of the 16-sided cylinder/flange along with the wooden mold setup. The pattern and setup were used to make the two-piece plaster mold required for slip casting the cylinder. The mold is shown in Figure 4-6. The mold was designed to produce the cylinder and flange in a single ceramic piece (note the flange pattern at the top of the photograph in Figure 4-6).

The cast cylinder is shown in Figure 4-4. The 16 sides of the cylinder are flat and straight, with no apparent defects in any area. The flange section of the receiver stripped from the mold with a minimum of effort. The flange had no stripping or drying cracks around its circumference or in the area where the flange attaches to the cylinder. No cracks were found on any part of the cast cylinder.

ASSEMBLY OF THE FINNED PLATES TO THE CYLINDER/FLANGE UNIT

Sixteen of the best finned panels were selected based on their dimensional accuracy and their flatness. It was found that all the finned panels had varying degrees of warpage resulting from the casting and drying technique used.

ORIGINAL PAGE IS
OF POOR QUALITY



F-35678

Figure 4-2. Aluminum Finned Panel Pattern



ORIGINAL PAGE IS
OF POOR QUALITY

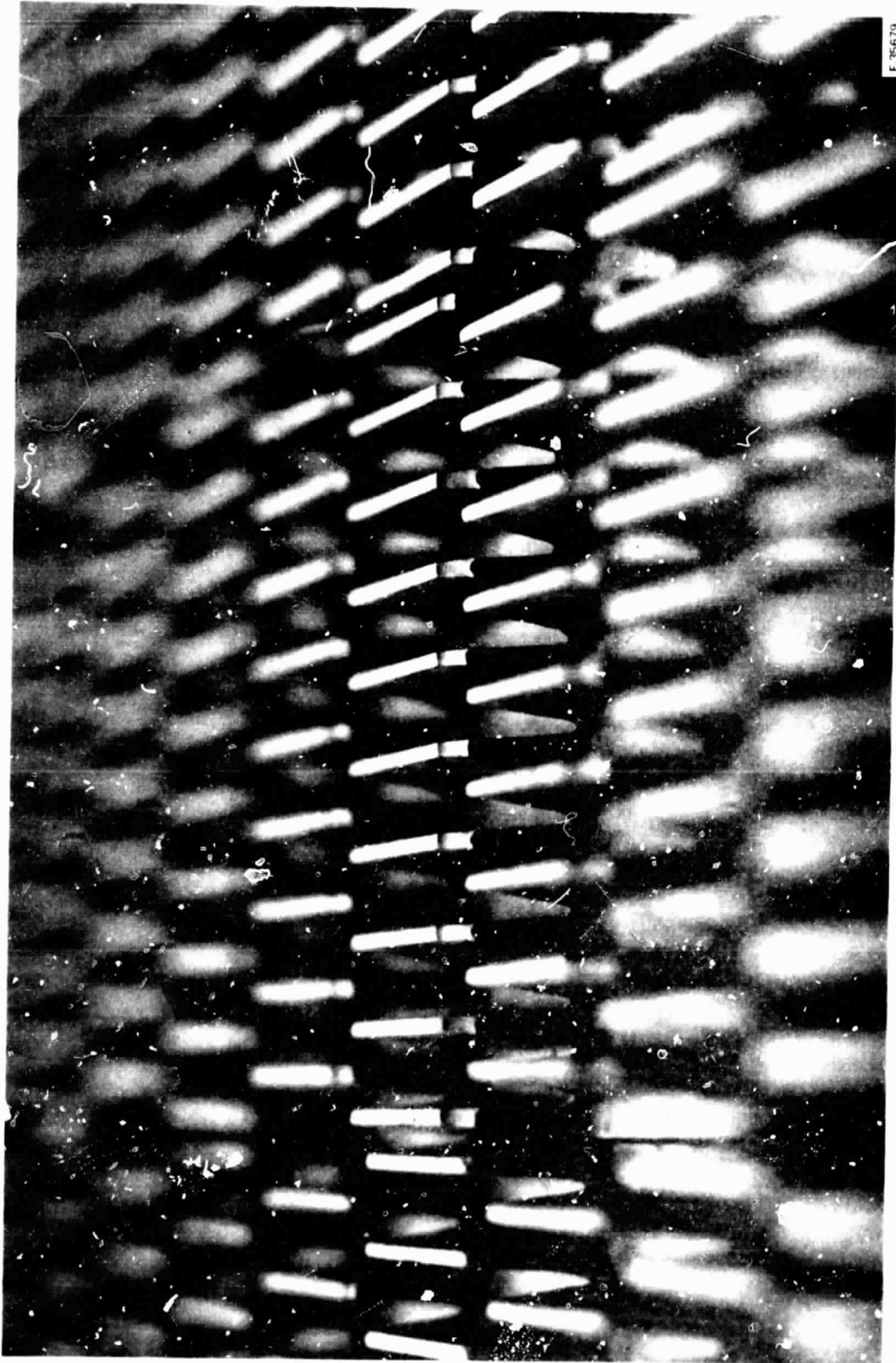


Figure 4-3. SiC Finned Panel Showing Incomplete Corner Formation on a Row of Fins



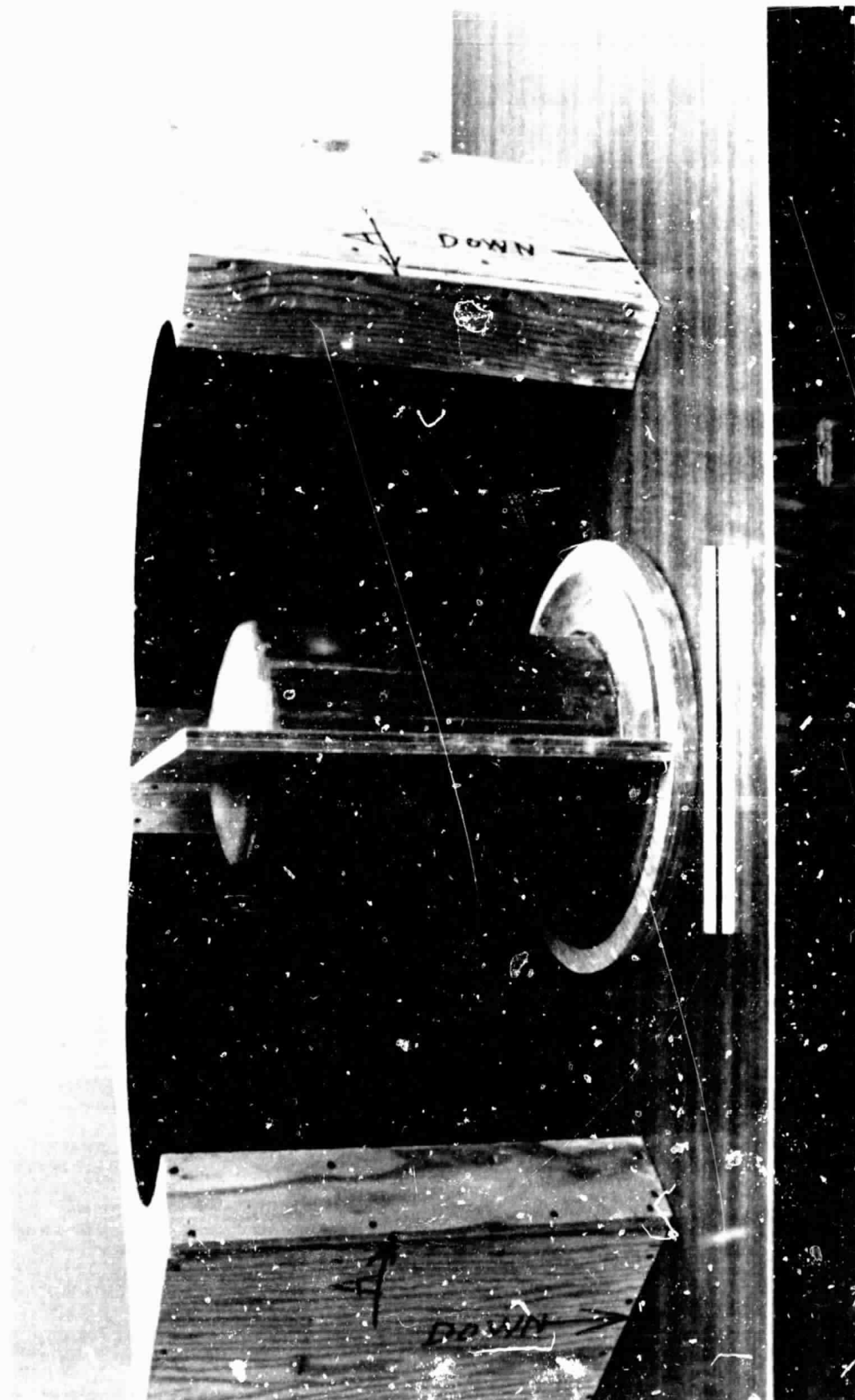
ORIGINAL PAGE IS
OF POOR QUALITY



Figure 4-4. Finned Plates and Cylinder Awaiting Assembly



ORIGINAL PAGE IS
OF POOR QUALITY



F 35680

Figure 4-5. 16-Sided Domed Cylinder Pattern and Setup



AIRESEARCH MANUFACTURING COMPANY

ORIGINAL PAGE
BLACK AND WHITE PHOTOGRAPH

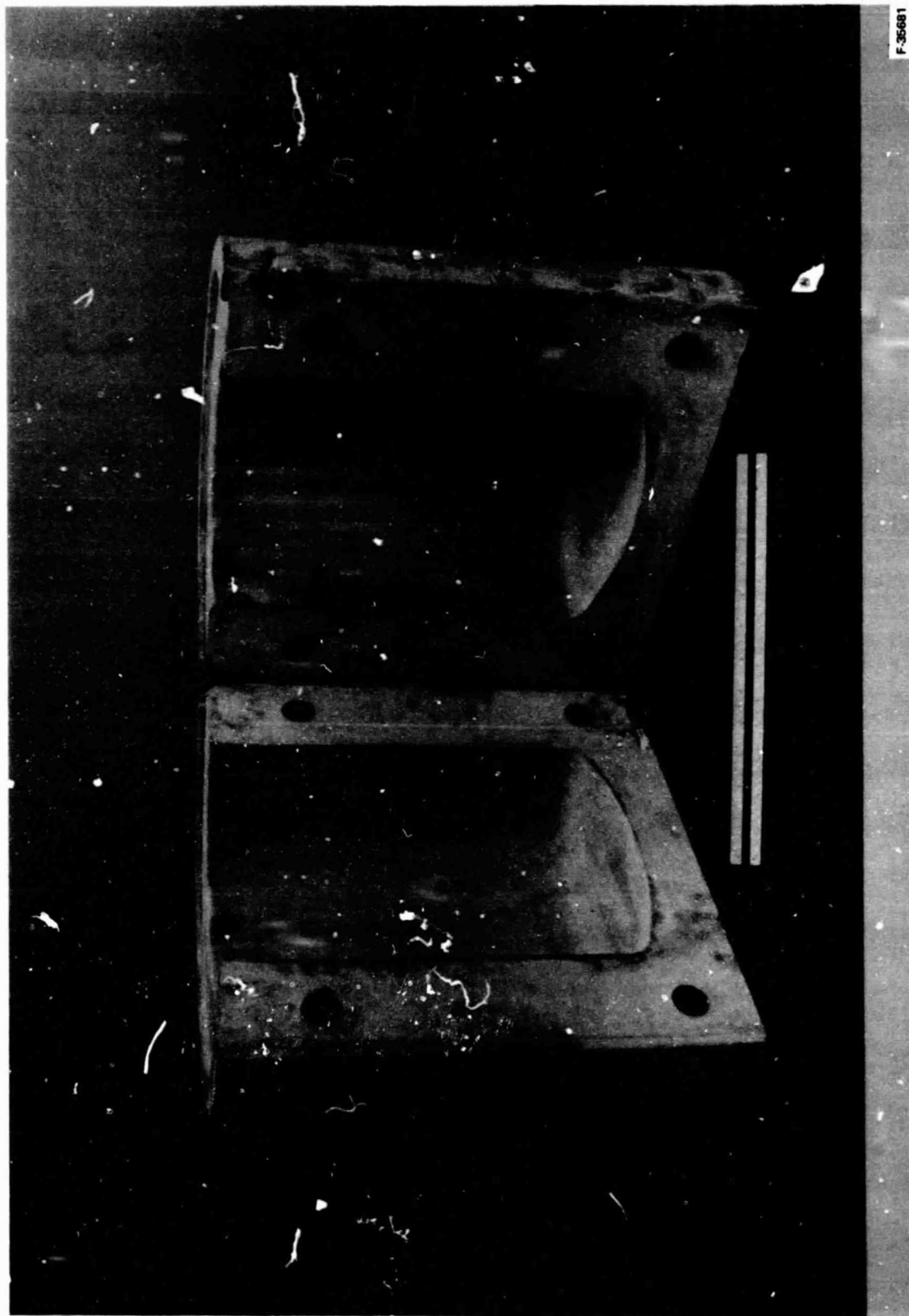


Figure 4-6. Two-Piece Domed Cylinder Plaster Mold

C-2



AIRESEARCH MANUFACTURING COMPANY

ORIGINAL PAGE IS OF POOR QUALITY

Humidity controlled drying will have to be used in the future to ensure uniform drying of the finned panels. The warpage was found to be as much as 0.125 in. over the 12-in. length on some panels. Average warpage was approximately 0.060 in. and occurred both toward and away from the finned side of the panel.

The finned plates and the cylinder were fired at low temperature to increase the strength and handling characteristics. The plates were then attached to the cylinder with a fine-grained adhesive SiC composition. Each panel was attached while holding the surface of the fins as parallel to the cylinder side as the warpage would allow. Figure 4-7 shows the cylinder with five panels attached in place, while Figure 4-8 is a close-up view of the panel to cylinder and panel to panel adhesion. The final assembly after attachment and drying is shown in Figure 4-9.

The time required for adhesion was in excess of the original projections due to the warpage of the panels which necessitated more adhesive and longer drying times. Improved warpage control will significantly reduce adhesion time per assembly.

SILICONIZATION/BONDING OF THE ASSEMBLY

The assembly was loaded into an induction furnace along with silicon metal in excess of that required to fill the porosity of the SiC microstructure and bond area. The assembly was fired to a temperature normal for the NC-430 product line.

Siliconization was successful, with the assembly showing no cracks or unimpregnated areas by visual inspection; complete bonding was achieved between the finned plates and the cylinder. There were, however, areas between adjoining fins where silicon metal had accumulated during firing. Clean-up of the ceramic liner was done by grit blasting. There were areas where the metal could not be completely removed without severe erosion of the fins. Excess metal also caused some of the fins on the ceramic liner to be completely or partially broken due to thermal expansion mismatch.

The broken fins were repaired and the ceramic liner was fired again with no additional silicon metal. It was hoped that the excess metal would melt and run off the receiver at elevated temperatures. When the receiver was removed from the furnace, the repaired fins were fully impregnated, but the excess metal problem persisted. The excess metal caused total blockage between approximately 40 adjoining fins which was not considered too severe when compared to the total number of fins on the ceramic liner (3040 fins).

To improve the overall appearance of the ceramic liner, the excess silicon was removed using a hand-held high speed drill with diamond plated (60-80 grit) grinding tools. Metal removal was fast and only two fins were broken off during grinding.

The completed ceramic liner is shown in Figure 4-10. Various close-up views are shown in Figures 4-11 through 4-13. These photographs show the excellent fin definition and the small amount of fin erosion and breakage.



ORIGINAL PAGE
BLACK AND WHITE PHOTOGRAPH

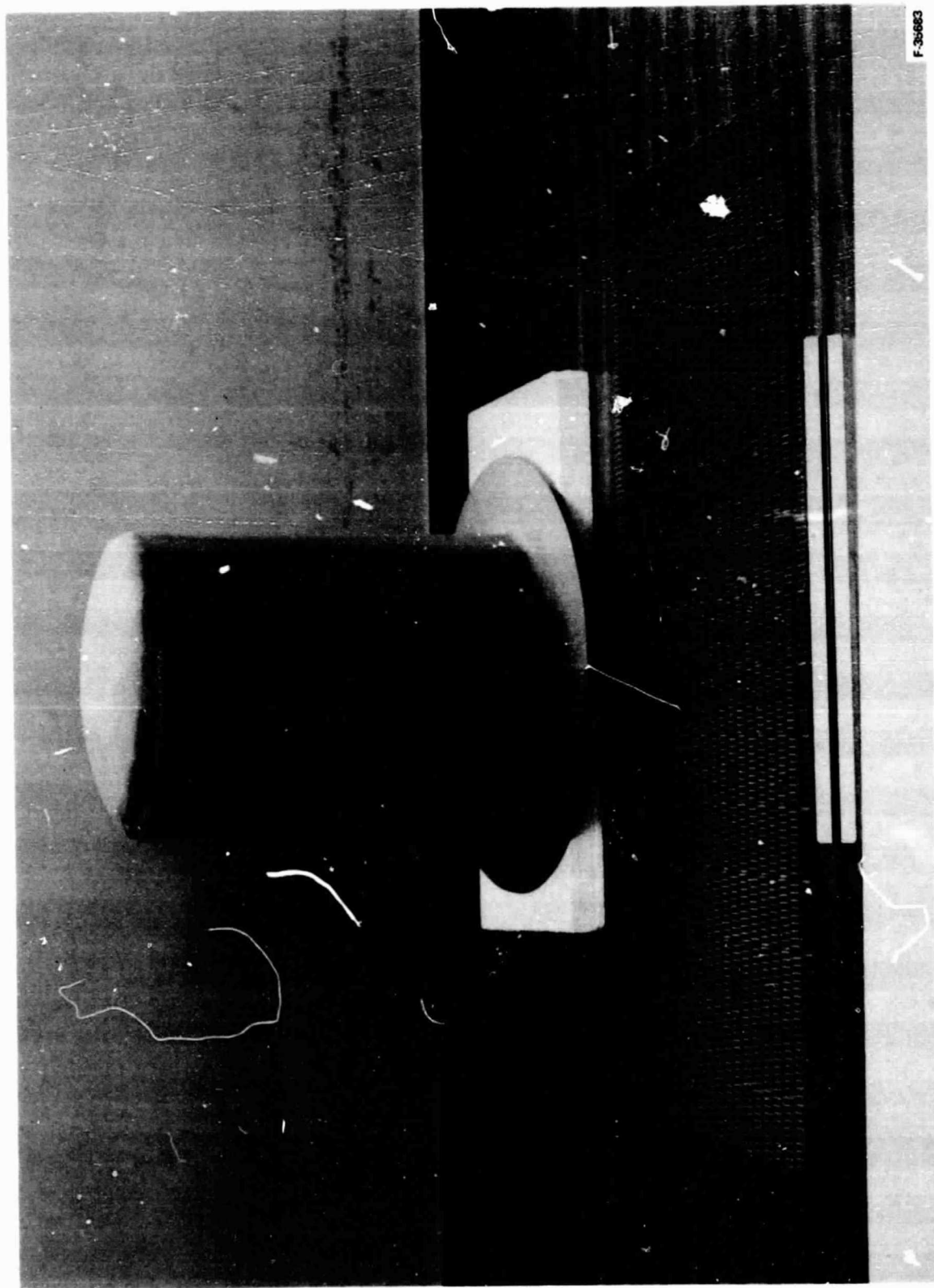


Figure 4-7. Appearance of Ceramic Receiver During Assembly Operation



ORIGINAL PAGE
BLACK AND WHITE PHOTOGRAPH

F-35684

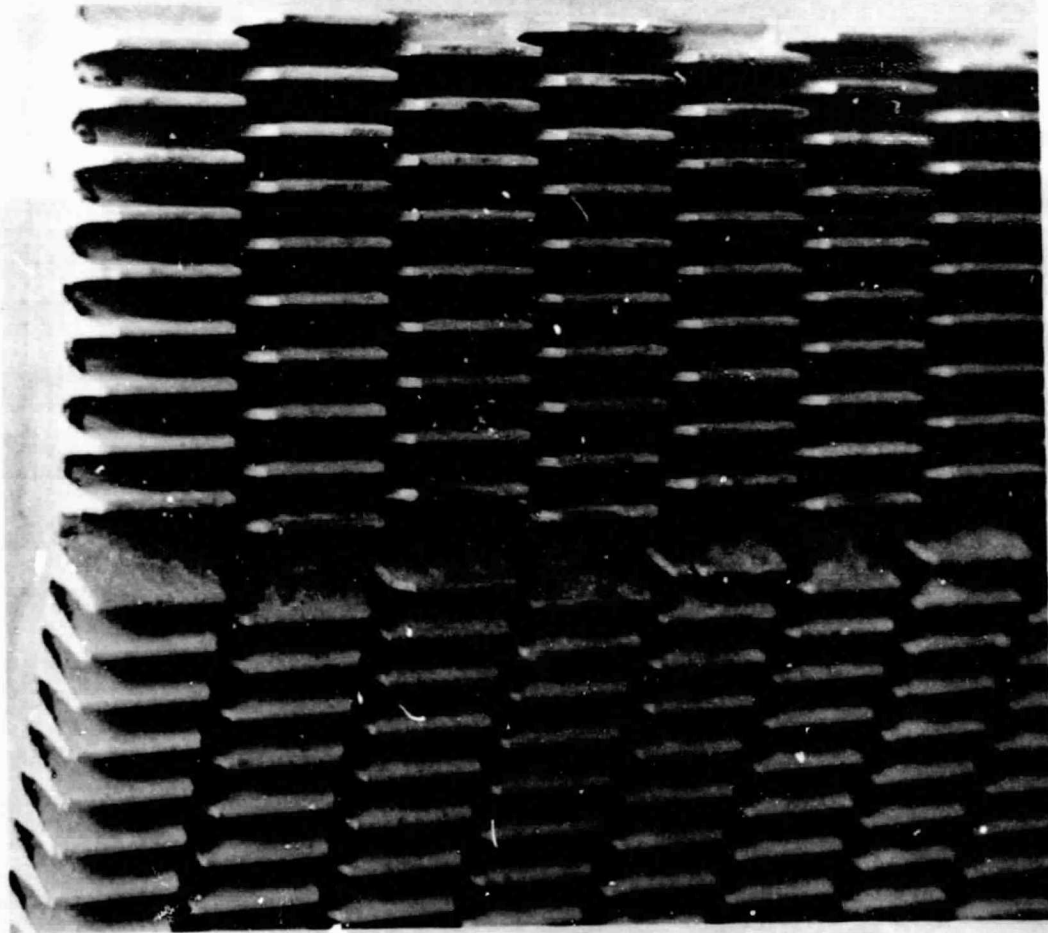


Figure 4-8. View of Finned Panel Assembled on the Cylinder



ORIGINAL PAGE
BLACK AND WHITE PHOTOGRAPH

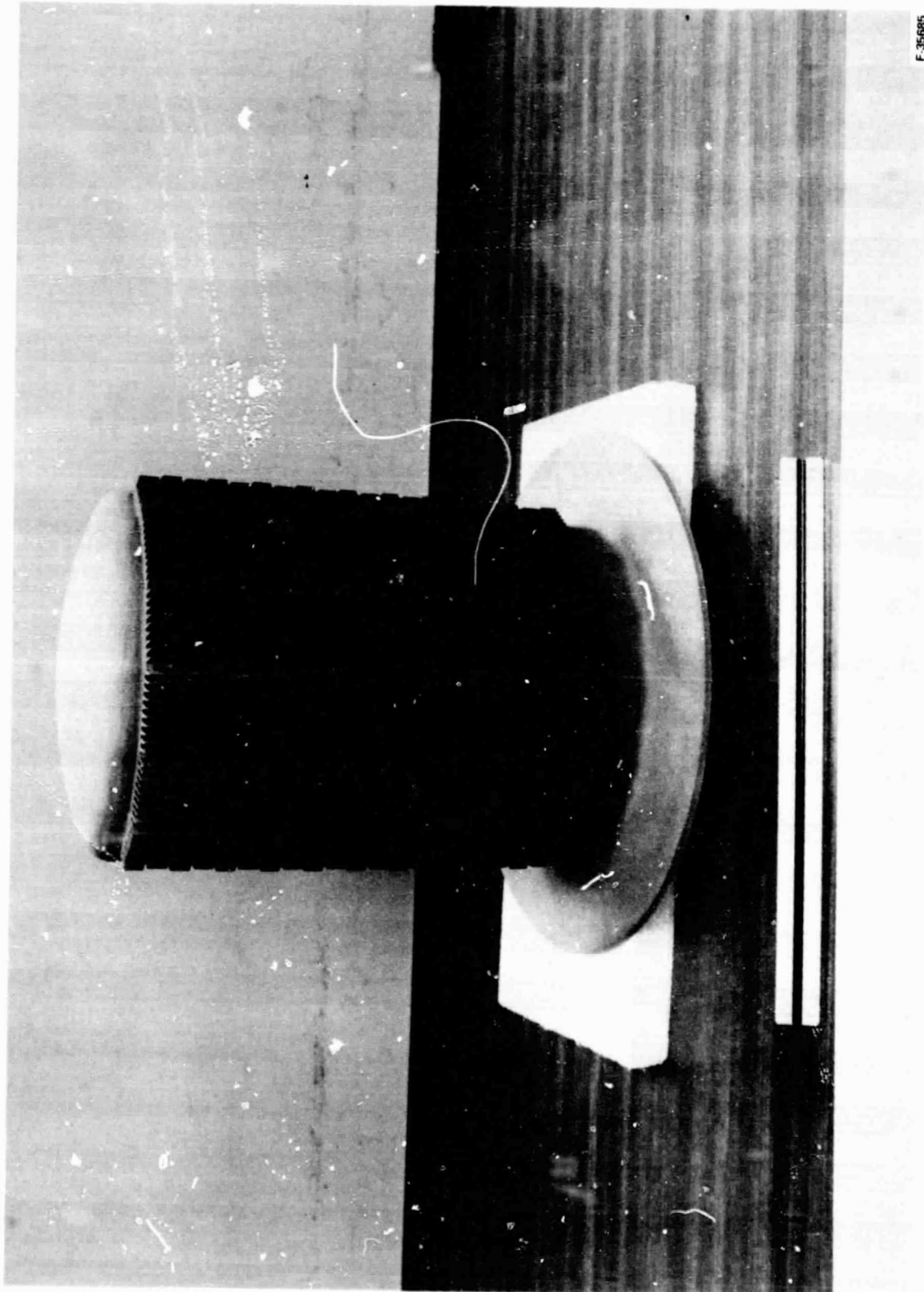


Figure 4-9. Final Assembly

ORIGINAL PAGE
BLACK AND WHITE PHOTOGRAPH



1 2 3 4 5 6 7 8 9 10 11 12

85601-7

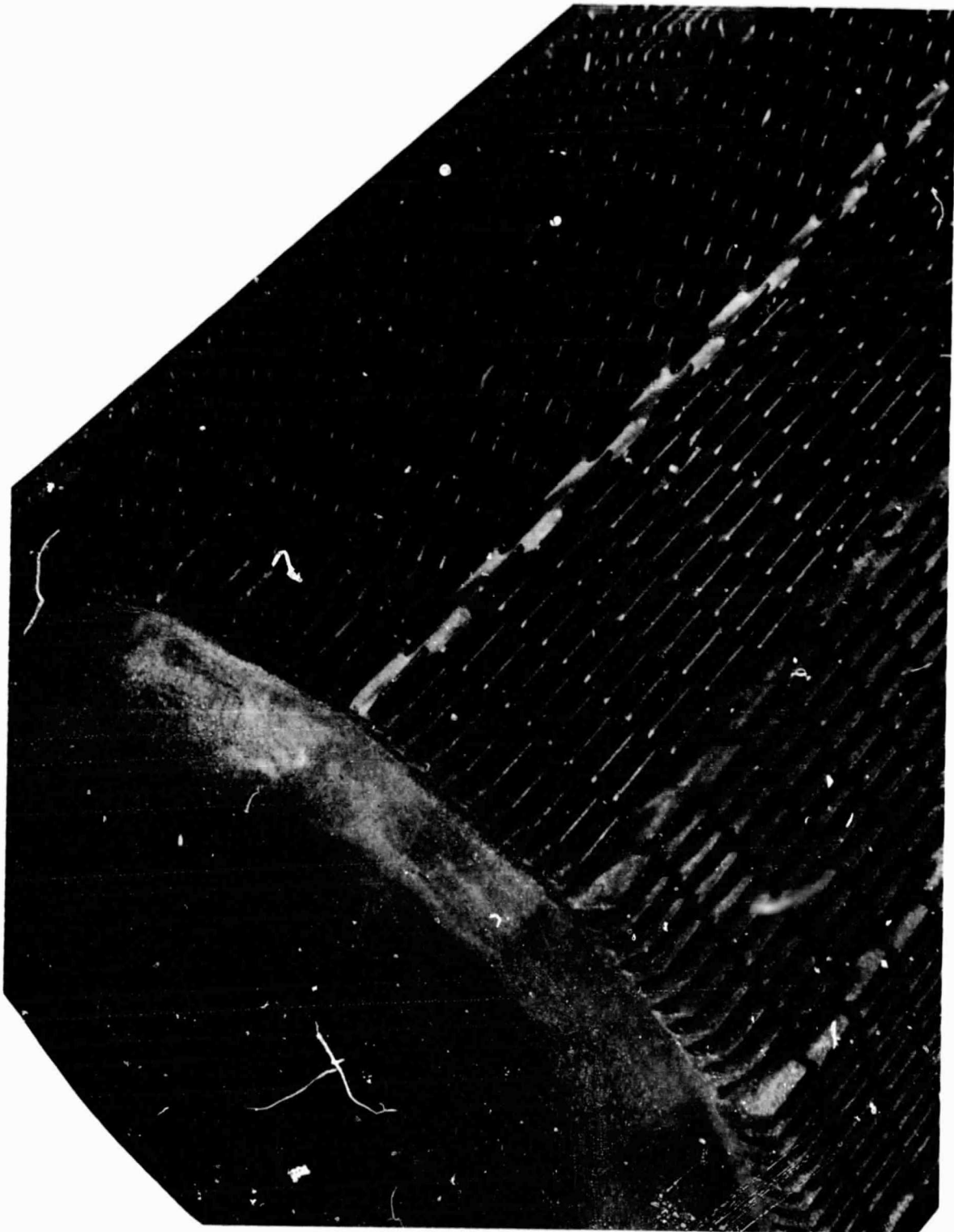
F.35716

Figure 4-10. Complete Ceramic Liner



AIRESEARCH MANUFACTURING COMPANY

ORIGINAL PAGE
BLACK AND WHITE PHOTOGRAPH



85601-3

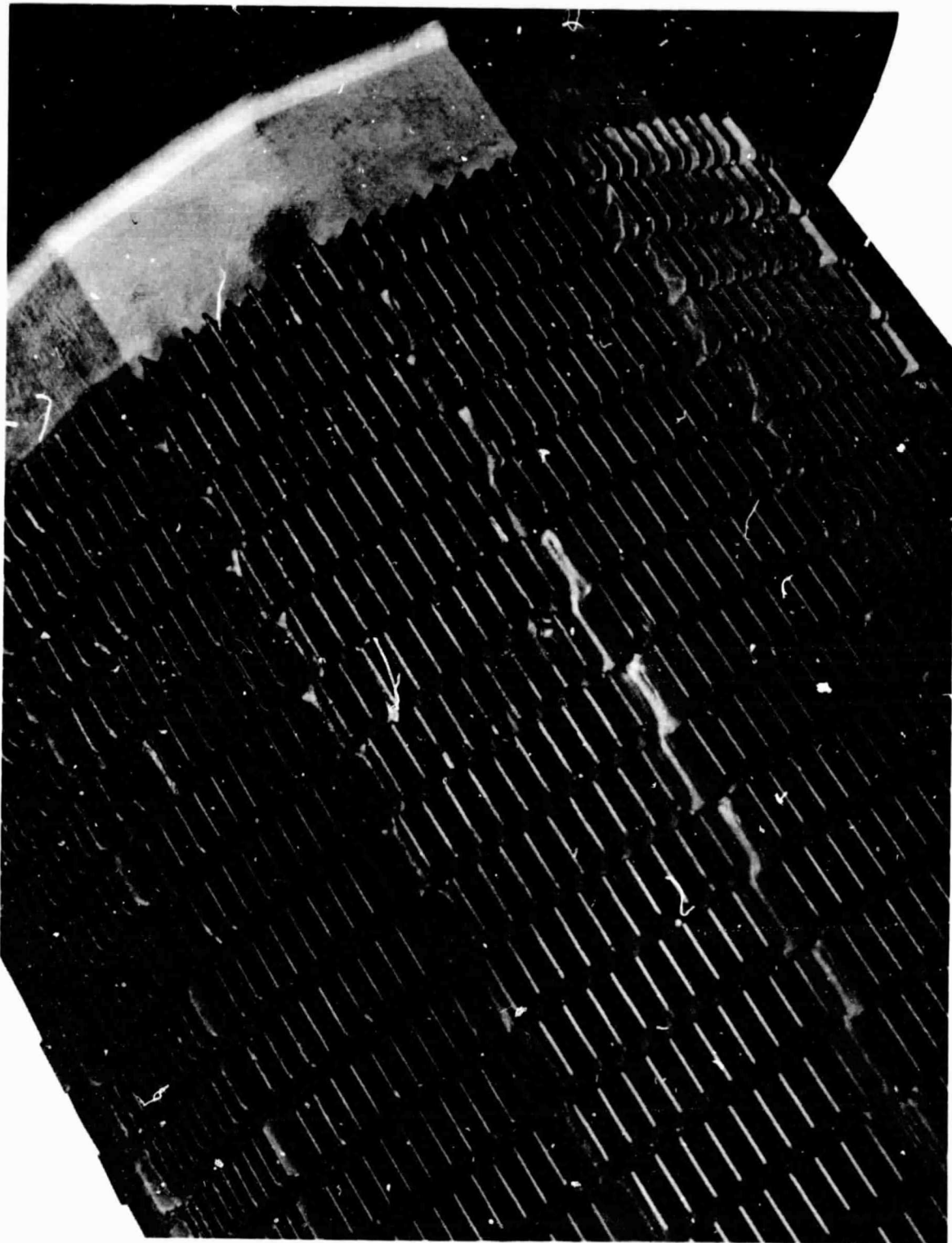
F 35714

Figure 4-11. Ceramic Liner Close-up



AIRESEARCH MANUFACTURING COMPANY

ORIGINAL PAGE
BLACK AND WHITE PHOTOGRAPH



85601-1

F.35713

Figure 4-12. Ceramic Liner Fin Detail



ORIGINAL PAGE
BLACK AND WHITE PHOTOGRAPH



85601-4

F-35715

Figure 4-13. Ceramic Liner Underside



**ORIGINAL PAGE IS
OF POOR QUALITY**

APPENDIX A
ALTERNATE MATERIAL SYSTEM DESIGN

APPENDIX A

ALTERNATE MATERIAL SYSTEM DESIGN

The present material for the ceramic receiver, NC-430 siliconized-silicon carbide, has some definite limitations. It is suggested that an alternate material, sintered alpha silicon carbide (SASC), be considered. According to a manufacturer of SASC, the Carborundum Company, the fabrication technology for SASC parts has advanced significantly over the past 2 years. Prior SASC technology had only limited fabrication and joining capability. Since all receiver concepts except one required joining (bonding), SASC did not appear to be a desirable material for the receiver. However, the selected design turned out to be the one that, in principle, could be fabricated without bonding (although the recommended fabrication approach with NC-430 does involve bonding). With its improved fabrication technology, Carborundum believes that a single piece (no bonding) receiver, of the ceramic-lined metal shell type, could be fabricated out of SASC. Carborundum has presented a proposal to AiResearch for the fabrication of a prototype full-size SASC receiver, with plain fins as the heat transfer surface.

The SASC material exhibits higher strength and higher temperature capability than does NC-430. The higher strength, when factored into the probabilistic analysis, results in a higher predicted receiver reliability. If operated at a higher temperature, the receiver size can be reduced. This is because a higher wall temperature affords a larger mean temperature difference between the wall and the working fluid; this reduces the required heat exchanger size.

A parametric design study was conducted using AiResearch computer program RECMDL for SASC receivers of the ceramic-lined metal shell type. Fin geometries expected to be achievable by Carborundum are assumed. The results of the study are presented in Table A-1.

The high temperature capability of the SASC allows selection of a 1.5-ft diameter by 1.5-ft length design, for example, the 8R-0.30-P-0.060 fin. This is 6 in. shorter than the NC-430 final design configuration. Operation at higher wall temperatures does result in a cavity efficiency penalty, however--0.824 as compared to 0.852 for the final design configuration.



ORIGINAL PAGE IS
OF POOR QUALITY

TABLE A-1
SASC RECEIVER STUDY

Diameter, ft	Length, ft	Fin Geometry	Maximum Wall Temperature, °F	Pressure Drop, percent	Cavity Efficiency
1.5	1.5	8R-0.30-P-0.060	2589	2.09	0.824
1.5	1.5	8R-0.28-P-0.060	2593	2.35	0.823
1.5	1.5	8R-0.26-P-0.060	2596	2.68	0.823
1.5	2.0	8R-0.30-P-0.060	2436	2.78	0.841
1.5	2.0	8R-0.28-P-0.060	2439	3.12	0.841
1.5	2.5	8R-0.30-P-0.060	2346	3.47	0.847
1.5	2.5	8R-0.28-P-0.060	2348	3.90	0.847



APPENDIX B
DESIGN WITH CERAMIC MATERIALS

APPENDIX B
DESIGN WITH CERAMIC MATERIALS

This appendix describes the structural design details for components fabricated from ceramic materials.

THEORY

Many structural ceramics are very strong, high-temperature materials. Some ceramic materials such as SiC and Si_3N_4 have thermal conductivities greater than stainless steel above 1400° F. Ceramics also are brittle and shatter with sharp impact. Unlike most metals, which show some plastic deformation before fracture, ceramic materials show linear elastic response (except near their melting point) to applied stress until catastrophic failure occurs. For this reason, ceramic materials are generally termed "unforgiving." This is shown schematically in Figure B-1 for a sintered silicon carbide and a mild steel. Note that the strain scale on each graph is quite different and that if the ceramic curve were plotted on the metal graph, it would rise almost vertically. Ceramic materials usually have compressive strengths that are three to four times greater than their tensile strength. For this reason, most ceramic components fail from tensile overloading. Ceramics have an unusual combination of properties for which the design engineer must use special design techniques.

Because ceramics do not deform plastically, small inclusions, cracks, point loading, and mechanical shock can cause catastrophic failure. In all of these cases, the inability of the ceramic material to locally deform to relieve the applied stress causes local stress concentrations that can promote crack formation or crack extension. If a crack develops to a critical size, spontaneous crack extension can proceed on stored elastic strain energy to cause catastrophic failure.

Maximum tensile stresses typically occur on the surface of stressed components where flaws of about 10 μm can cause failure of high-performance ceramics at very high stresses. Therefore, the surface finish usually controls the ultimate strength of ceramic components. If components are processed in a consistent way, their surfaces will have a characteristic distribution of flaws that will control the ultimate strength. Because strength is controlled by a distribution of flaws, measured strengths can have a wide variation within a group of samples processed and tested under the same conditions. The observed distribution (skewed to the high strengths) is most accurately described by a Weibull distribution, which is a subcase of the compound Poisson process used to describe natural events that are random in time (such as traffic flow or agricultural and ecological events). The Weibull "Weakest Link Theory" assumes that in a uniformly stressed body, surface element, or volume element, the largest flaw (weakest link) causes failure. The parameters of the Weibull distribution (which must be experimentally determined) are a function of the type of material and its surface and volume condition. The Weibull parameters are engineering design parameters that describe flaw distributions on a particular set of samples. The Weibull parameters are not material constants and they do not define flaw severity or material strength.



ORIGINAL PAGE IS
OF POOR QUALITY

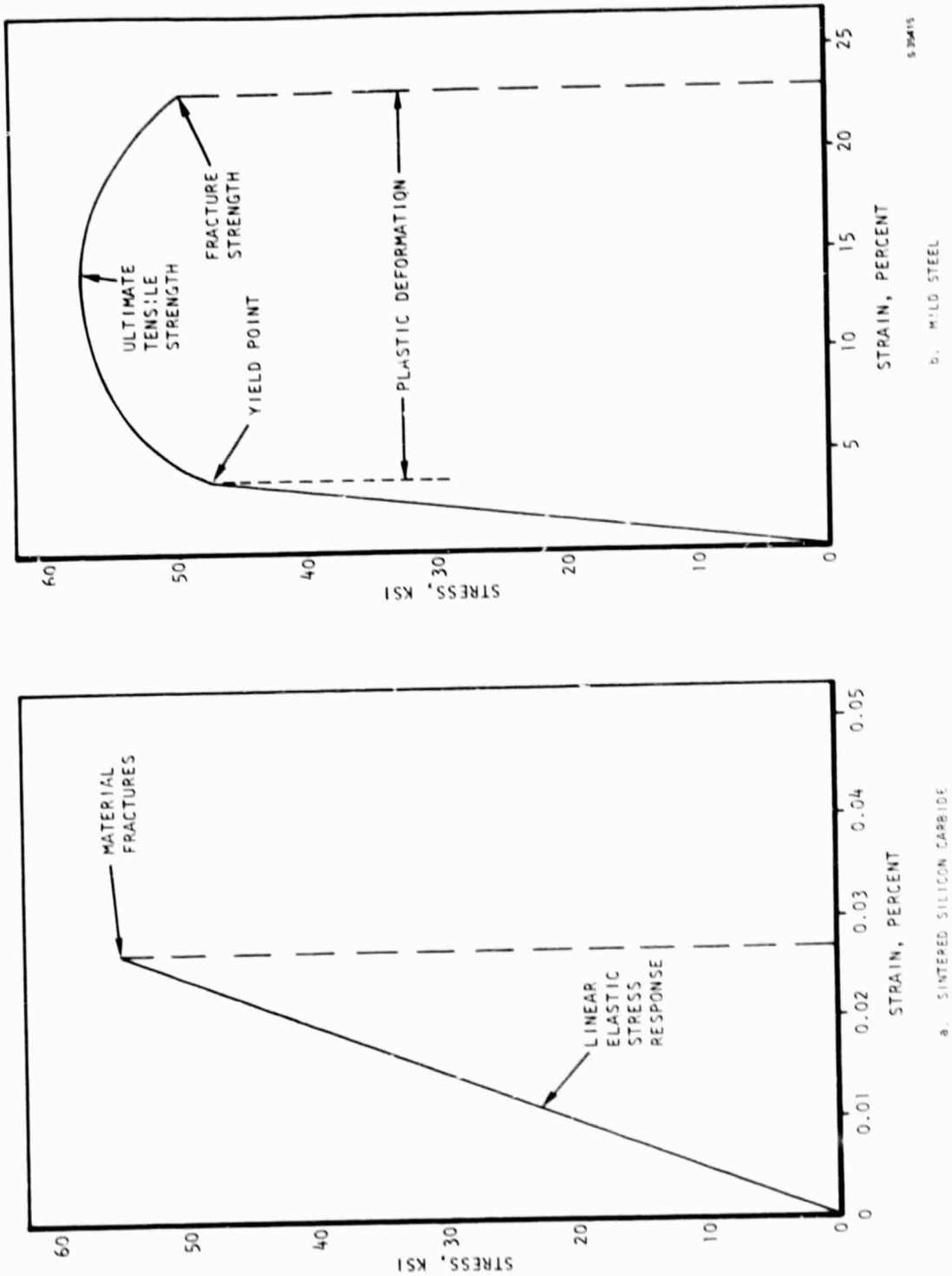


Figure B-1. Comparison of Elastic Properties of Sintered Silicon Carbide and Mild Steel



The Weibull distribution function allows the comparison of strength distribution parameters with calculated stress fields. This comparison then can be used to estimate the failure probability of a component design at a particular stress level using computer finite-element analysis. Use of this method implies that test data are collected from samples processed in exactly the same manner as production components, and that material testing is conducted under the same conditions that components will experience in service.

The probability of failure of ceramics has been most accurately characterized by means of the standard Weibull statistics expression as:

$$S = 1 - \exp \left[- V \left(\frac{\sigma_f}{\sigma_0} \right)^m \right] \quad (B-1)$$

where S is the failure probability, V is a normalized stressed volume or surface area depending on the type of flaws causing failure, σ_f is the fracture stress, σ_0 is the characteristic stress (which is a normalizing constant), and m is the Weibull modulus. The fracture strengths of a group of samples can be used to estimate m and σ_0 when Eq. B-1 is rewritten as:

$$\ln \ln \frac{1}{1-S} = m \left\{ \ln V - \ln \sigma_0 \right\} + m \ln \sigma_f \quad (B-2)$$

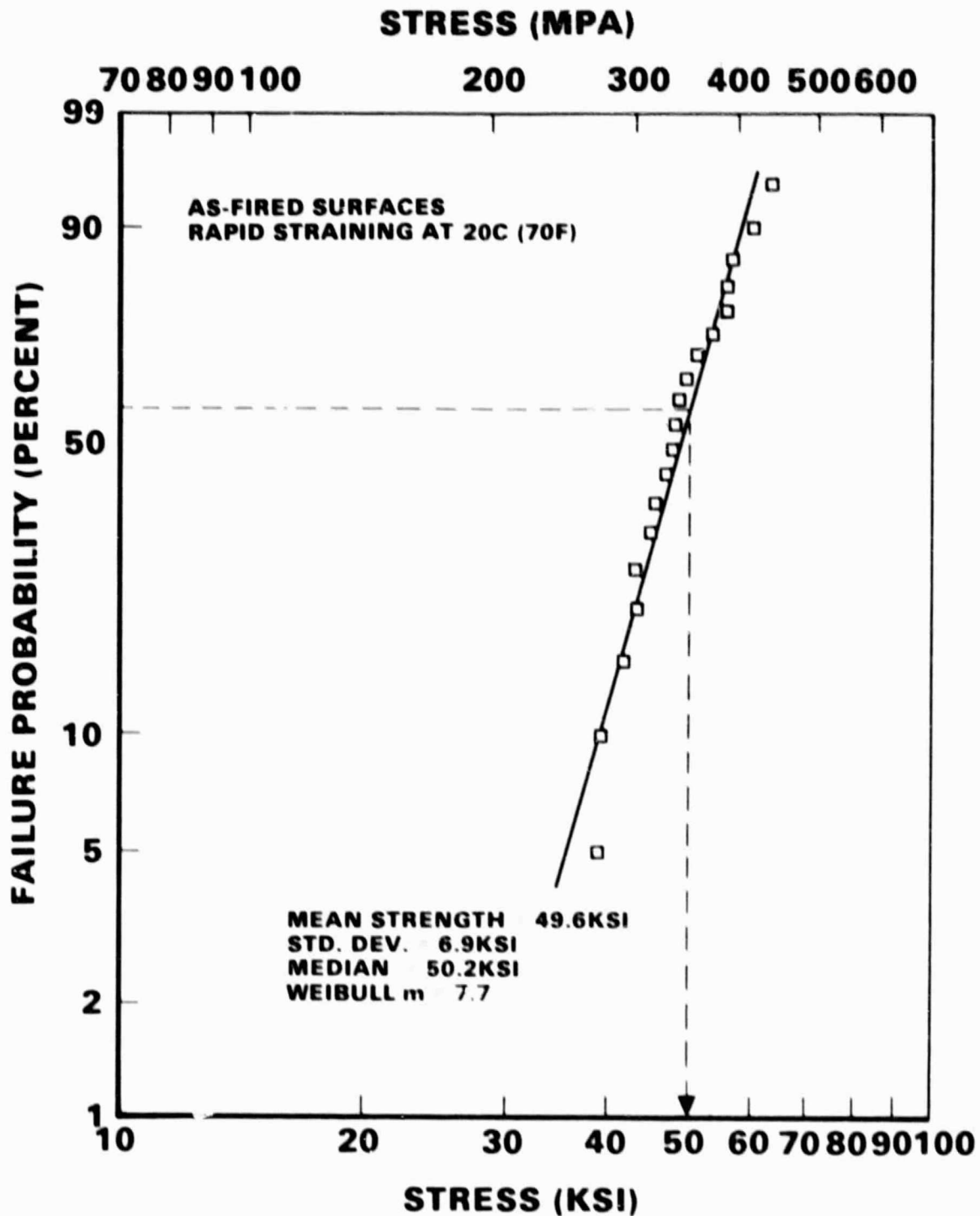
The value of S can be estimated from $S = s/(n + 1)$, where n is the total number of samples in a test and s is the number of the sample when the group is arranged in increasing order of fracture stress. When $\ln \ln 1/(1-S)$ is plotted versus $\ln \sigma_f$, m is the slope and σ_0 can be taken as the value that will make the data best fit a straight line. For a good representative set of Weibull data, σ_0 is the median stress and is found at $S = 0.632$. Figure B-2 shows an actual computer-drawn plot and calculated Weibull m for a group of strength data. The plot is used for design purposes by selecting a designated failure probability that defines the design stress level.

The reliability of the estimated slope or Weibull modulus (m) is increased with large sample populations. For design purposes, sample sizes larger than 20 should be used. Sample sizes that are too small can easily cause the spread in the data to be underestimated. Thus, an unrealistically high Weibull modulus will be estimated. This in turn will result in an erroneous prediction of lower failure probabilities than will actually be observed for a given stress level.

Eq. B-1 can be used to calculate the probability of failure of a particular volume or surface represented in a finite-element analysis. The following describes how local probabilities can be combined to obtain an overall probability for an entire structure, and to relate the material constants σ_0 and m to appropriate material test data.



ORIGINAL PAGE IS
OF POOR QUALITY



S 3504B A

Figure B-2. Computer-Drawn and Calculated Weibull m



ORIGINAL PAGE IS
OF POOR QUALITY

Assuming independence, the probability of success of an entire structure can be found by combining individual local probabilities of success according to the following:

$$(1 - S_T) = (1 - S_{1_i}) (1 - S_{1_{i+1}}) \dots (1 - S_{1_n}) \quad (B-3)$$

where S_T = probability of failure for the entire structure of n segments

S_1 = probability of failure for a local segment

The process is more easily described if a simple situation is considered. If the individual probabilities of success are equal, Eq. B-3 can be rewritten as:

$$(1 - S_T) = (1 - S_1)^n \quad (B-4)$$

In addition, if the local volumes are equal, the probability of success of a total volume may be considered as the product of the probabilities of success of V equal volumes, resulting in:

$$(1 - S_T) = (1 - S_1)^V \quad (B-5)$$

Taking the natural log of both sides of Eq. B-5 and multiplying by -1 results in:

$$-\ln (1 - S_T) = -V \ln (1 - S_1) \quad (B-6)$$

The left side of Eq. B-6 is commonly defined as the risk of rupture, R ; thus,

$$R = -V \ln (1 - S_1) \quad (B-7)$$

Eq. B-7 allows Eq. B-6 to be rewritten in the form of:

$$S_T = 1 - \exp (-R) = 1 - \exp [V \ln (1 - S_1)] \quad (B-8)$$

To establish a necessary relation with the test data, the number of unit volumes (V) can be treated as the volume of a finite element (v) divided by the stressed volume (v_s) of a suitable test specimen. The material characteristics obtained from test specimens are characterized for both volume and surface failure modes and stored within computer programs.



ORIGINAL PAGE IS
OF POOR QUALITY

The probability of failure of a stressed volume equal to the stressed test volume can be expressed as:

$$S = 1 - \exp \left(- \left(\frac{\sigma}{\sigma_0} \right)^m \right) \quad (B-9)$$

where σ is the design stress and

σ_0 and m are supplied by the test data available for the chosen specimen and failure mode.

This allows Eq. B-8 to be rewritten as the probability of failure of a given element due to a single stress component. Thus, the expected survival probability, S_E , can be represented as,

$$S_E = 1 - \exp \left(- \frac{V}{V_T} \left(\frac{\sigma}{\sigma_0} \right)^m \right) \quad (B-10)$$

The probability of success of a given element can thus be written in the form of:

$$1 - S_E = \exp \left(- \frac{V}{V_T} \left(\frac{\sigma}{\sigma_0} \right)^m \right) \quad (B-11)$$

A similar approach can be employed for surface area effects, resulting in:

$$1 - S_E = \exp \left(- \frac{A}{A_T} \left(\frac{\sigma}{\sigma_0} \right)^m \right) \quad (B-12)$$

An estimate of the probability of success of a local volume or surface (i.e., a particular finite element) must consider the three principal stresses. The total probability of success is assumed to be equal to the product of the individual probabilities associated with each principal stress. Considering the brittle nature of ceramic materials, the principal stresses are considered to be a better measure of failure than equivalent or octahedral shear stresses. In addition, most failures in ceramics are mode I types, even at high temperatures, indicating that the principal stresses are a good estimate. Compressive stresses contribute little to crack growth and failure. Therefore, it has been assumed that compressive stresses can be neglected. The probability of success of the total structure is taken as the smallest of the calculated probabilities of success of all the local volumes or surface areas that are readily obtained during the finite-element analysis.

Design criteria embodying aspects of a deterministic approach, and utilizing a probabilistic basis built into the analytical tools on an individual finite-element volume and surface area basis, are felt to provide the best approach to

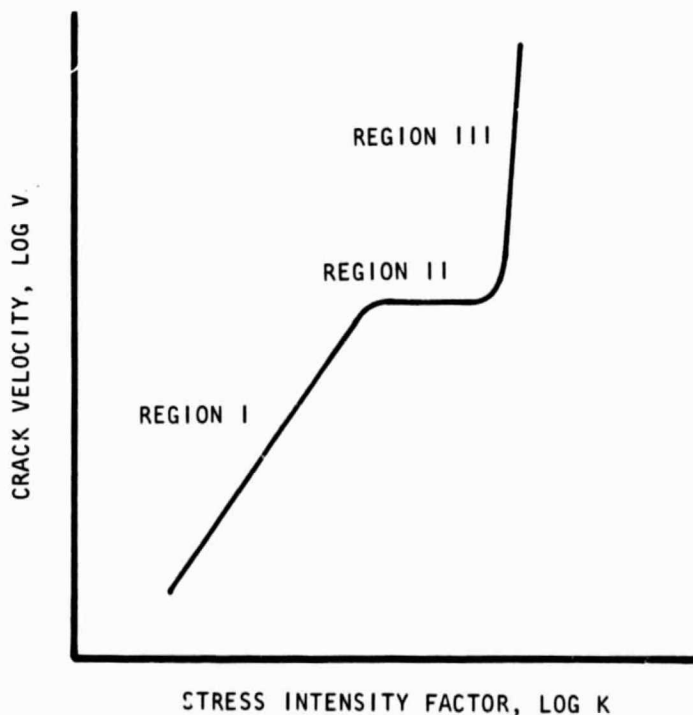


effective design with ceramics. In the presence of adequate materials and component test data, this approach is valid; even with a lower level of materials data, it provides a realistic method of comparing designs. This approach is currently being employed by AiResearch in the analysis of all ceramic designs, including ceramic rotor-blade attachment designs, the evaluation of spin-pit data from tests on ceramic turbine wheels, and ceramic heat exchanger component designs. Initial test results, when compared with prior predictions, have thus far been very encouraging.

The data used in the Weibull probabilistic analysis should accurately represent the expected component operating conditions. Many experimenters make the mistake of generating material data in short-time, rapid-loading experiments. Because ceramic materials can be susceptible to slow crack growth (SCG), simulation of actual component performance may require stress rupture or cyclic fatigue tests over a long time to accurately characterize performance.

Slow crack growth is the subcritical extension of preexisting cracks under stress to a critical size where catastrophic failure can occur by spontaneous crack growth (energetically favored crack growth). SCG can be controlled by corrosive environments that affect the rate of crack extension (crack velocity).

The relation between stress and crack velocity can be graphically shown. A schematic representation of the ideal K/V (stress intensity/crack velocity) diagram is shown in Figure E-3.



S-26123

Figure E-3. Stress Intensity vs Crack Velocity



**ORIGINAL PAGE IS
OF POOR QUALITY**

The stress intensity factor (K) is usually expressed as $K = \sigma Y C/2$ for ceramics where σ = stress, C = crack length, and Y = a geometrical factor. In Region I, the rate of reaction between the corrosive species and the atoms under stress at the crack tip is controlling. In Region II, the diffusion of corrosive species to the crack tip is rate-controlling. Region III expresses the crack growth independent of the environment, since the crack would be traveling faster than the diffusion of the corrosive species.

These data can be generated from crack propagation tests of large preformed cracks by the double torsion method. Determination of the K/V slope by double torsion methods may not be characteristic of crack propagation of inherent surface flaws, which usually are the cause of failure in ceramics. Stress rupture and dynamic fatigue testing (variable strain rate testing) are alternative methods.

In Regions I and III, the slope of the K/V diagram, n, can be determined from the ratio of strengths (σ) at two strain rates ($\dot{\epsilon}$) by

$$\left(\frac{\sigma_1}{\sigma_2}\right)^{n+1} = \left(\frac{\dot{\epsilon}_1}{\dot{\epsilon}_2}\right) \quad (B-13)$$

The value of n can then be used to define the relation between the failure time in a constant strain rate test, $\tau_{\dot{\epsilon}}$, and the failure time under the maximum stress sustained in a constant stress test, τ_{σ} , using

$$\tau_{\sigma} = \frac{\tau_{\dot{\epsilon}}}{n+1} \quad (B-14)$$

If the flaw distribution does not change with time in the operating environment, the Weibull modulus should remain constant for all data tested to failure in the same lifetime. Then the ratio of failure times, τ , at different applied stresses can be written as

$$\left(\frac{\sigma_1}{\sigma_2}\right)^n = \left(\frac{\tau_2}{\tau_1}\right) \quad (B-15)$$

Using this relation, data from the experimentally determined failure probability curve can then be used to predict the family of failure probability curves as a function of time to failure, which can be used to predict stressed lifetime. If the time to failure of samples tested at greatly different strain rates (at least two orders of magnitude) is used to predict the failure probability at long life-times, it is possible that a refinement of the prediction can be made. Furthermore, the reliability of the predicted failure curves can be estimated with a limited number of stress rupture tests.



ORIGINAL PAGE IS OF POOR QUALITY

Because the most vigorous stress requirements for high-temperature ceramic components are during heatup and cooldown, dynamic and cyclic tests that characterize the stress-probability-lifetime curves most accurately represent the material response in ceramics. Furthermore, cyclic fatigue tests can be incorporated into the lifetime prediction curves from

$$\tau_f = g^{-1} \tau_c \quad (B-16)$$

where the time to failure under static fatigue conditions, τ_f , is related to the cyclic time to failure, τ_c , by the constant g^{-1} , which can be derived for various cyclic loading conditions.

Because ceramics are a relatively new and uncharacterized set of materials, much of the data described above do not exist for many environmental and high-temperature cases. Furthermore, most data found in the literature have been collected on machined surfaces and are not applicable to components with as-received or as-fired surfaces.

APPLICATION OF THEORY

Structural analysis on ceramic components is routinely performed with the AiResearch ANSTAT computer program. The ANSTAT program takes the results of a finite-element computer analysis using the ANSYS computer program and calculates the cumulative percent of failure of the entire model. Inputs of material properties are obtained from test specimens that were made by the same manufacturing technique as the part being analyzed.

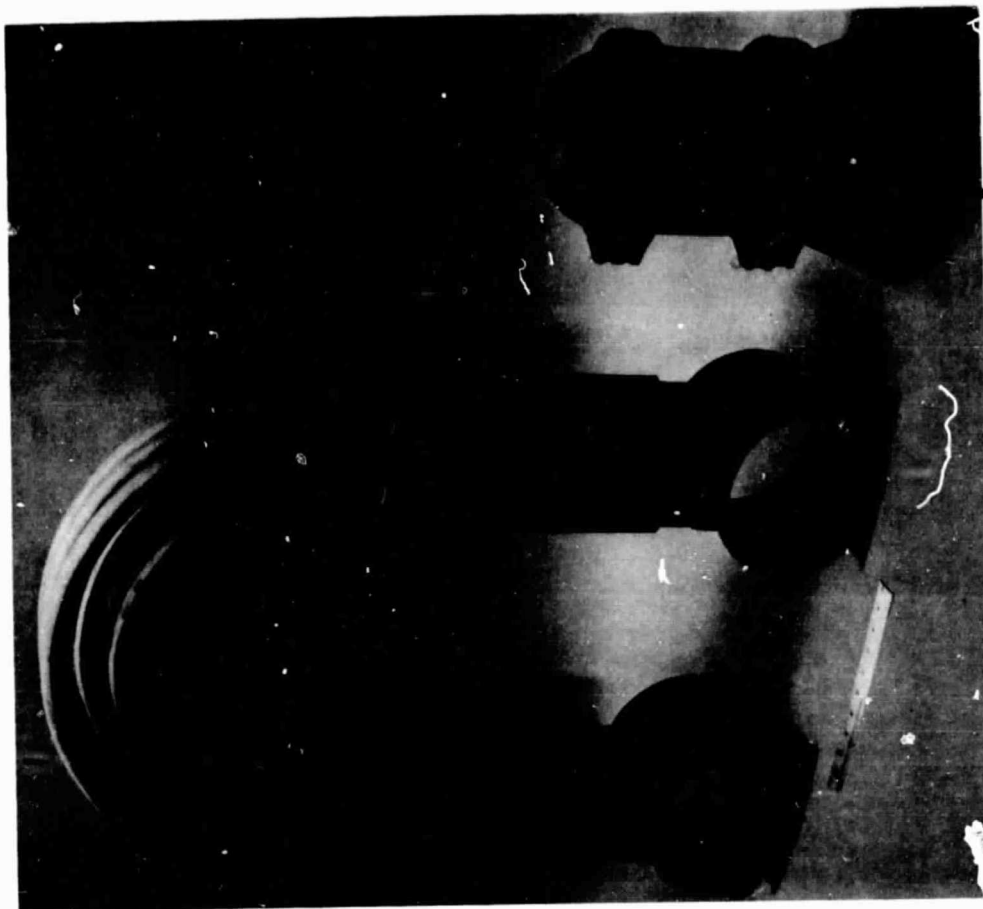
This statistical method was successfully demonstrated in a program for the Electric Power Research Institute (EPRI) to design a high-temperature ceramic heat exchanger (Figure B-4). Basic material tests on standard bar specimens and components were used to design the heat exchanger with a 90-percent reliability. The ANSTAT program uses the median strength and the Weibull slope obtained from a statistical analysis of material test data. An in-house computer program was used to reduce the test data to obtain these needed parameters. In addition, ANSTAT requires the surface area and volume definition of the test specimen, which is subject to the maximum stress. The volume and surface area of the bar specimens subjected to the maximum stress were calculated using a technique outlined in Westinghouse report WAHL-TME-2688, "Theory and Structural Design Applications of Weibull Statistics."

Finite-element computer models were constructed to aid in the analysis of the various components of the reference design of the heat exchanger. Included were models of the entire tube assemblies, the finned tube sections, and a part of the manifolds. The manifold model is shown in Figure B-5. These models also were used to analyze the data obtained from the component tests performed.

The operating temperatures and pressures were applied to a representative section of the heat exchanger to determine the loading in the various components. The technique was used to predict the probability of the components successfully withstanding the operating loads. From the component results, a reliability



FINNED TUBE



F-31440

PLAIN TUBE

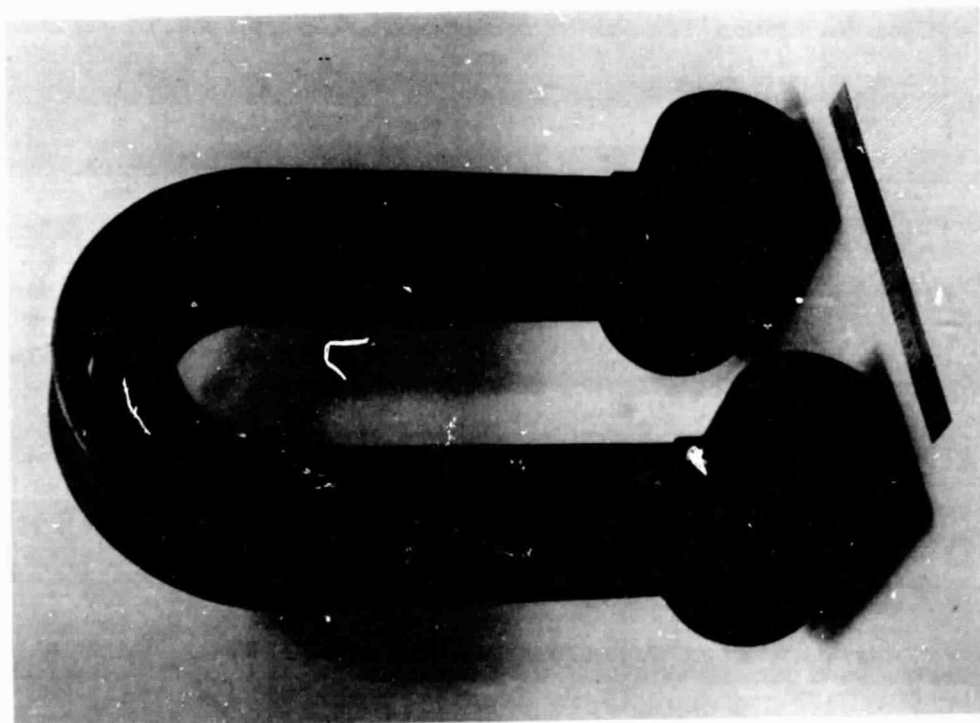


Figure B-4. Ceramic (Si-SiC) Heat Exchangers

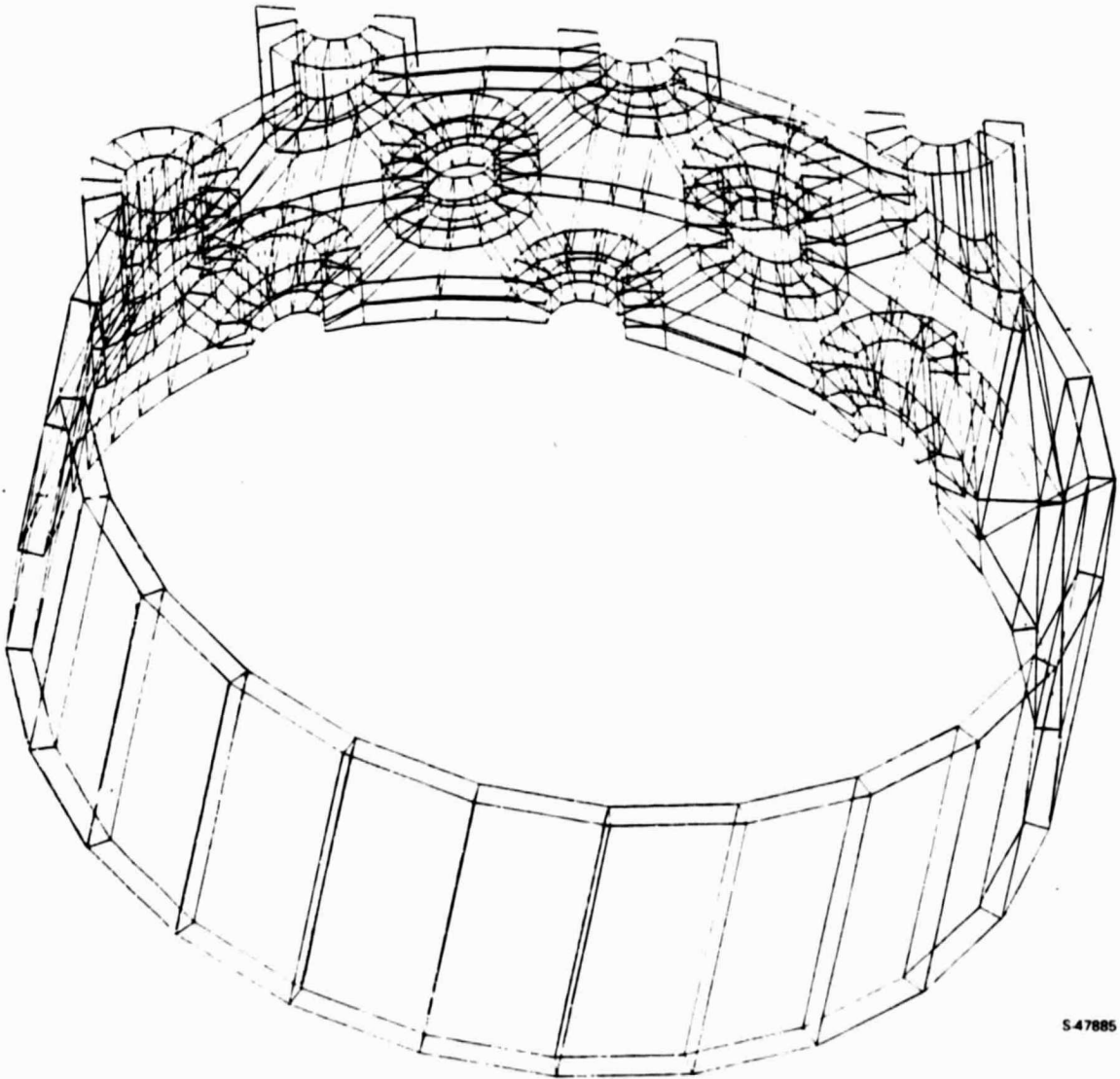
ORIGINAL PAGE
BLACK AND WHITE PHOTOGRAPH

81-18452
Page B-10



AIRESEARCH MANUFACTURING COMPANY

ORIGINAL PAGE IS
OF POOR QUALITY



S47885

Figure B-5. Manifold Finite-Element Model



**ORIGINAL PAGE IS
OF POOR QUALITY**

model was constructed to determine the probability of the heat exchanger withstanding the application of operating loads. The resulting value was 83.46 percent, which is below the design goal of 90 percent. The calculated value for the tubes is 94.68 percent. The manifolds, with an overall probability of success of 88.15 percent, represent the weakest link. If the manifold diameter were reduced by approximately 2 inches, reliability of 90 percent would be predicted for the heat exchanger.

This demonstration of the design methodology also served to confirm the basic theory upon which it was predicated. Collected data were found to fit the Weibull form and the performance of components followed the general trends predicted by computer simulation. One of the most important aspects of the experiment was the determination of a volume scaling factor. Figure E-6 shows the average fracture strength of a variety of test specimens plotted as a function of their volume normalized to that of the smallest specimen (standard test bar). Rearranging Eq. E-2 gives

$$m \ln V = \ln \ln \frac{1}{1-S} + m \ln \sigma_0 - m \ln \sigma_f \quad (E-17)$$

indicating that the slope of Figure E-6 is the negative inverse of the Weibull modulus. The data for both room temperature and high temperature seem to indicate a Weibull m of 7.0 when considering the major components (test bars, tubes, and flasks). It is difficult to determine if the effective stressed volume of the U-tube specimens has been accurately estimated. These points are included for completeness, but were not used in the estimation of m . Results of this type confirm the basic mechanical properties theory and make the design of complex components possible.

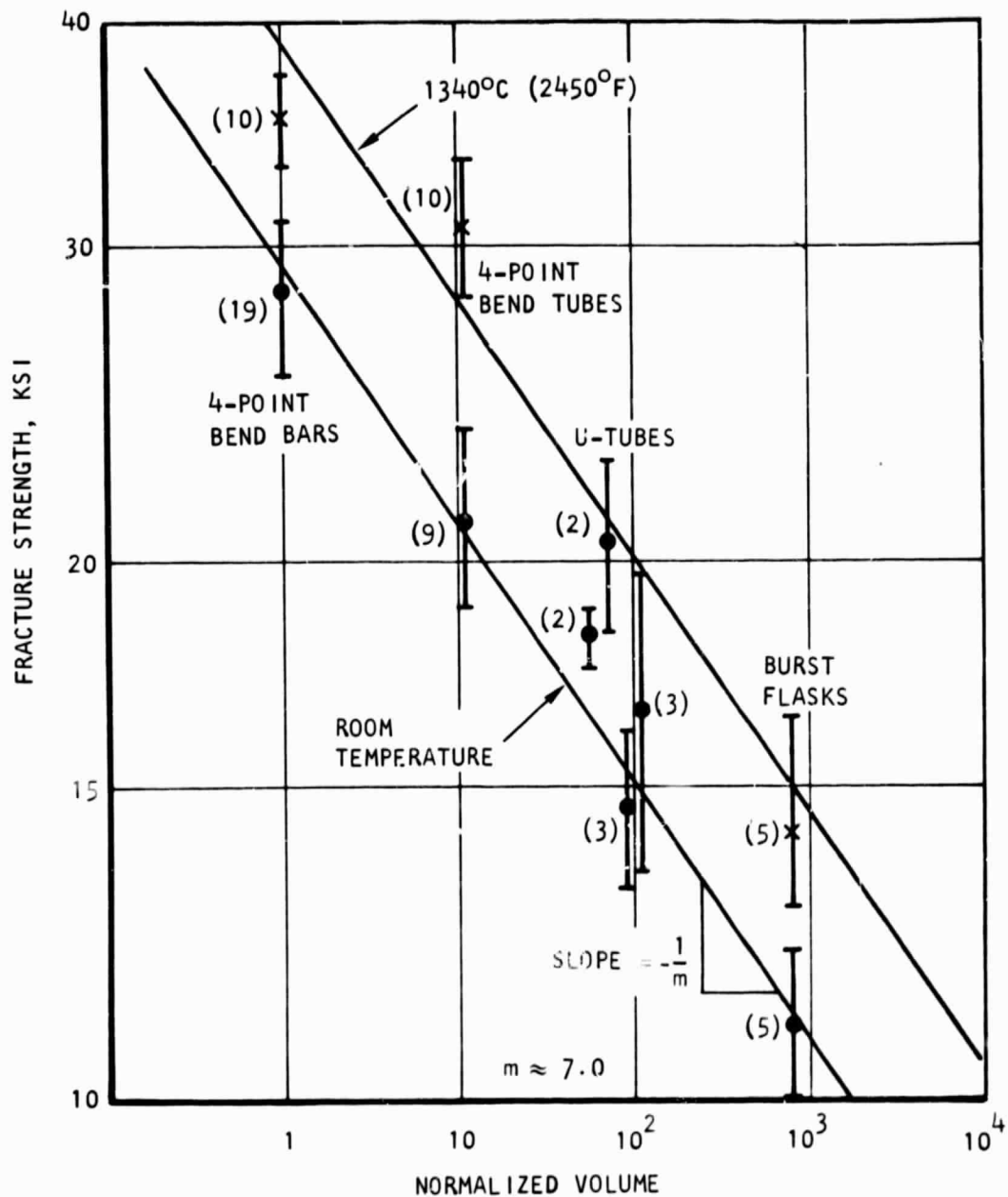
OTHER DESIGN PROBLEMS

In addition to conventional material property characterization, it is necessary to evaluate the properties of special configurations such as permanent and mechanical joints, environmental impact on material properties, and the fabrication technology development.

To produce large complex ceramic components, it is often necessary to form permanent joints between separately fabricated components and mechanically joined individual components. Permanent joining techniques have only been successfully demonstrated on a large scale for siliconized silicon carbide. Norton Company fabricated the complex Si-SiC heat exchanger (shown in Figure E-4) from 32 separate components using 40 permanent ceramic joints to ceramically bond all components into one piece. Characterization of similar joints on tubes showed that the joints had strengths of about 90 percent of the parent material. Similar joining techniques on other ceramic materials are currently under study. Mechanical joining techniques are also necessary to incorporate ceramic components with metallic components, to join large ceramic components, and to promote replaceability and repairability of large and expensive complex ceramic structures. The mechanical sealing problem is further complicated when high temperatures and high pressure containment are necessary. Relatively little research has been done in this area. The EPRI program briefly addressed this problem with encouraging results.



ORIGINAL PAGE
BLACK AND WHITE PHOTOGRAPH



A.2651-A

Figure B-6. Normalized Volume



**ORIGINAL PAGE IS
OF POOR QUALITY**

Although many studies have been done on ceramic materials in aggressive environments, few have addressed the problem of prolonged environmental exposure where diffusional mechanisms might significantly alter the properties of candidate materials. These studies often are beyond the scope and resources of most hardware-oriented programs.

Many ceramic materials have outstanding properties for use in advanced applications, but they have limited fabricability. Considerable development is necessary in this area. Near-net shape fabrication techniques are necessary to avoid the high cost of machining large and complex ceramic components.

